10-2015

Seismic Behavior Prediction Of Concentrically Braced Steel Frames

Hani Mohamed Mayez Akkari

United Arab Emirates University

College of Engineering

Department of Civil and Environmental Engineering

SEISMIC BEHAVIOR PREDICTION OF CONCENTRICALLY
BRACED STEEL FRAMES

Hani Mohamed Mayez Akkari

This thesis is submitted in partial fulfilment of the requirements for the degree of
Master of Science in Civil Engineering

Under the Supervision of Dr. Amr M.I. Sweedan

October 2015

Declaration of Original Work

I, Hani Mohamed Mayez Akkari, the undersigned, a graduate student at the United Arab Emirates University (UAEU), and the author of this thesis entitled "*Seismic behavior prediction of concentrically braced steel frames*", hereby, solemnly declare that this thesis is my own original research work that has been done and prepared by me under the supervision of Dr. Amr Sweedan, in the College of Engineering at UAEU. This work has not previously been presented or published, or formed the basis for the award of any academic degree, diploma or a similar title at this or any other university. Any materials borrowed from other sources (whether published or unpublished) and relied upon or included in my thesis have been properly cited and acknowledged in accordance with appropriate academic conventions. I further declare that there is no potential conflict of interest with respect to the research, data collection, authorship, presentation and/or publication of this thesis.

Student's Signature: _____   Date: _____

Advisory Committee

1) Advisor: Dr. Amr M.I. Sweedan

Title: Associate Professor

Department of Civil and Environmental Engineering

College of Engineering

Approval of the Master Thesis

This Master Thesis is approved by the following Examining Committee Members:

1) Advisor (Committee Chair): Dr. Amr M.I. Sweedan

   Title: Associate Professor

   Department of Civil and Environmental Engineering

   College of Engineering, UAE University

   Signature _____   Date _____

2) Member: Dr. Aman Mwafy

   Title: Associate Professor

   Department of Civil and Environmental Engineering

   College of Engineering, UAE University

   Signature _____   Date _____

3) Member (External Examiner): Prof. Jerome F. Hajjar

   Title: CDM Smith Professor and Chair,

   Director, Laboratory for Structural Testing of Resilient and Sustainable Systems (STReSS Laboratory)

   Department of Civil and Environmental Engineering

   Northeastern University, USA

   Signature _____   Date _____

This Master Thesis is accepted by:

Dean of the College of Engineering: Prof. Mohsen Sherif

Signature _____   Date _____

Dean of the College of the Graduate Studies: Prof. Nagi Wakim

Signature _____   Date _____

Copy ____ of ____

Abstract

Concentrically braced steel frames (CBFs) are efficient and commonly used steel systems for resisting seismic loads through a complete truss action. In strong earthquake events, multi-storey concentrically braced steel frames (CBFs) are prone to form a storey-collapse mechanism after buckling and yielding of the braces in a storey.

This thesis evaluates the seismic performance of steel concentrically braced frames (CBFs) in Abu Dhabi, UAE. The aim of this study is to assess the overall lateral capacity of multi-storey buildings and the associated sequence of formation of plastic hinges using inelastic pushover analysis technique. The time history analysis approach is employed to assess the local and global seismic performance of braced frame structures under various earthquake records representing the potential seismic loading scenarios. In addition, the adequacy of using inelastic pushover analysis as a simplified means to examine the seismic integrity of braced frame structures and to predict the sequence of development of plastic hinges within the system is evaluated. This study shows that under the expected level of Abu Dhabi's seismicity the designed concentrically braced steel frames (CBFs) perform in an excellent manner by suffering of repairable damages with no life safety threatening.

This study puts a step forward in the effort of spreading the knowledge of using the concentrically braced steel frames as lateral force resisting system in Abu Dhabi for mid and high rise buildings.

Keywords: Concentrically braced steel frames, storey-collapse mechanism, buckling, yielding, push over, time history, plastic hinges

Title and Abstract (in Arabic)

التنبؤ بالسلوك الزلزالي للهياكل المعدنية المقواه بدعامات مركزية

الملخص

تعد الهياكل المعدنية المقواه بدعامات مركزية (CBFs) من الأنظمة الفعالة والشائعة الاستخدام لمقاومة أحمال الزلازل من خلال القوى المحورية، وعند حدوث زلزال قوي قد يحدث انهيار لبعض طوابق الهياكل المعدنية المقواه بدعامات مركزية (CBFs) نتيجة التواء وليونة الدعامات المستخدمة في هذه الطوابق ولذلك تركز هذه الدراسة على تقييم الأداء الانشائي للهياكل المعدنية المقواه بدعامات مركزية (CBFs) تحت تأثير الهزات الأرضية المتوقع حدوثها في أبوظبي بدولة الإمارات العربية المتحدة.

الهدف من هذه الدراسة هو تقييم قدرة التحمل الجانبية الشاملة للمباني متعددة الطوابق وتسلسل تكوين المفصلات البلاستيكية باستخدام أسلوب التحليل المبني على القوى الافقية المتزايدة الشدة (Inelastic Pushover Analysis) و أيضا باستخدام أسلوب التحليل الديناميكي (Time History Analysis) لتقييم الأداء الزلزالي للعناصر الحرجة و لكامل الهياكل المعدنية المدعمة تحت تأثير سجلات الزلازل المختلفة التي تمثل السيناريوهات المحتملة للزلازل، بالإضافة إلى تقييم مدى كفاية استخدام تحليل الدفع المتتالي غير المرن كوسيلة مبسطة لفحص السلوك الزلزالي للهياكل المعدنية المدعمة والتنبؤ بتسلسل تكوين المفصلات البلاستيكية داخل عناصر الهيكل.

تخلص هذه الدراسة الى أنه في ظل المستوى المتوقع للنشاط الزلزالي في أبوظبي فإن الهياكل المعدنية المقواه بدعامات مركزية (CBFs) التي تم تصميمها بشكل كامل باستخدام مواصفات التصميم الدولية تؤدي دورها بطريقة ممتازة من خلال تحمل أضرار قابلة للإصلاح بدون تهديد سلامة أرواح مستخدمي هذه المباني عند تعرضها لهزة أرضية قوية، و لذلك تمثل هذا الدراسة خطوة للإمام في خضم الجهود المبذولة لنشر الوعي بفائدة استخدام الهياكل المعدنية المقواه بدعامات مركزية كنظام مقاوم للقوى الجانبية المؤثرة على المباني المتوسطة أو العالية الارتفاع المقامة في أبوظبي.

مفاهيم البحث الرئيسية: الهياكل المعدنية المقواه بدعامات مركزية، التواء، ليونة، التحليل المبني على القوى الافقية المتزايدة الشدة، التحليل الديناميكي، المفصلات البلاستيكية.

Acknowledgements

Foremost, I would like to express my sincere gratitude to my advisor Dr. Amr Sweedan for the continuous support of my Master's study and research, for his patience, motivation, enthusiasm, and immense knowledge. His guidance helped me in all the time of research and writing of this thesis.

My sincere thanks also go to Dr. Aman Mwafy for his guidance, support, and assistance. I would like to thank the chair and all members of the Department of Civil and Environmental Engineering at the United Arab Emirates University for assisting me all over my studies and research.

I would also like to thank my dad and mom for the support they provided me through my entire life. In particular, I must acknowledge my wife and best friend, without her love, encouragement and editing assistance, I would not have finished this thesis. Finally, I want to acknowledge my twin daughters source of my inspiration and encouragement.

Dedication

To my beloved dad (Mayez), mom (Nadia), wife (Mayssa) and twin daughters (Lilia & Myriam)

Table of Contents

List of Tables

List of Figures

List of Abbreviations

A_g Gross cross sectional area of the brace element (mm^2)

b   Width of section (mm)

B_1 Multiplier to account for P-δ effects

c   Actual damping coefficient

Ccritical   Critical damping coefficient

C   Equivalent viscous damping coefficient (N.s/m)

C_o modification factor to relate spectral displacement of an equivalent SDOF system to the roof displacement of the building MDOF system

C_1 modification factor to relate expected maximum inelastic displacements to displacements calculated for linear elastic response

C_3 is the modification factor to represent increased displacements due to dynamic P-Δ effects

C_{BR} Expected compressive strength in compression and post-buckling strength of the bracing element (MPa)

C_d Deflection amplification factor

C_m Coefficient accounting for non-uniform moment

CP   Collapse Prevention

D   Outside diameter, in. (mm)

E   Modulus of elasticity of steel (MPa)

f_D Total damping force experienced by the structure (N)

F_{cr} Critical compressive strength of axially-loaded elements (MPa)

F_{cre} Critical stress calculated using expected yield stress (MPa)

F_e Elastic buckling stress (MPa)

f_y	Specified minimum yield stress of the type of steel to be used (MPa)
G_f	Wind gust Factor
h_{sx}	Storey height below level x
I	Moment of inertia, (mm^4)
IDR	Inter-storey Drift Ratio
IO	Immediate Occupancy
K_0	Initial stiffness of member
k	Effective length factor
L_b	Length between points which are either braced against lateral displacement of compression flange or braced against twist of the cross section, in. (mm)
L	Half brace length (mm)
LS	Life Safety
M_1	Calculated from a first-order analysis, is the smaller moment at the ends of that portion of the member unbraced in the plane of bending under consideration.
M_2	Calculated from a first-order analysis, is the larger moments, at the ends of that portion of the member unbraced in the plane of bending under consideration.
M_n	Nominal flexural strength (N-mm)
Mu	Required flexural strength using LRFD load combinations (N-mm)
NSP	Non-linear Static Procedure
OCBF	Ordinary Concentrically Braced Frames

P.O.S.C.   A certain output determined from Pushover Analysis at Storey Collapse limit

P.O.B.C.   A certain output determined from Pushover Analysis at Building Collapse limit

P_{e1} Elastic critical buckling strength of the member in the plane of bending (N)

P_{ncr} Nominal compressive strength of a member (N)

P_y Nominal axial yield strength of a member equal to F_yA_g, (N)

P_u Required axial strength in compression, kips (N)

P_D Column axial load from Dead load (N)

P_L Colum axial load from live load (N)

$P_{(D.S.)}$ Column axial load at strength level, resulting from direct summation (N)

PGA   Peak ground acceleration (m/s^2)

r_i Radius of gyration (mm)

R   Response modification factor

R_y Ratio of expected yield stress to the specified minimum yield stress

SCBF   Special Concentrically Braced Frames

S_S Mapped maximum considered earthquake spectral response acceleration for short period

S_1 Maximum considered earthquake spectral response acceleration for 1-second period

T_e Effective fundamental period of the building in the direction under consideration, sec.

Ts   Characteristic period of the response spectrum, defined as the period associated with the transition from the constant acceleration segment of the spectrum to the constant velocity segment of the spectrum

T_{BR}	Expected strength of the bracing elements in tension (N)
t	Thickness of element (mm)
V_d	Design base shear (N)
V_m	Base shear carried by the system at a particular mechanism (N)
$\dot{x}$	Velocity (m/s)
Z_p	Plastic section modulus of section about the axis of bending (mm^3)
λ	Slenderness parameter
λ_{md}	Limiting slenderness parameter for moderately ductile compression elements
λ_{mh}	Limiting slenderness parameter for highly ductile compression elements
α	ASD/LRFD force level adjustment factor
Φ	Resistance factor for flexure (0.9)
Ω_o	Structural overstrength
μ	Structural Ductility factor
Δ_u	Ultimate structural drift
Δ_y	Displacement corresponding to the yield strength
ζ	Critical damping coefficient, known as the damping ratio

Chapter 1: Introduction

1.1 Overview

In the early twenty first century, almost all six Gulf Cooperation Council (GCC) countries, Bahrain, Kuwait, Oman, Qatar, Saudi Arabia and the United Arab Emirates (UAE), showcased levels of economic development and infrastructure expansion not seen since the 1970s oil boom. High oil revenues in conjunction with low interest rates made for a very fruitful soil for building construction boom with UAE being the biggest construction market in the GCC. Tall buildings construction is spreading in the UAE especially in Dubai where the tallest building in the world "Burj Khalifa" is located and Abu Dhabi where several iconic buildings have been built such as the Capital Gate tower and Al Dar Headquarters building. For many years, the UAE was known to be a region of low seismicity even though being in close proximity to high seismic zones. Until few years back, the Uniform Building Code (UBC, 1997) was used for seismic design and recommended the use of seismic zone '0' for the cities of Abu Dhabi and Dubai. Recent earthquakes recorded within the region have emphasized the necessity to revise the adopted seismic design provisions. In 2013, Abu Dhabi's Department of Municipal Affair released the Abu Dhabi International Building Code that is based on the International Building Code (IBC, 2009) with the use of specific-generated Abu Dhabi seismic maps. The IBC (2009) takes into account more factors in deriving values for each criterion as compared to the UBC (1997). It introduced the seismic design category (SDC) that combines the building's occupancy category, seismic hazards and soil characteristics at the construction site. For example, IBC (2009) restrictions on building height, lateral force resisting system, structural irregularity, choice of analysis procedure and

level of detailing required are dependent on seismic design category (SDC) whereas UBC (1997) relies on zone categories for calculating seismic loads (Anthony, 2007; Pong et al., 2006).

The current study focusses on using steel concentrically braced frames (CBFs) as lateral resisting force system. Early in the Twentieth century, the steel braced frames were primarily used to resist wind-induced forces in buildings. Later on, their usage was extended to resist seismic forces. More complete bracing systems were developed in the 1960s and 1970s, along with the dissemination of more detailed seismic regulations. Unlike moment-resisting frames, braced framing systems proved popular in regions of high seismicity because more materials savings could be achieved and control of frame drift due to high earthquake-induced inertial forces could be efficiently realized (Bruneau et al., 2011). The efficient drift control arises from the fact that braced frames may be considered as cantilevered vertical trusses resisting lateral loads primarily through the axial stiffness of columns and braces. The columns act as the chords in resisting the overturning moment. The diagonals work as the web members resisting the horizontal shear in axial compression or tension, depending on the direction of inclination. The resulting deformed shape of the braced frame is a combination of the effects of the flexural and shear patterns, with a resultant configuration depending on their relative magnitudes as depicted by Fig. 1.1. Nevertheless, the flexural deflection most often dominates the deflection characteristics. CBFs can provide a ductile response through inelastic action in braces. In general, failure of this system is controlled by two potential failure modes; braces yield in tension or braces buckle in compression.
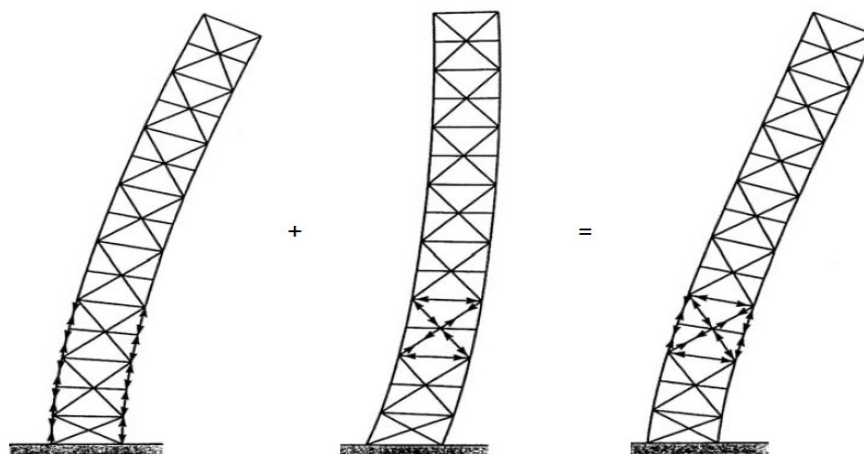
(a) Flexural deformations   (b) Shear deformations   (c) Combined profile

Figure 1.1: Lateral Deformation Patterns of Braced Frames (Taranath, 2005)

There are several types of CBFs depending on the system of triangulation used to form the brace members. Common CBF configurations are presented in Fig. 1.2 (Bruneau et al., 2011).
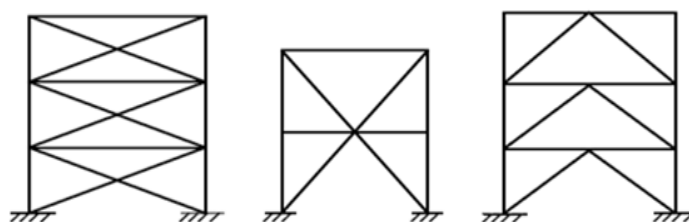
(a) X-bracing   (b) Split X-bracing   (c) Chevron inverted
                                              V bracing
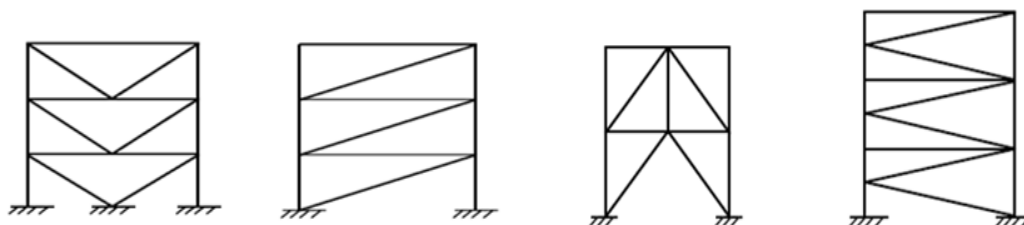
(d) Chevron V-bracing   (e) Diagonal bracing   (f) Zipper column   (g) K-bracing
                                                      bracing

Figure 1.2: Common Configurations of CBFs (Bruneau et al., 2011)

To understand the inelastic response of CBFs under earthquake loading, consider the CBF in Fig. 1.3(a) subjected to lateral force (P).

(a)   (b)

(c)
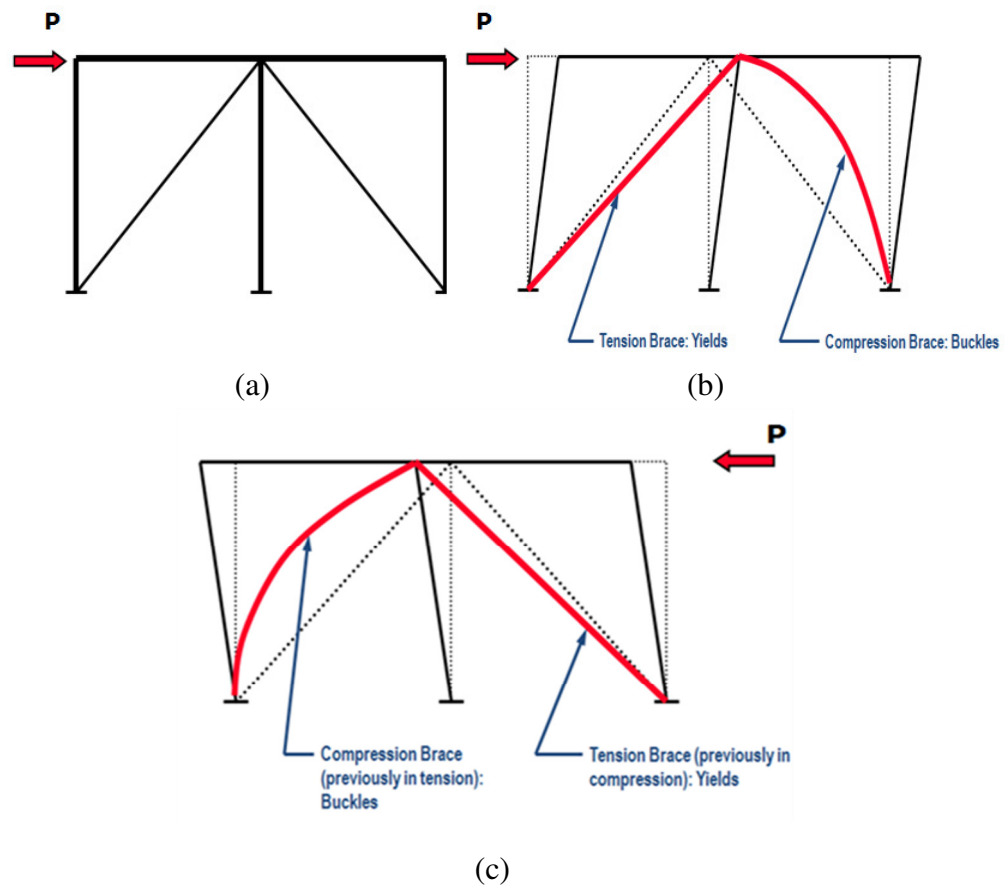
Figure 1.3: Basic Response of CBFs to Lateral Loading (Engelhardt, 2007)

This load will induce a tensile axial force in the left bracing diagonal and a compressive axial force in the right bracing diagonal as shown in Fig. 1.3(b). Ultimately, the tension brace will respond in a yielding ductile behavior whereas the compression brace will buckle in a non-ductile manner. Meanwhile, columns and beams remain essentially elastic. The inelastic response of both bracing elements will be reversed once the applied load reverses its direction to (-P) as depicted by Fig. 1.3(c). The inelastic cyclic response of a CBF under cyclic loading is dependent upon several factors including the following (Bruneau et al., 2011):

- The slenderness and compactness of the bracing members.

- The relative axial strength of the brace in compression and tension .

- The strength of the brace connections to the beams and columns.

- The degree of lateral restraint provided to the brace-to-beam connection.

- The stiffness, strength, and compactness of the beam (or column) into which the brace frames.

The basic inelastic response of a bracing element subjected to reverse cyclic axial loading is shown in Fig. 1.4.
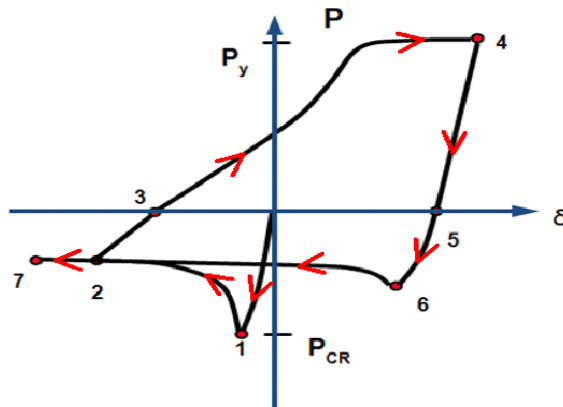
Figure 1.4: Hysteresis Loop of an Axially Loaded Element (Engelhardt, 2007)

The brace is assumed to be carrying an axial load (P) that causes axial deformation (δ). Meanwhile, the mid-length transverse displacement is noted (Δ) as shown in Fig. 1.5.
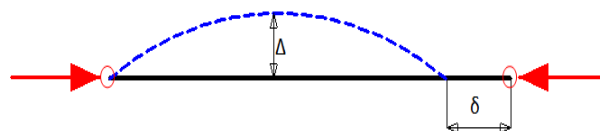
Figure 1.5: Axial (δ) and Transverse (Δ) Deformation of a Typical Bracing Element (Engelhardt, 2007)

The major points identifying the basic hysteresis loop are explained herein (Engelhardt, 2007):

1. Brace loaded in compression to peak compression buckling capacity (P_{cr}).

2. Continue loading in compression. Compressive resistance drops rapidly. Flexural plastic hinge forms at mid-length (due to P-Δ moment in member).

3. Remove load from member (P=0). Member has permanent out-of-plane deformation.

4. Brace loaded in tension to yield.

5. Remove load from member (P=0). Member still has permanent out-of-plane deformation.

6. Brace loaded in compression to peak compression buckling capacity (P_{cr}). Peak compression capacity is reduced from previous cycle due to the fact that the beginning of the second cycle, the brace undergoes mid-length plastic kink that results at the end of the first cycle. This magnifies the (P-Δ) moment in the brace and reduces its axial compressive load carrying capacity.

7. Continue loading in compression. Flexural plastic hinge forms at mid-length (due to P-Δ moment in member).

Most of Abu Dhabi buildings built in the eighties and start of nineties were not designed specifically as seismic resistant structures. Thus, in order to assess the actual condition of these buildings and their capabilities to withstand lateral forces, performance based studies should be conducted on these existing buildings. This could be attained by applying the pushover analysis technique to the existing lateral system to provide preliminary evaluation of the structural performance limit states as per FEMA P-750 (2009) and FEMA 356 (2000). According to the pushover analysis

results, structure will be safe or a retrofitting action should be implemented like incorporating steel braces at storeys or adding full braced frames at elevations (if architecturally permissible). For offices, governmental and industrial buildings ranging from six- to fifteen-storey, concentrically steel braced frames provide an economical alternative compared to steel moment resisting frames, which yield bigger sections for beams and columns. The economy of CBFs arises also from the inexpensive, nominally pinned connections between beams, columns and bracing elements (Sabelli et al., 2013).

1.2 Study Objectives

The main objective of this thesis is to investigate the efficiency of utilizing CBF systems in resisting seismic loads that are expected to act on multistorey buildings in Abu Dhabi, UAE. This is achieved by pursuing the following objectives:

1) Review available data related to seismic performance of multi-storey steel buildings with braced frames as the main lateral load resisting system.

2) Evaluate seismic loads and design of model buildings with different heights. All buildings are equipped with CBF systems to provide resistance to the seismic loads.

3) Assess the overall lateral capacity of modelled multi-storey buildings and the associated sequence of formation of plastic hinges using inelastic pushover analysis technique.

4) Use time history analysis approach to assess the local and global seismic performance of braced frame structures under various earthquake records representing the potential seismic loading scenarios.

5) Evaluate the adequacy of using inelastic pushover analysis as a simplified means to examine the seismic integrity of braced frame structures and to predict the sequence of development of plastic hinges within the system until an overall failure mechanism is formed.

1.3 Thesis Organization

The work conducted in this thesis to address the above-mentioned objectives is reported in six chapters. Detailed information on the contents of each chapter is provided herein.

Chapter 1 provides a general overview about concentrically steel braced frames, braces configuration, behavior and efficiency. The chapter proceeds by discussing the current research problem statement, the objectives of conducting the study and the thesis organization.

Chapter 2 introduces the conducted literature review of previously published research work related to the performance of CBFs from global behavior perspective. The literature survey is also extended to review the performance of CBFs at the local behavior level as well.

Chapter 3 is about modeling and design of reference buildings with concentric braced frame (CBF) system. It presents the selected building type and the different heights considered (six-, nine- and fifteen-storey). It also discusses the design criteria and demonstrates the detailed design procedure of the reference CBFs considered in the current study.

Chapter 4 discusses the static pushover analysis of the chosen CBFs. It introduces the employed software to conduct the pushover analysis, the modeling

concept of braces, the specified levels of structural performance along with the corresponding failure mechanism. The chapter presents the validation of the developed finite element model followed by exploring the failure sequence of structural members corresponding to a specific performance level. Finally, analyzed systems overstrength and ductility are evaluated and discussed.

Chapter 5 discusses time history analysis of Special Concentrically Braced Frames (SCBFs) under the effect of eight ground motion records scaled to represent the expected level of seismicity in Abu Dhabi. It shows the response of three different heights of SCBFs to the eight scaled ground motion records. The damage sequence of structural members and a comparison between pushover analysis predictions and time history analysis results and inter-storey drift patterns are introduced in chapter 5.

At the end of the thesis, chapter 6 presents conclusions regarding the effectiveness of using SCBF with six-, nine- and fifteen-storey as seismic lateral system in Abu Dhabi City. It also provides conclusions regarding the capability of pushover technique as compared to time history analysis to assess the seismic behavior of CBFs. The chapter provides recommendations for future research work based on the findings of this study.

Chapter 2: Literature Review

2.1 Introduction

Performance of concentrically steel braced frames (CBFs) was the subject of several studies since seventies of the last century. The focus on studying CBFs is increasing especially for the special concentrically braced frames (SCBFs) as they have the strength and stiffness needed to assure economy and serviceability during small, frequent earthquakes. Larger, more infrequent earthquakes invoke the nonlinear lateral response of SCBFs, which is dominated by tensile yielding and post buckling behavior of the braces. This inelastic deformation is intended to assure life safety and collapse prevention during these seismic events (Yoo et al., 2008a). In the last decade, some of the performance studies focused on the local behavior such as fracture in steel braces, while others focused on the global behavior of CBFs by assessing response modification factor (R), ductility factor (μ), overstrength factor (Ω_o), damage index and residual drifts.

This chapter reviews the experimental and analytical studies that were conducted in an attempt to investigate the behavior of the CBFs under seismic loading. The discussion is presented in several sections beginning with a brief description of the conducted studies and area of focus. This is followed by detailed presentation of the conducted researches on global and local performance of CBFs. Finally, a conclusion will introduce the necessity of conducting the current thesis.

2.2 Performance of Concentrically Braced Frames (CBFs) from Global Behavior Perspective

Concentrically braced frames (CBFs) are commonly used as lateral-load resisting systems in mid- and high-rise buildings. SCBFs are currently used in regions of high seismicity (Johnson et al., 2014). In recent years, typical steel construction in regions of high seismic risk has shifted from moment-resisting frames to CBFs. As a result of the increased popularity of braced frames, a series of experimental and analytical studies were initiated by many researchers over the last decade to investigate the poor performance of some conventionally braced frames in past earthquakes, and the limited experimental data available on the inelastic response and the failure characteristics of braced-frame systems (Uriz and Mahin, 2008).

Wakabayashi et al. (1974) conducted an experimental and theoretical study on the inelastic behavior of full-scale steel frames with and without bracings. Eight experiments were performed on large-scale portal frame models with different dimensions and loading conditions. The storey height and the span of test frames were approximately equal to those of actual building frames. Horizontal load was monotonically applied on the first four frames and alternatingly repeated on the other four; two of each with the vertical load acting constantly. It was concluded from the experimental and theoretical investigations on frames subjected to the simultaneous effect of constant vertical load and monotonic or repeated horizontal load that the existence of vertical load significantly affected the hysteresis behavior of unbraced frames. Meanwhile, the hysteresis loops of the braced frames were reversed S shaped and hardly affected by the vertical load. Load carrying capacity of unbraced frames

under combined constant vertical load and repeated horizontal load was increased in every loading cycle. This took place when extensive yielding occurred in the column cross section due to the strain-hardening phenomenon caused by the accumulated compressive strain in the section. In the case of braced frames, as well as unbraced frames without vertical load, such a phenomenon was not observed. Local buckling alone did not disturb the stability of restoring force characteristics. Under repeated horizontal load, lateral buckling was induced due to the decrease in rigidity caused by excess deformation in the locally buckled portion and the resulting restoring force characteristics showed deterioration. Experimental behavior of unbraced frames was well predicted by the theoretical analysis described in this research. This conclusion implies that experimental behavior of braced frames can be adequately predicted by the theoretical assessment that combines load-displacement relationship of unbraced frame with that of bracing system with both of them being obtained based on the plastic hinge method.

Moghaddam et al. (2005) presented a methodology for optimization of the dynamic response of concentrically braced steel frames subjected to seismic excitation based on the concept of uniform distribution of deformation. In order to obtain the optimum distribution of structural properties, an iterative optimization procedure has been adopted in which the structural properties are modified so that inefficient material is gradually shifted from strong to weak areas of the structure. This process is continued until a state of uniform deformation is achieved. For this purpose, three steel concentric braced frames with five, ten and fifteen storeys have been selected. An arbitrary lateral load pattern, such as that of UBC (1997), was chosen and used for design of the frames. For static and nonlinear dynamic analysis,

computer program Drain-2DX was used to predict the frame responses. Four strong ground motion records with PGA that ranges from 0.44g to 0.66g were used to evaluate and compare the seismic performance of the frames. In this study, the shear-building model was modified by introducing supplementary springs to account for flexural displacements in addition to shear displacements. A nonlinear time history analysis under the design earthquake was carried out for the modified shear-building model. By using a modified shear-building model, an optimization procedure can be conducted on simple nonlinear spring elements without a need to perform any nonlinear dynamic analysis on a full frame models. Results from two proposed methods were compared with UBC 97 design for the fifteen-storey braced frame subjected to the Northridge earthquake 1994. The cumulative damage was calculated for both optimum and conventional models in different earthquakes. It was concluded that optimum structures suffer less damage as compared with conventional structures.

Moghaddam and Hajirasouliha (2006) investigated the potential of the pushover analysis to estimate the seismic deformation demands of concentrically braced steel frames. Reliability of the pushover analysis has been verified by conducting nonlinear dynamic analysis on five-, ten-, and fifteen-storey frames subjected to 15 synthetic earthquake records representing a design spectrum. It was shown that pushover analysis with predetermined lateral load pattern provides questionable estimates of inter-storey drift. To overcome this inadequacy, the same simplified analytical model for seismic response prediction of CBFs introduced in Moghaddam et al. (2005) was proposed. In this approach, a multistorey frame is reduced to an equivalent shear-building model while performing a pushover analysis.

A conventional shear-building model has been modified by introducing supplementary springs to account for flexural displacements in addition to shear displacements. It was shown that modified shear-building models have a better estimation of the nonlinear dynamic response of real framed structures compared to nonlinear static procedures. Evaluating the deformation demands using modified shear-building models was demonstrated to be about the same as using the corresponding full-frame models, which are significantly more time-consuming to analyze.

Broderick et al. (2008) conducted a research on earthquake testing and response analysis of concentrically braced sub-frames. The experimental response of three single-storey braced frames measured in shake table tests was compared with the results of two different types of inelastic response analyses: time-history analysis and pushover analysis. The nonlinear finite element analysis program ADAPTIC that accounts for material and geometric nonlinearities was used to conduct the pushover analysis. A strain-hardening bilinear stress–strain material law was selected for the analysis carried out in this investigation. The comparison of experimental and analytical results implied that the use of inelastic fiber elements with a bilinear material relationship to represent the behavior of bracing members leads to accurate modelling of earthquake response. However, in one of the three tests, good agreement was only observed for the first half of the test, after which the cumulative effect of local buckling and possible modelling idealizations led to a discrepancy between the experimental and analytical results. Similar levels of agreement were observed at the member level by examining the variation in brace axial force throughout the test. The results illustrated that the design approach adopted in

European provisions whereby the lateral frame resistance is only based on the tension diagonals provides a reasonable representation of the behavior within practical ranges of brace slenderness. However, in terms of satisfying the objectives of capacity design, it is important that additional checks be considered to account for possible adverse effects caused by the contribution of the braces in compression.

An Experimental evaluation of the seismic performance of modular steel-braced frames was carried out by Annan (2008) where the hysteretic characteristics of modular steel-braced frames (MSB) under reversed cyclic loading were evaluated. The design and construction of the test specimen accounted for the unique detailing requirements of these frames. A regular concentrically braced frame with similar physical characteristics was also tested for comparison. Both test specimens consisted of a one-storey X-braced system with tubular brace cross-section that were designed in accordance with the Canadian standard CSA-S16.1 (2001). The test specimens were subjected to symmetric reversed-cyclic loading histories to characterize their performance. Analytical prediction of the behavior of each frame specimen was carried out to develop suitable loading history, evaluate need for instrumentation and to avoid unexpected behavior during testing. Two-dimensional models were developed using the nonlinear computer program, SeismoStruct (2012). A bilinear material model for steel was employed, with a kinematic strain-hardening parameter of 2%. Inelastic beam-column frame element was used to represent the behavior of all frame members. Both the MSB- and regular-braced specimens showed stable and ductile behavior up to very high drift levels. The MSB specimen reached a ductility of 10 at 3.5% drift and the regular specimen reached a ductility of nine at 3.1% drift at a load level equal to the load capacity of the actuator. The

regular specimen further sustained 20 more cycles at 3.05% drift before the test was terminated. For the regular specimen, the first sign of nonlinearity occurred as a result of buckling in a brace member while in the MSB specimen, flexural response due to column yielding caused the initial nonlinearity. The regular-braced specimen was found to be slightly superior in terms of lateral stiffness at low ductility (below 2) and at high ductility (above 6). Between these ductility levels, both frame specimens showed similar stiffness levels. For both specimens, initial stiffness degraded by about 45% at a ductility level of six. Within each load step in the regular-braced specimen, there was no significant strength and stiffness degradation with cycling. The MSB specimen also showed no significant stiffness degradation but only slight reduction (less than 10% at 3.5% drift) in strength with cycling beyond a 2.1% drift. For the MSB specimen, the test was terminated after a high level of ductility was reached. The brace members in this specimen did not suffer severe deformation. For the regular-braced specimen, the test was terminated after several inelastic cycles at sufficiently high ductility level. Prior to this point, a lower half side of a brace member experienced severe out-of plane buckling at its mid-section. Both specimens dissipated significant and similar amount of cumulative energies.

In 2010, Hajirasouliha and Doostana (2010) investigated again the proposed simplified shear-building model for seismic response prediction of CBFs. The adequacy of the modified model has been verified by conducting non-linear dynamic analysis on five-, ten-, and fifteen-storey CBFs subjected to fifteen synthetic earthquake records representing a design spectrum as per UBC 97 (1997). It was shown that the proposed simplified shear-building models provide a better estimate

of the non-linear dynamic response of the original framed structures, as compared to the conventional models. While simplifying the analysis of CBFs to a large extent, and thus reducing the computational efforts significantly. The study showed that conventional shear-building models provide accurate estimates of maximum roof and storey displacements of CBFs, but are not able to provide good estimates of inter-storey drifts. While the maximum errors in the estimation of maximum roof and storey displacements are usually less than 15%, they are particularly large for the maximum drift at top storeys where the estimated drift could be more than 40% higher than the actual value. It was shown also that the accuracy of modified shear-building models to predict storey displacements and peak inter-storey drifts is significantly higher than conventional models. Finally, it was shown that the modified shear-building model is not sensitive to the ground motion intensity and maximum storey ductility and, therefore, could be utilized to estimate the seismic response of CBFs from elastic to highly inelastic range of behavior. The results indicate that the proposed modified model is also capable to estimate the global damage experienced by the CBFs from low (less than 20%) to high (more than 70%) level of damage intensity.

Mahmoudi and Zaree (2010) carried out a study about the evaluation of response modification factors of concentrically braced steel frames. 30 conventional CBFs and 20 buckling restrained braced frames (BRBFs) with three, five, seven, ten and twelve storeys as well as a bay of 5m long were selected. For conventional CBFs, three different bracing types (X, chevron V and chevron-inverted V) and for BRBFs two bracing types (chevron V and chevron-inverted V) were considered. To evaluate behavioral factors, nonlinear static (pushover) analysis was performed by

subjecting the structure to monotonically increasing lateral forces with an invariant height-wise distribution using SNAP-2DX program. The analysis was conducted using life safety structural performance level as well as the nonlinear behavior of braces as suggested by FEMA 356 (2000). It was observed that the overstrength and response modification factors of CBFs and BRBFs decrease with an increase in the height of buildings. However, the reduction factors due to ductility of CBFs and BRBFs are different. In addition, the overstrength and response modification factors increase with the increase in the number of bracing bays. Code's seismic provisions for brace member design have a profound effect on the conventional CBFs overstrength factors. These cause overstrength to have higher values while ductility decreases because of the deterioration in strength and degradation of stiffness due to buckling in cyclic loading.

In BRBFs, because of the brace energy dissipating capacity in tension and compression, the maximum roof displacement, and reduction factors due to ductility have higher values that cause these parameters to have considerable effect on the response modification factor. The overstrength factors for CBFs in type V, inverted V and X with single bracing bay were evaluated as 2.90, 3.75 and 3.10 and for double bracing bays as 3.80, 4.80 and 4.20, respectively. The overstrength factors for different types of BRBFs with single and double bracing bay were 1.90 and 2.40, respectively. The type of brace configuration in BRBFs has no effect on overstrength factors. The obtained reduction factors due to ductility for different types of CBFs with single and double bracing bays were 1.35 whereas it varied between 4.7 and 8.0 for BRBFs. The response modification factors for CBFs in type V, inverted V and X with single bracing bay were evaluated as 4.10, 5.10 and 4.80 and for double bracing

bays as 5.00, 6.25 and 6.10, respectively. Meanwhile, the obtained response modification factors for different type of BRBFs with single bracing bay varied between 7 and 16 and for double bracing bays between 8 and 22.

In 2012, Brandonisio et al. (2012) investigated the seismic design of concentric braced frames. In this research, it was mentioned that capacity design procedure aims to obtain a ductile and dissipative ultimate behavior by imposing that the yielding of diagonal members occurs before the damage and premature failure of beams, columns and connections. This approach, involving overstrength requirements and diagonal slenderness limitations, strongly affects the design of CBFs and generally leads to oversized structural members. The proposed approach by the authors in this research consists of some modifications to the current design provisions of the European seismic codes, with the major aim of controlling the overstrength requirements to the non-dissipative members of braced frames, thus reducing the associated structural weight premium while preserving a satisfactory inelastic behavior. For this purpose, three, six and nine-storey buildings, characterized by the same floor plan (18×54 m) were considered (X-braces, one bay). For each building height, two structural layouts, with columns respectively spaced at 9m (M9) and 6m (M6), were considered. Considering the different number of storeys, six basic building cases have been examined: 3-storey-9×9m grid (3St.M9), 6 storey-9×9m grid (6St.M9), 9-storey-9×9m grid (9St.M9), 3-storey-6×6m grid (3St.M6), 6-storey-6×6m grid (6St.M6), 9-storey-6×6m grid (9St.M6). The buildings are located in high seismic zone (PGA=0.35g), on a soil type B. Pushover analyses using SAP2000 (2009), have been performed on the single braced frames designed according to the different approaches considered in this paper. The application of

elastic, Eurocode 8 (EC8, 2005) and the proposed approach design procedures to 30 case studies has shown that the proposed approach appears as a more flexible tool for designing ductile CBFs than the EC8 approach; in particular it allows for tuning the structural solutions and for obtaining a more uniform distribution of overstrength with less structural weight than the EC8 (2005). The results of non-linear static analyses presented in the paper have underlined the ability of the proposed approach to obtain CBFs characterized by a satisfactory non-linear behavior in terms of ductility and number of yielded diagonals without introducing the excessive overstrength requirements emerged by applying the procedure proposed by the EC8 (2005). However, the authors recognize that the performance of the structural solutions designed according to the proposed approach needs to be assessed through non-linear time history analyses and future research is being planned in this direction towards this goal. In fact, it has to be pointed out that the possibility of the proposed approach of selecting the number of diagonals to be involved in the dissipative mechanism of the braced frame can lead to high plastic demand (level of damage in the braced frame) and to potential damage concentrations (soft-storey mechanism).

In 2012, a study on seismic behavior of dual steel concentric braced frames was conducted by D'Aniello et al. (2012). It was mentioned in the study that according to capacity design principles the non-dissipative zones should behave elastically. This implies that these elements are subjected to high strength demand. Therefore, it is rational and convenient to design steel frames with the combined use of high strength steel for non-dissipative elements and the mild steel for those dissipative. Such a structure is termed dual-steel structure. The analyzed CBFs are extracted from a reference building of eight and sixteen storeys. The eight storeys

braced frames were studied for span of 5m and 7.5m, meanwhile, the sixteen-storey ones were studied for 7.5m span. The examined frames were designed according to EC8 (2005). Two different soil conditions were examined: soil type C and soft soil. The design PGA=0.32g, which is typical of Bucharest (Romania). SeismoStruct (2012) was used for the analytical computations. Static (Pushover Analysis) and dynamic (Incremental Dynamic Analysis, IDA's) nonlinear analyses were carried out to identify the collapse modes and deformation demands. It was observed that the average overstrength factor for eight storey frames is equal to 1.28, while for sixteen storey frames is 1.05. IDAs showed that soft soil conditions experienced inter-storey drift ratio demands larger than those for stiff soil by comparing pushover curves to IDAs, it was observed that IDA maximum base shear-to-maximum roof displacement curves are closely bounded by the capacity curves. It is worth mentioning that all frames exhibited a lateral capacity at least 2 times the design base shear value. Residual inter-storey drift ratios were always smaller than 0.3%, thus being compatible with easy repairing of the frames after earthquake. The behavior factors obtained in this study were calculated based on the conservative assumption that failure criteria were the local collapse of members.

2.3 Performance of Concentrically braced frames (CBFs) from Local Behavior Perspective

Wakabayashi et al. (1977) conducted an experimental study on the elastic-plastic behavior of braced frames under repeated horizontal loading. Braces with an H-shaped cross section are tested in a single or a doubled bracings system. The effects of the slenderness ratio, the buckling plane and the local buckling were investigated. Furthermore, the fundamental properties of a brace for the formulation of the hysteretic characteristics under repeated loading were extracted. Twelve

specimens were subjected to monotonic load and twelve specimens were subjected to cyclic load. It was shown that the effective slenderness ratio for buckling could be estimated by the use of the slope-deflection method, taking into account the secondary effect of axial force. According to the result of calculation, when bracing members are rigidly connected to a surrounding frame with relatively rigid members, the effective length of a single brace is a half of the bar length. It is about 0.6 times of the bar length for a double brace which buckles in the plane of a frame, and it is about a 7 times of the bar length for a double brace which buckles out of the plane of a frame. The effective slenderness ratio used in this test is about 40-120 for the single brace, and about 22-84 for the double brace. The hysteretic characteristics of braces deteriorate even if the slenderness ratio is as small as 22. A certain amount of the compressive load carrying capacity can be expected even if the slenderness ratio is as large as 120. Though the load carrying capacity is not changed very much by the occurrence of local buckling, local buckling is significant in the sense that it induces cracks and breakage of the member. The effect of width-thickness ratio on the breakage remains to be investigated in the future. Though the boundary condition of a single brace is not simple i. e., a single brace is subjected to the compulsory end deformation due to the storey drift of a surrounding frame, a single brace is substituted for simply supported bar whose length equals the effective length. The effective length for the behavior under repeated loading and for buckling is identical. The effective slenderness ratio of a double brace for the behavior under repeated loading is regarded to be essentially different from the one for buckling. Braces with a small slenderness ratio may buckle about the strong axis of a cross section unexpectedly. Their behavior under repeated loading is stable, and their load carrying capacity and energy absorbing capacity are larger than that of braces which have

identical length and which buckle about a weak axis originally. However, after several cycles of loading, they come to deflect about the weak axis of a cross section, and they behave as if they would have buckled about a weak axis originally.

Yoo et al. (2009) investigated the analytical and experimental performance of special CBFs. A numerical investigation on the behavior of multi-storey X-braced frames and gusset plate connections was conducted using the inelastic finite element program ANSYS. The design of this frame closely simulated the size and geometry of single-storey, single-bay diagonally braced frames, tested and analyzed in previous research studies by Lehman et al. (2008) and Yoo et al. (2008b). The previous study by Yoo et al. (2008b) used the equivalent plastic strain to estimate weld crack initiation and brace fracture. This estimate was found to be accurate and consistent when the equivalent plastic strains are calibrated to experimental results. As such, the numerical model results presented by this study employed these methods to consider both the yield mechanisms and failure modes of the braced frames. A series of simulations to investigate the impact of different gusset plate connection design parameters on connection and system performance were performed. The parametric study included evaluation of the sizes of framing elements, elliptical and linear 8tp (8 times the gusset plate thickness) clearance model for mid-span gusset plates, weld length joining the brace to the gusset plate connection, out-of-plane constraints on top and bottom beam flanges, loading pattern, and frame configuration. This parametric study concluded that frames with intermediate member sizes provided the best performance. Very light members sustained high inelastic stress and strain demands on the middle beam and mid-span gusset plates, while heavy framing members reduced inelastic stress and strain

demands on the middle beam but retained demands on mid-span gusset plates. The 8tp linear clearance for the mid-span gusset plates provided improved performance relative to the 8tp elliptical clearance, which provides the best performance for the corner gusset plates. The 8tp linear clearance model resulted in smaller more compact gusset plates, and reduced potential for premature gusset plate buckling. The concentration of inelastic deformation at a single storey is a major concern for braced frames. Although concentration of damage was noted in this analytical study, it was much less severe than noted in previous research on alternative multi-storey braced frame configurations. This reduction in damage concentration is beneficial, and it is partly due to the characteristics of the multi-storey X-braced system. The study suggests that the multi-storey, X-braced configuration has the potential to decrease the tendency for concentrating inelastic action into a single storey and is a promising solution for seismic design.

In 2009, Fell et al. (2009) carried out an experimental investigation of inelastic cyclic buckling and fracture of steel braces. Eighteen large-scale tests of steel bracing members were tested under cycling loading to examine their inelastic buckling and fracture behavior as related to the seismic design of CBFs. The brace specimens included square hollow structural shapes HSS, pipe, and wide-flange sections. The effect of various parameters, including width thickness and slenderness ratios, cross-section shape, loading history and loading rate on the performance of these braces was investigated. Among these parameters, loading history, width thickness ratio and slenderness ratio were shown to have the largest influence on brace ductility. Qualitatively, the tests all followed a similar sequence of events leading to failure. It was observed that global buckling of the brace at displacements

corresponding to 0.2–0.4% storey drift leads to the formation of a plastic hinge at the midpoint of the brace. Subsequently, local buckling takes place in the hinge region at 2–5% storey drift that amplify the strains and trigger fracture initiation at 2–8% storey drift. Soon after this, the fracture propagates through the entire cross section, severing the brace. One of the main conclusions of this study is that brace fracture ductility is primarily a function of section compactness and to a lesser extent member slenderness and loading history. Specifically, fracture ductility increases with more compact cross sections and more slender members. Furthermore, the standard loading protocols modeled to represent general or far-field ground motions are more damaging than loading protocols developed to represent pulse-like near-field ground motions. The tests further demonstrated that the local buckling in HSS sections results in more severe straining of the steel material, leading to fracture initiation near the corners of the brace. This is in contrast to pipe and wide-flange sections that exhibit more gradual local buckling modes that delay fracture initiation. The tests suggest that the section width–thickness ratios in the ANSI/AISC 341-10 Seismic Provisions (2010) for HSS and pipe sections may not result in adequate deformation capacities for seismic design. HSS members with width–thickness ratios equal to about 90% of the limiting compactness criteria, and subjected to the general loading protocol, fractured at drift ratios in the range of 2.7–3.0%. Pipe members with diameter-to-thickness ratios equal to 60% of the limit fracture at drift ratios of 2.7%. Although the drifts achieved by these members are larger than the approximate design level drift of 2%, they are smaller relative to the 4% drift demand criteria implied by several previous investigations and current design requirements. On the other hand, W-shape braces, which slightly violated the compactness criteria, sustained drift ratios of up to 5%. These results are sensitive to loading history, as the

endurance for all of the braces increased considerably up to two or three times when subjected to the near-fault loading protocol that subjected the braces to fewer reverse loading cycles. Tests to investigate the effect of loading rate on fracture performance demonstrated essentially no difference in response between quasi-static and earthquake loading rates. Comparison of measured and calculated strengths for brace strength and stiffness generally confirm expectations and the legitimacy of standard assumptions. In particular, ratios of measured compressive buckling strengths to calculated strengths using the standard AISC column curve equation and expected yield strengths with R_y factors specified by AISC have a mean value of 1.23 and a standard deviation of 0.25. Ratios of measured tensile strengths are estimated fairly well by the average of the expected yield and ultimate brace strengths calculated using R_yF_y and R_tF_u values specified by AISC with a mean value of 1.01 and a standard deviation of 0.08.

In 2012, Hsiao et al. proposed an improved analytical model for SCBFs that accounts for the requirements of Performance Based Seismic Design (PBSD). In this study, thirty single-storey closed frame specimens were tested at University of Washington under the effect of axial load and reversed lateral loading. Three 2-storey and three 3-storey SCBFs were tested at the National Center for Research on Earthquake Engineering (NCREE) Laboratory in Taiwan. These frames included composite floor slabs with realistic test boundary conditions. The frames were subjected to reversed cyclic lateral loading at the top storey only; axial loading was not simulated. Several variations of connection design and brace type were tested. Experimental data was used for development, calibration and verification of the proposed model. Models of the concentrically braced frame were developed in

OpenSees framework in which simplified discrete component models including nonlinear beam–column elements and concentrated springs are used. The novel aspect was the model for the gusset plate connection, which included rotational springs. All models provided good but similar variability in accuracy in predicting stiffness and tensile resistance. Relative to the proposed approach, the conventional modeling approaches reduced the accuracy of the compressive response predictions. The fixed-end brace model significantly overestimated the compressive resistance of the brace and the deterioration of resistance in post-buckling deformation. The pinned end brace models significantly underestimated the compressive resistance of the brace. The proposed improved model provided an accurate estimate of compressive capacity of the brace and post buckling deformation. The proposed improved model resulted in consistently accurate and reliable predictions at both of the global and local response levels. The results reveal the importance of considering accurate modeling approach for the connection to achieve this level of accuracy.

2.4 Conclusions

As UAE started to be a leading country in the Middle East in the construction of mid- and high-rise buildings, steel systems became of such importance due to their lightweight, which generates smaller seismic forces and consequently an optimum use of construction material and achieving the required safety. After reviewing the various studies related to the performance of steel CBFs, it is evident that none of these studies focuses on the performance of CBFs in the UAE and specifically in Abu Dhabi. This lack of information provided a motivation to conduct the work reported in this thesis. As such, the current research focuses on investigating the

efficiency of using steel CBFs as the lateral load resisting system in mid and high-rise buildings constructed in Abu Dhabi.

Chapter 3: Modeling and Design of Reference Buildings with concentrically Braced Frame (CBF) System

3.1 Buildings Characteristics and Design Data

The study is carried out on a set of multi-storey office buildings that are assumed to be located in the city Abu Dhabi, UAE. The selected set includes three different buildings with six-, nine- and fifteen-storey height. All buildings have a typical storey height of 3.6 m (Fig.3.1), with the same floor plan dimensions of 38.7 m x 38.7 m, as shown in Fig.3.2. These reference buildings are selected to provide a representative sample of the dimensions and heights of office buildings that are commonly constructed in the study area. Structural loads are calculated in accordance with the ASCE7-10 (2010) standards and the requirements of the International Building Code (IBC, 2012). Design of the various structural elements is performed according to the regulations of the American Institute of Steel Construction for structural steel buildings (ANSI/AISC 360-10, 2010) and the corresponding seismic provisions (ANSI/AISC 341-10, 2010).
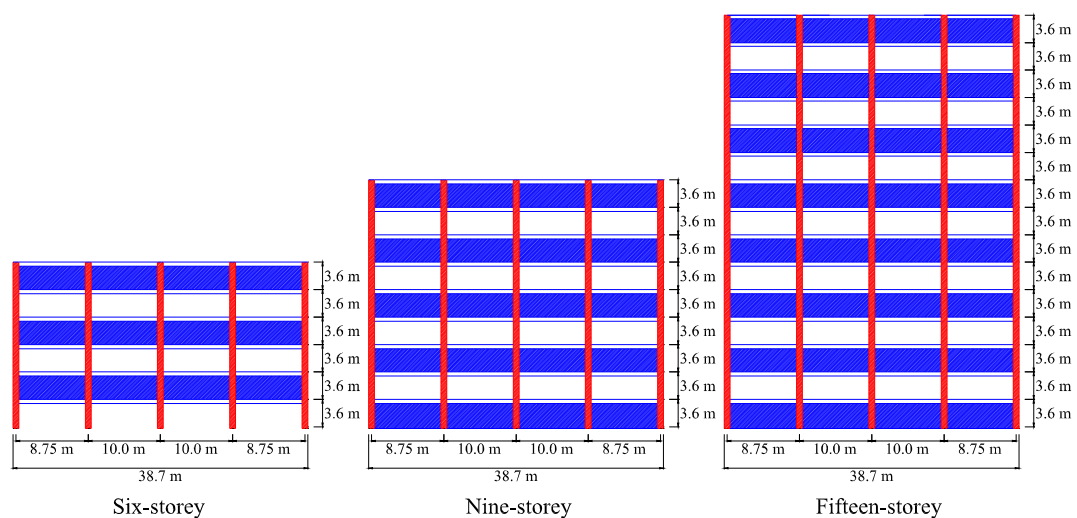
Figure 3.1: Considered Heights of Model Buildings
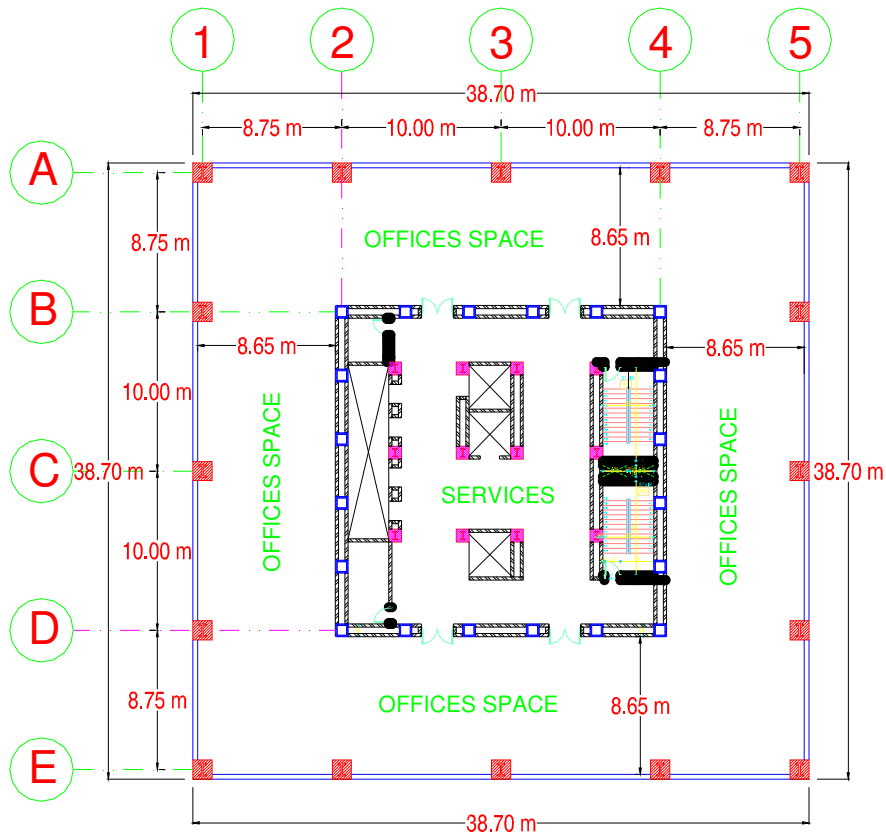
Figure 3.2: Typical Building Plan of Modeled Buildings (Six-, Nine- and Fifteen-Storey Buildings)

3.1.1 Structural System and Building Materials

The gravity loads resisting system consists of a composite floor system supported by encased composite columns in which I-shaped steel sections are embedded in the concrete as shown in Fig. 3.3(a). The composite floors are constructed using formed steel deck and are linked to the reinforced concrete slabs using shear connectors as shown in Fig. 3.3(b) (Kowalczyk et al., 1995).
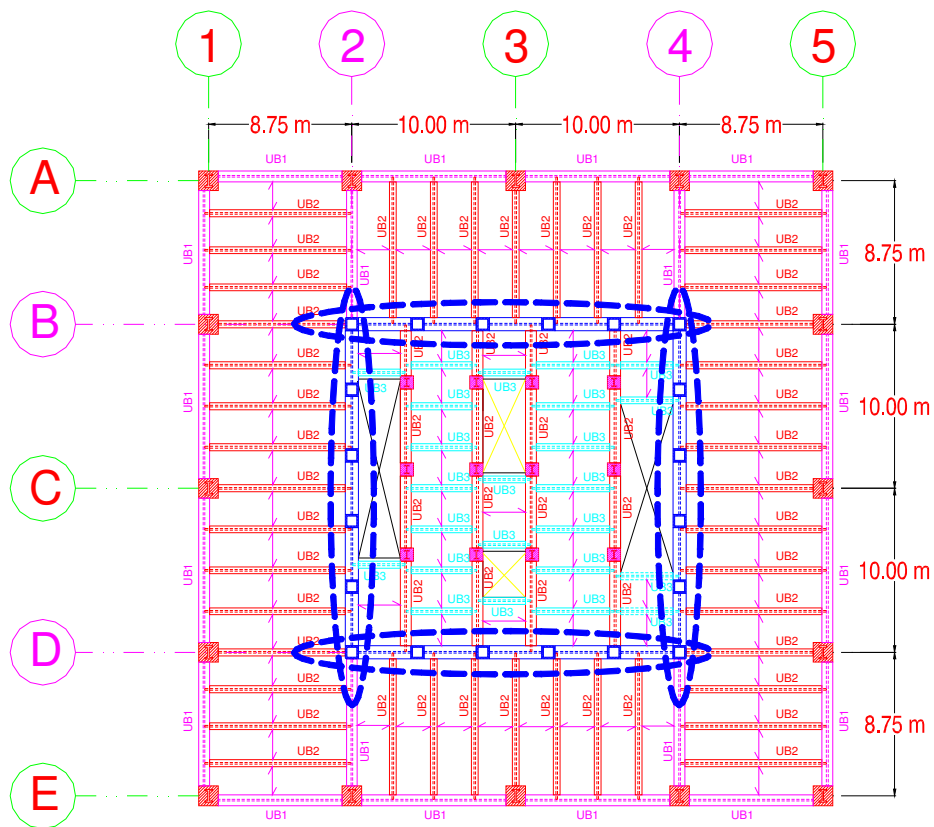
(a) Composite Floor Plan
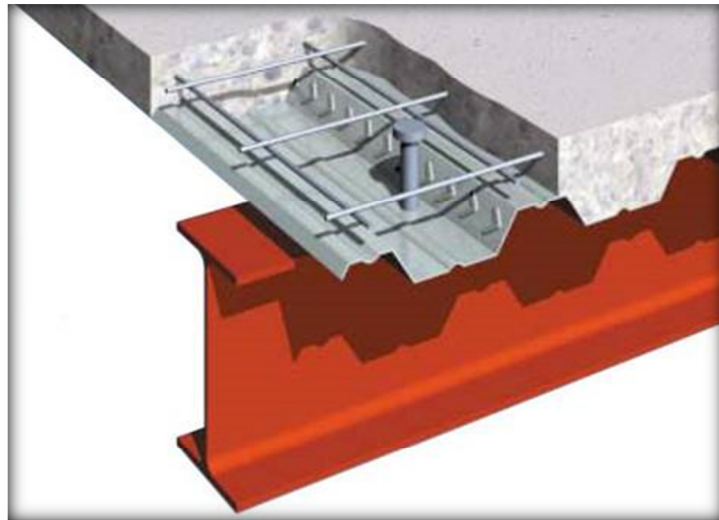
(b) 3-D Detailing of Composite Floor System (Tegral Comflo, 2014)

Figure 3.3: Composite Floor Details

The service areas in all analyzed building are enclosed by the building's core, in a 20 m x 20 m square tube structure where the lateral load resisting system is utilized to provide resistance in the two orthogonal directions. Such system includes four identical steel braced frames along axes 2, 4, B and D as presented in Fig. 3.3(a). The triangulation system is chosen as cross bracing to form Concentrically Braced Frames (CBFs) as shown in Fig.3.4 for all three buildings.
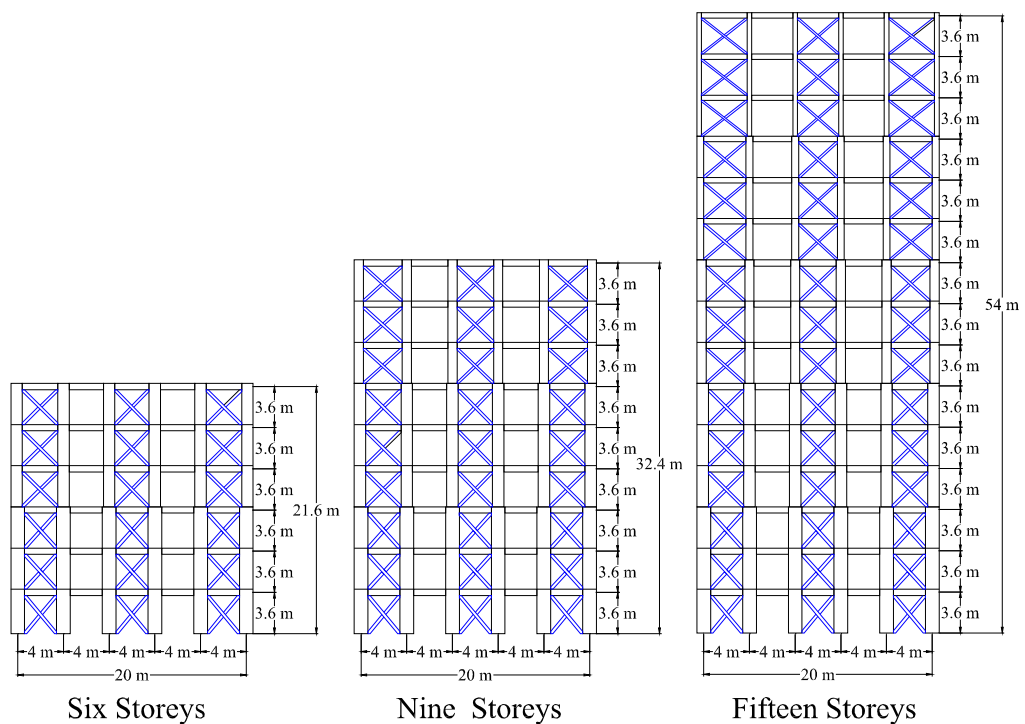
Figure 3.4: Steel CBFs (Three Heights Considered in this Study)

The selection of the braced bays avoids blocking the door ways leading to the office areas presented in Fig.3.2. In the design of the CBFs, steel tube sections are used for the columns, Universal Beam (UB) sections for the beams and circular Hollow Steel Sections (HSS) for the braces (diagonal members). An evaluation and verification for the selection of the seismic load resisting system will be presented in section 3.1.4 following the determination of the Seismic Design Category. For reinforced concrete elements, the unconfined compressive strength is taken as 40

MPa with the reinforcing steel yielding strength of 420 MPa. Meanwhile, structural steel sections are assumed to be made of A572-Gr 50 construction steel with yielding strength of 345 MPa and ultimate tensile stress of about 450 MPa (Salmon et al., 2009).

3.1.2 Gravity Loads

The considered buildings are designed to sustain dead, superimposed and live loads. Dead loads are considered from the weight of the elements constituting the flooring system. Each floor consists of a 0.11 kN/m^2 unit weight metal deck with 127 mm thick normal density concrete slab. This combination is equivalent to a uniform slab thickness of 132 mm leading to a dead load intensity of 3.3 kN/m^2. The superimposed dead load is assumed to originate from a 2.0 kN/m^2 floor finishing in addition to a 0.5 kN/m^2 as mechanical, electrical and plumbing fixtures (MEP) loads attached to the ceiling. Meanwhile, the live load for office use areas is taken as 2.4 kN/m^2 (ASCE7-10, 2010) in addition to 1.0 kN/m^2 to account for the weight of movable partitions. For corridors and stairs areas, a live load of 4.8 kN/m^2 is considered (ASCE7-10, 2010).

3.1.3 Wind Loads

Wind loads are calculated in accordance with ASCE7-10 (2010) standards based on a basic wind speed of 45 m/sec (100 Mph), as per Abu Dhabi common practice, along with wind directionality factor of 0.85, a topographical factor (K_{zt}) of 1, an occupancy category II and an importance factor of 1. An exposure Category C that represents open terrain with scattered obstructions with heights less than 30 ft. is adopted in wind calculations. An important wind load parameter is the Gust Factor G_f that accounts for dynamic amplification of loading in the along-wind direction

due to wind turbulence, flexibility of the building system and wind-structure interaction. For rigid lateral load resisting systems with natural frequency greater than 1.0 Hz, a minimum gust effect factor (G = 0.85) is employed (ASCE7-10, 2010), otherwise detailed calculations need to be carried out to account for estimated building frequency. For the six-storey buildings considered in this study, the natural frequencies exceeded 1.0 Hz and, therefore, a gust factor G = 0.85 is used. On the other hand, the nine- and fifteen storey buildings showed more flexible behavior with natural frequencies that are less than 1.0. For these buildings, the estimated gust factor ranged between 0.86 and 0.89.

3.1.4 Seismic Loads and Seismic Load Resisting System (SLRS) Verification

Seismic loads are estimated based on ASCE7-10 (2010) requirements and the most recent UAE seismic maps that are developed similar to those of the International Building Code (IBC, 2012). Estimation of the seismic forces necessitates the identification of the Seismic Design Category (SDC), based on which several important design-related decisions can be made, including (Fanella, 2012; Taranath, 2005):

- Permissible seismic force-resisting systems

- Limitations on building height.

- Consideration of structural irregularities.

- The required level of strength and detailing

In the current study, the structure is assigned a Seismic Importance Factor 1.0, an Occupancy Category II and a site class C (ASCE7-10, 2010). A mapped maximum

considered earthquake spectral response acceleration for short period; S_S, of 0.6g is identified based on UAE seismic maps for the city of Abu Dhabi. Similarly, the maximum considered earthquake spectral response acceleration for 1-second period, S_1, is found to be 0.19g. More detailed calculations are presented in Appendix A. Based on this information; the SDC is classified as C. It should be, however, noted that it is a borderline case that is very close to being at SDC D, which is more severe than SDC C. In the current study, SDC D will be also considered due to the following reasons:

1- The seismic classification of Abu Dhabi city is a borderline between SDC C and the more severe seismic category D.

2- The recent noticeable increase in seismic activity of the UAE.

Table 12.2-1 of ASCE7-10 (2010), indicates that for SDC C, Steel Ordinary Concentrically Braced Frames (OCBF) can be used as a seismic laod resisting system without height limitation. On the other hand, when considering the SDC D, the OCBF will be only permitted for a maximum height of 35 ft. (10.70 m) (ASCE7-10, 2010). Given that this height limit is shorter than all building heights considered in the current study, a Steel Special Concentrically Braced Frame (SCBF) is considered for SDC D.

The distribution of seismic forces along the height of the building is derived from the base shear (V), which is a function of the response modification factor (R). The response modification factor, R, reflects the redundancy of the structure and its ability to dissipate energy through inelastic action (Wight and Macgregor, 2011). As a result, every structural system has its own R-value that depends on its ductility (i.e.,

energy dissipation through inelastic action)**.** From Table 12.2-1 of ASCE7-10 (2010) standards, R = 3.25 for OCBF. Meanwhile for the SCBF, R = 6.0. Detailed discussion and comparison between the performances of each of these systems are presented in Chapter 4 of this study.

3.2 Modeling and Design of the Considered CBFs

Three buildings are considered in this study representing six-storey, nine-storey and fifteen-storey structures. As it was mentioned before, all buildings have the same overall plan dimensions and typical storey height of 3.6 m.

As a result of the symmetry in geometry and structural system (Fig. 3.3(a)), a two-dimensional CBF model was developed for each building. Given that the entire building is equipped with two CBFs, each CBF is considered to carry half the building weight. The Structural Analysis Software SAP2000 (2009) is used to model all the CBFs (Fig. 3.5). All elements are designed in accordance with the strength design requirements of the ANSI/AISC 360-10 (2010) for the imposed gravity, wind and seismic loads.

    (a) OCBFs SAP 2000 models   (b) SCBFs SAP 2000 models
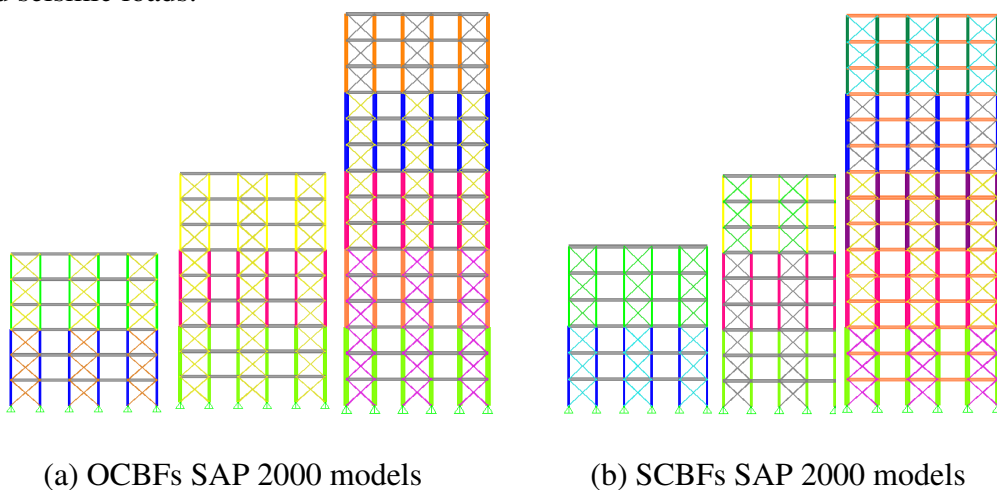
Figure 3.5: SAP2000 models for the six-, nine- and fifteen-storey CBFs

The elastic inter-storey drifts of the CBFs were multiplied by the deflection amplification factor C_d to allow for evaluation of the anticipated inelastic inter-storey drifts and then compared to inter-storey drift (ID) limits provided in Table 12.12-1 of ASCE7-10 (2010) standards:

$$ID \ limit = 0.02 \times h_{sx} \tag{3.1}$$

where

h_{sx} is the Storey height below level x

These limits were found to be fulfilled by the original design of all members constituting the six-storey CBFs. However, with increased height of buildings, the storey drift values increased considerably and originally designed section sizes were found insufficient to satisfy the code drift limits. As a result, brace and column sections in the nine-storey and fifteen-storey CBFs were enlarged to reduce the drift values within acceptable limits. This oversizing action is clearly reflected in the design-to-capacity (D/C) ratios reported later in Tables 3.5 and 3.6 where D/C ratios are much less than the optimum value of 1.0.

In general, seismic design codes adopt the philosophy that it is not economical to design a structure to remain elastic during strong earthquake and if an effort is made to ensure that the structure possesses ductility, the required base shear force can be significantly reduced. As a result, the elements requested to insure ductility to a structure should yield to dissipate energy while the supporting members of these ductile elements should remain elastic to prevent the structure from collapse. In other words, the supporting members of the ductile ones should be sized to withstand the full capacity load of the ductile ones, which is typically referred to as

capacity design. In the current study, brace elements, columns and beams constituting the lateral load resisting system (Fig. 3.5) are evaluated and resized, as necessary, to ensure fulfilling the ductility design requirements and capacity design procedures of the ANSI/AISC 341-10 (2010). Given the fact that such requirements differ for various lateral load-resisting systems, each structure is designed twice with the lateral load resisting system being an Ordinary Concentrically Braced Frame (OCBF) or Special Concentrically Braced Frame (SCBF).
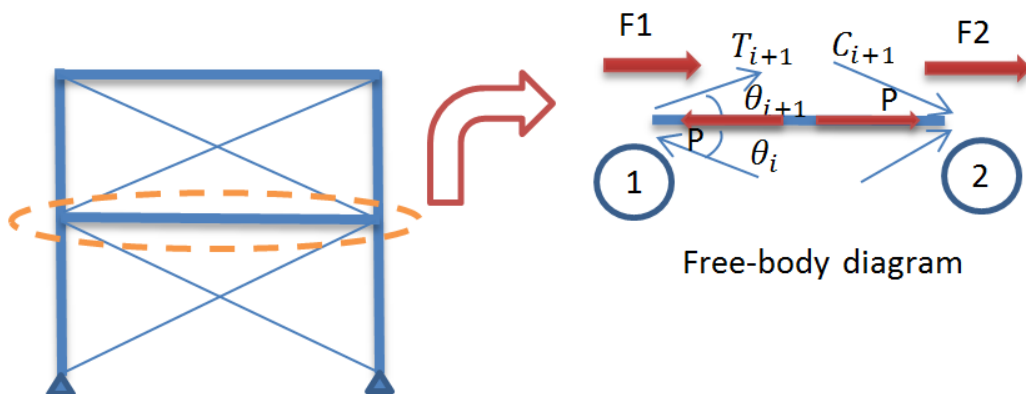
Figure 3.6: Free Body Diagram for Brace Forces in CBF Beam

3.2.1 Ductility and Capacity Design Requirements for OCBFs

From design standpoint, OCBF are not expected to be subject to large inelastic demands due to the relatively low response modification factor ($R=3.25$) assigned to the system as per ASCE7-10 (2010) provisions. From analysis point of view, due to the expected limited inelastic demands on OCBF, a strength design is considered sufficient. Ductility of CBF depends largely on buckling characteristics of brace elements characterized by overall buckling (slenderness ratio kl/r) and local buckling of the cross section elements (Bruneau et al., 2011). The Seismic Provisions for Structural Steel Buildings ANSI/AISC 341-10 (2010) indicates that braces of OCBF should conform to the moderately ductile members' requirements defined by

the limiting value $\lambda_m = 0.044(E/F_y)$. In the current study, all brace sections resulting from the strength design approach are found to satisfy the local buckling limitation stated above. Meanwhile, no special requirements are provided for columns and beams in OCBF. Results of strength and capacity design of the six-storey, nine-storey and fifteen-storey OCBFs are summarized in Tables 3.1, 3.2 and 3.3, respectively.

Table 3.1: Member Sections of Six-Storey OCBF

| Storey # | Strength design of **OCBF** (Six-storey building) | | |
	Element	Section	D/C Ratio
4 to 6	Beams	UB 406x140x46	**0.81**
	Braces	HSS 174.6.3x9.5	**0.92**
	Columns	Col 200x200x11	**0.89**
1 to 3	Beams	UB 406x140x46	**0.81**
	Braces	HSS 177x12.7	**0.90**
	Columns	Col 250x250x22	**0.97**

Table 3.2: Member Sections of Nine-Storey OCBF

| Storey # | Strength design of **OCBF** (Nine-storey building) | | |
	Element	Section	D/C Ratio
7 to 9	Beams	UB 406x140x46	**0.81**
	Braces	HSS 190.5x12.7	**0.46**
	Columns	Col 300x300x25	**0.24**
4 to 6	Beams	UB 406x140x46	**0.81**
	Braces	HSS 190.5 x12.7	**0.72**
	Columns	Col 300x300x25	**0.65**
1 to 3	Beams	UB 406x140x46	**0.81**
	Braces	HSS 190.5 x12.7	**0.80**
	Columns	Col 350x350x35	**0.71**

Table 3.3: Member Sections of Fifteen-Storey OCBF

Storey #	Strength design of **OCBF** (Fifteen-storey building)		
	Element	Section	D/C Ratio
13 to 15	Beams	UB 406x140x46	**0.81**
	Braces	HSS 168.3x 12.7	**0.46**
	Columns	Col 450x450x35	**0.10**
10 to 12	Beams	UB 406x140x46	**0.81**
	Braces	HSS 190.5x12.7	**0.58**
	Columns	Col 500x500x40	**0.22**
7 to 9	Beams	UB 406x140x46	**0.81**
	Braces	HSS 190.5x12.7	**0.70**
	Columns	Col 550x550x50	**0.30**
4 to 6	Beams	UB 406x140x46	**0.81**
	Braces	HSS 219x12.7	**0.59**
	Columns	Col 600x600x60	**0.35**
1 to 3	Beams	UB 406x140x46	**0.81**
	Braces	HSS 219x12.7	**0.68**
	Columns	Col 650x650x65	**0.40**

3.2.2 Ductility and Capacity Design Requirements for SCBFs

Unlike OCBF, SCBF are expected to provide significant inelastic deformation capacity primarily through brace buckling and yielding of the brace in tension. This is reflected in the high response modification factor (*R=6.0*) set by ASCE7-10 (2010) standards to this special type of CBFs. As a result, the ANSI/AISC 341-10 (2010) provides a set of special provisions for the various SCBF members to insure achieving the desired level of ductile behavior. Braces of SCBFs are expected to satisfy the highly ductile members' requirements defined by the limiting value $\lambda_h = 0.038(E/F_y)$. Local buckling in columns of SCBF should be avoided by conforming to the highly ductile members requirements $\lambda_h =$

$0.55 \sqrt{(E/F_y)}$. Columns should be checked and resized (if necessary) to ensure they can withstand the expected strength of the bracing elements in tension given by (Bruneau et al., 2011; Williams, 2014):

$$T_{BR} = R_y F_y A_g \tag{3.2}$$

In addition, brace forces based on their expected compressive strength and post-buckling strength should be evaluated using Eqs. (3.3) and (3.4), respectively:

$$C_{BR} = smaller\ of\ (R_y F_y A_g\ and\ 1.14 F_{cre} A_g\ ) \tag{3.3}$$

$$C_{BR} = 0.3 F_{cr} A_g \tag{3.4}$$

where

A_g is the gross cross sectional area of the brace element

R_y is the ratio of expected yield stress to the specified minimum yield stress

F_y is the minimum yield stress

F_{cr} is the critical compressive strength of axially loaded elements

F_{cre} is the critical compressive strength of axially loaded elements calculated as per the regular equations of Chapter (E) of the ANSI/AISC 360-10 (2010) but replacing F_y with $R_y F_y$.

Forces in each column are calculated based on the direct summation of all vertical seismic forces represented by the brace strength component. Use of SRSS method is not recommended since it has been found to be un-conservative for strong earthquake loads (Bruneau et al., 2011). It should be noted that seismic-induced

forces are determined, as mentioned above, for external columns only as they are likely to be subjected to greater effective brace-induced loads than internal columns. (Annan, 2008). The resulting column section at a certain level is to be applied to all other columns of braced bays on the same level of the frame.

Beams in SCBF are expected to abide by the moderately ductile members' requirements λ_m provided by ANSI/AISC 360-10 (2010). Besides, in the ductility design of floor beams, the effect of redistribution of loads due to brace buckling or yielding should be considered in designing the beams in braced bays. Such beams are redesigned as beam-column elements to withstand moment due to gravity loads and axial compression due to horizontal component of maximum brace force, i.e., nominal brace strength (Bruneau et al., 2011). The axial compression (P) resulting from unequal capacity of braces in tension and compression is determined considering a horizontal equilibrium of brace-induced forces at each beam end as presented in Fig. 3.5:

$$P = 0.5(T_i - C_i) \cos \theta_i + 0.5(T_{i+1} - C_{i+1}) \cos \theta_{i+1} \tag{3.5}$$

In this expression, i refer to the storey number while θ indicates the inclination angle of the brace element with respect to the beam.

An in-house developed spreadsheet is developed to allow for automated calculations of the capacity design calculations for SCBF. Detailed calculations are provided in Appendix B. The outcomes of the strength design and capacity design calculations of the six-storey, nine-storey and fifteen-storey SCBFs are summarized in Tables 3.4, 3.5 and 3.6, respectively.

Table 3.4: Member Sections of Six-Storey SCBF

Storey #	Strength design of **SCBF** (Six-storey building)			Changes due to capacity design (for D/C ratios, refer to the Excel spreadsheet in Appendix B)
	Element	Section	D/C Ratio	
4 to 6	Beams	UB 406x140x46	**0.81**	Unsafe, use: UB 533x210x109
	Braces	HSS 141.3x12.7	**0.97**	Ok
	Columns	Col 200x200x15	**0.71**	Unsafe, use: Col 300x300x20
1 to 3	Beams	UB 406x140x46	**0.81**	Unsafe, use: UB 533x210x109
	Braces	HSS 152.4x12.7	**0.95**	Ok
	Columns	Col 250x250x25	**0.92**	Unsafe, use: Col 400x400x35

Table 3.5: Member Sections of Nine-Storey SCBF

Storey #	Strength design of **SCBF** (Nine-storey building)			Changes due to capacity design (for D/C ratios, refer to Appendix B)
	Element	Section	D/C Ratio	
7 to 9	Beams	UB 406x140x46	**0.81**	Unsafe, use: UB 533x210x109
	Braces	HSS 141.3x12.7	**0.89**	Ok
	Columns	Col 200x200x15	**0.65**	Unsafe, use: Col 300x300x20
4 to 6	Beams	UB 406x140x46	**0.81**	Unsafe, use: UB 533x210x109
	Braces	HSS 168.3x12.7	**0.73**	Ok
	Columns	Col 300x300x25	**0.69**	Unsafe, use: Col 400x400x35
1 to 3	Beams	UB 406x140x46	**0.81**	Unsafe, use: UB 533x210x109
	Braces	HSS 168.3x12.7	**0.81**	Ok
	Columns	Col 350x350x30	**0.86**	Unsafe, use: Col 500x500x45

Table 3.6: Member Sections of Fifteen-Storey SCBF

Storey #	Strength design of **SCBF** (Fifteen-storey building)			Changes due to capacity design (for D/C ratios, refer to Appendix B)
	Element	Section	D/C Ratio	
13 to 15	Beams	UB 406x178x74	**0.33**	Unsafe, use: UB 533x210x122
	Braces	HSS 152.4x12.7	**0.47**	Ok
	Columns	Col 350x350x35	**0.14**	Ok
10 to 12	Beams	UB 406x178x74	**0.33**	Unsafe, use: UB 533x210x122
	Braces	HSS 168.3x12.7	**0.57**	Ok
	Columns	Col 450x450x40	**0.26**	Ok
7 to 9	Beams	UB 406x178x74	**0.33**	Unsafe, use: UB 533x210x122
	Braces	HSS 190x12.7	**0.55**	Ok
	Columns	Col 500x500x40	**0.42**	Unsafe, use: Col 550x550x50
4 to 6	Beams	UB 406x178x74	**0.33**	Unsafe, use: UB 533x210x122
	Braces	HSS 190x12.7	**0.57**	Ok
	Columns	Col 550x550x55	**0.44**	Unsafe, use: Col 650x650x60
1 to 3	Beams	UB 406x178x74	**0.33**	Unsafe, use: UB 533x210x122
	Braces	HSS 219x12.7	**0.51**	Ok
	Columns	Col 600x600x60	**0.50**	Unsafe, use: Col 700x700x70

3.3 Conclusions

This chapter described the selection and design of the steel CBFs used in the current study. Three different buildings assumed to be located in the city of Abu Dhabi, UAE (S_S = 0.6g and S_1 = 0.19g), with six-, nine- and fifteen-storey height were selected. All buildings have a typical storey height of 3.6 m with the same floor plan dimensions of 38.7 m x 38.7 m to represent the dimensions of office buildings that are commonly constructed in the study area. The gravity loads resisting system consists of a composite floor system supported by encased composite columns in which I-shaped steel sections are embedded in the concrete. Structural loads (gravity, wind and seismic) are calculated in accordance with the ASCE7-10 (2010) standards and the requirements of the International Building Code (IBC, 2012). Design of the various structural elements was performed according to ANSI/AISC 360-10 (2010), and the corresponding seismic provisions ANSI/AISC 341-10 (2010). Seismic calculations showed that although the seismic design category (SDC) is classified as C, it is a borderline with the more severe SDC D. As a result, both categoreis (SDC C) and (SDC D) were considered. For SDC C where no height limitation is imposed by the code, a steel ordinary OCBF, with R=3.25, was used as a seismic laod resisting system. Meanwhile, for SDC D, a SCBF, R=6, was considered due to the strict height limitation imposed by ASCE7-10 (2010) on OCBFs constructed in SDC D. Thus, for SDC C, three OCBFs with six-, nine- and fifteen-storey were studied and for SDC D, three SCBFs with six-, nine- and fifteen-storey were considered. The structural analysis software SAP2000 (2009) was employed to model and design all six CBFs. With the increased height of buildings, the storey drift values increased considerably and strength-designed section sizes were found insufficient to satisfy the code drift limits. As a result, brace and column sections in the nine-storey and

fifteen-storey CBFs were enlarged to reduce the drift values within acceptable limits. OCBFs were designed in accordance with strength design requirements only since they are not expected to be subjected to large inelastic demands due to their relatively low response modification factor ($R=3.25$). Meanwhile, the SCBFs were subjected to capacity design and ductility requirements as per ANSI/AISC 341-10 (2010) in order to provide significant inelastic deformation capacity primarily through brace buckling and yielding. It is worth to note that with increase of height (nine-storey and above), designed sections of OCBFs started to approach those of SCBFs (resulting from capacity design) due to the need to control the inter-storey drift values of OCBFs within acceptable limits.

Chapter 4: Static Pushover Analysis of Structures with Concentrically Braced Frames (CBFs) as Lateral Load Resisting System

4.1 Static Pushover Analysis

4.1.1 Concept of Static Pushover Analysis

The Static Pushover Analysis provides a simplified solution to complex problems for predicting force and deformation demands imposed on structures and their elements by severe ground motion. It uses a nonlinear technique in which the structure is subjected to monotonically increasing lateral loads with a specific distribution along the height of the building until a predetermined target displacement is reached (Krawinkler, 1996; FEMA 356, 2000). The static term implies that a static method is being employed to represent a dynamic phenomenon; a representation that may be adequate in many cases but is doomed to failure sometimes. The pushover technique is employed to evaluate the solution and modify it as needed. The pushover does not create good solutions, it only evaluates solutions. In other words, If the engineer starts with a poor lateral system, the pushover analysis may render the system acceptable through system modifications, or prove it to be unacceptable (Krawinkler, 1996). The process is to prepare an analytical model of the structure in a two or three-dimensional space, the model should accounts for all important linear and nonlinear response characteristics. Two methods exist to perform Static Pushover Analysis :

(1)   Load-controlled procedure involves incremental application of a monotonic load to the structure until the maximum load is reached or the structure collapses, whichever occurs first. Force control should be

used when the magnitude of load is known (such as gravity load), and the structure is expected to support the load.

(2)   Displacement-controlled procedure involves incremental application of a monotonic load until the target displacement has reached a pre-specified value or the structure collapses, whichever comes first. Displacement control is used when the value of the applied load is not known in advance, or when the structure is expected to lose strength.

Since the maximum value of earthquake load can not be determined precisely in advance, the displacement-controlled method is employed in this thesis where the behavior of the Concentrically Braced Frames (CBF) under seismic loads is studied. Lateral loads are applied in a predetermined pattern that represents the lateral load distribution as proposed by the IBC (2012). The structure is then pushed under these loads to specific target displacement levels to obtain the pushover or capacity curve (Fig. 4.1).
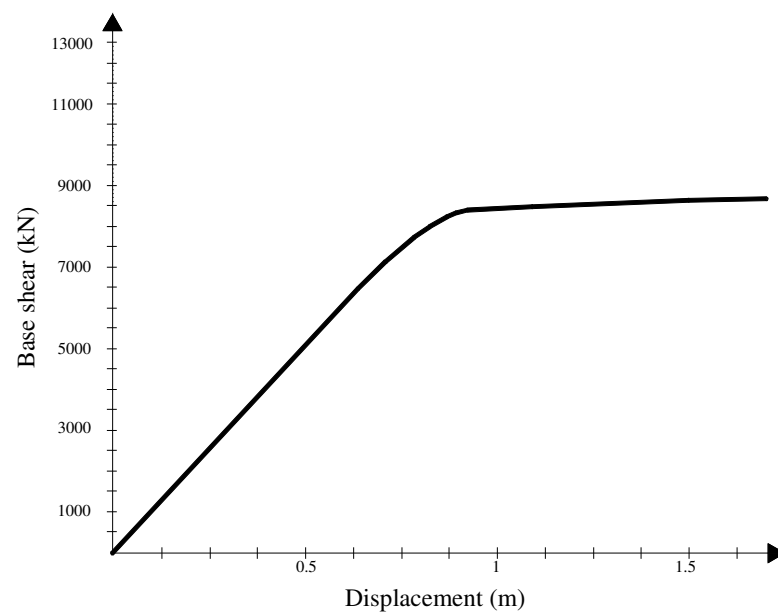
Figure 4.1: Typical Pushover Response Curve

The internal forces and deformations computed at the target displacement levels are estimates of the strength and deformation demands, which need to be compared to available capacities. (Krawinkler, 1996).

A target displacement is a characteristic displacement in the structure that serves as an estimate of the global displacement experienced by the structure in a design earthquake associated with a specified structural performance level. A common definition of target displacement is the roof displacement at the center of mass of the structure and is given by FEMA 356 (2000):

$$\delta_t = C_0 C_1 C_2 C_3 S_a \frac{T_e^2}{4\pi^2} \ g \tag{4.1}$$

where

C_o is a modification factor to relate spectral displacement of an equivalent SDOF system to the roof displacement of the building MDOF system. The appropriate value of C_o can be found in Table 3.2 of FEMA 356 (2000) based on the building height, lateral load resisting system and pattern of distribution of lateral load along the height of the building.

C_1 is the modification factor to relate expected maximum inelastic displacements to displacements calculated for linear elastic response:

$$C_1 = 1.0 \ \text{for} \ T_e \geq T_s \tag{4.2}$$

$$C_1 = [1.0 + (R-1)T_S/T_e]/R \ \text{for} \ T_e < T_s \tag{4.3}$$

but not greater than the values given in Section 3.3.1.3, FEMA 356 (2000) nor less than 1.0.

T_e is the eEffective fundamental period of the building in the direction under consideration, sec.

T_s is the characteristic period of the response spectrum, defined as the period associated with the transition from the constant acceleration segment of the spectrum to the constant velocity segment of the spectrum per Sections 1.6.1.5 and 1.6.2.1 of FEMA 356 (2000).

R is the ratio of elastic strength demand to calculated yield strength coefficient calculated by Eq. (3-16) FEMA 356 (2000):

$$R = \frac{S_a}{\frac{V_y}{W}} \times C_m \qquad (4.4)$$

C_2 is the modification factor to represent the effect of pinched hysteretic shape, stiffness degradation and strength deterioration on maximum displacement response. Values of for different framing systems and Structural Performance Levels shall be obtained from Table 3.3, FEMA 356 (2000). Alternatively, use of $C_2 = 1.0$ shall be permitted for nonlinear procedures.

C_3 is the modification factor to represent increased displacements due to dynamic P-Δ effects. For buildings with positive post-yield stiffness, shall be set equal to 1.0. For buildings with negative post-yield stiffness, values of shall be calculated using Eq. (3-17), FEMA 356 (2000):

$$C_3 = 1.0 + \frac{|\alpha|(R-1)^{3/2}}{T_e} \qquad (4.5)$$

but not to exceed the values set forth in Section 3.3.1.3 of FEMA 356 (2000).

S_a is the response spectrum acceleration, at the effective fundamental period and damping ratio of the building in the direction under consideration, g, as calculated in Sections 1.6.1.5 and 1.6.2.1 of FEMA 356 (2000).

g is the acceleration of gravity.

V_y is the yield strength calculated using results of the NSP (Non-linear Static Procedure) for the idealized nonlinear force displacement curve developed for the building in accordance with Section 3.3.3.2.4 of FEMA 356 (2000).

W is the effective seismic weight, as calculated by Section 3.3.1.3.1 of FEMA 356 (2000).

C_m is the effective mass factor obtained from Table 3.1, FEMA 356 (2000). Alternatively, C_m taken as the effective model mass calculated for the fundamental mode using an Eigenvalue analysis shall be permitted.

α is the ratio of post-yield stiffness to effective elastic stiffness, where the nonlinear force displacement relation shall be characterized by a bilinear relation as shown in Fig. 3.1 (FEMA 356, 2000).

4.1.2 Interpretation of Pushover Capacity Curves

As mentioned above, a major outcome of the Static Pushover Analysis is the capacity curve. Carful interpretation of this curve should provide understanding of the response of the structure under increasing lateral loads. FEMA P-750 (2009) and FEMA 356 (2000) provide an interpretation to these curves by dividing them into three main types namely; Type 1, Type 2 and Type 3 as shown in Fig. 4.2.
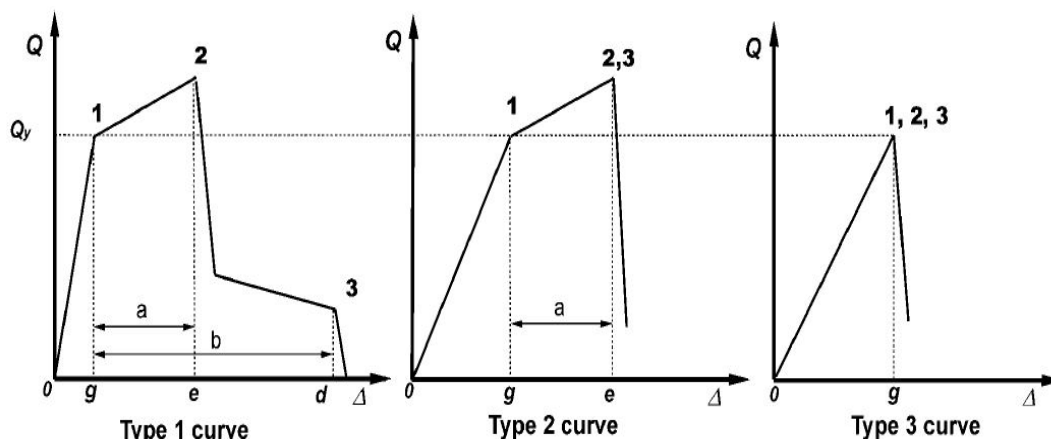
Figure 4.2: Types of Pushover Curves (FEMA P-750, 2009; FEMA 356, 2000)

Type 1 curve depicted in Fig. 4.2 represents a ductile behavior where there is an elastic range (point 0 to point 1 on the curve) followed by a plastic range (points 1 to 3). The plastic range includes a strain hardening or softening range (points 1 to 2) and a strength-degraded range (points 2 to 3). The residual strength at point (3) is considered to provide support to gravity loads. Primary lateral load resisting system component exhibiting this behavior shall be classified as deformation-controlled if the strain-hardening or strain softening range is such that e > 2g; otherwise, they shall be classified as force-controlled. For secondary component (i.e., an element that does not contribute significantly or reliably in resisting earthquake effects because of low lateral stiffness, strength, or deformation capacity) actions exhibiting Type 1 behavior shall be classified as deformation-controlled for any e/g ratio. Meanwhile Type 2 curve, shown in Fig. 4.2, is representative of ductile behavior where there is an elastic range (point 0 to point 1) and a plastic range (points 1 to 2) followed by loss of strength and loss of ability to support gravity loads beyond point 2. Primary and secondary component actions exhibiting this type of behavior shall be classified as deformation-controlled if the plastic range is such that e > 2g; otherwise, they shall be classified as force-controlled. On the contrary, Type 3 curve provided in Fig.

4.2 reflects a brittle or non-ductile behavior where there is an elastic range (point 0 to point 1 on the curve) followed by a sudden loss of strength and loss of ability to support gravity loads beyond point 1. Primary and secondary component actions displaying Type 3 behavior shall be classified as force-controlled.

The interpretation of these curves remains incomplete until the Structural Performance Levels defined in FEMA P-750 (2009) and FEMA 356 (2000) are introduced to allow for full description of the structure's behavior under seismic loads.

4.1.3 Structural Performance Levels

The structural performance levels defined by FEMA P-750 (2009) and FEMA 356 (2000), as shown in Fig. 4.3, are discrete damage states that express the possible damage conditions that buildings could experience during an earthquake event. The structural performance level of a building is selected from four discrete structural performance levels and two intermediate structural performance ranges as defined herein:

- Immediate Occupancy (S-1),(IO)
- Life Safety (S-3), (LS)
- Collapse Prevention (S-5), (CP)
- Not Considered (S-6)

Meanwhile, the intermediate structural performance ranges are:

- The Damage Control Range (S-2)
- The Limited Safety Range (S-4)

Acceptance criteria for performance within the Damage Control Structural Performance Range shall be obtained by interpolating the acceptance criteria provided for the Immediate Occupancy and Life Safety Structural Performance Levels. Acceptance criteria for performance within the Limited Safety Structural Performance Range shall be obtained by interpolating the acceptance criteria provided for the Life Safety and Collapse Prevention Structural Performance Levels.

Immediate Occupancy Structural Performance Level (IO) (S-1)

Structural Performance Level S-1, Immediate Occupancy, means the post-earthquake damage state in which only very limited structural damage has occurred. The basic vertical- and lateral-force-resisting systems of the building retain nearly all of their pre-earthquake strength and stiffness. As such, the risk of lifethreatening injury due to structural damage is very low.

Damage Control Structural Performance Range (S-2)

Design for the Damage Control Structural Performance Range may be desirable to minimize repair time and operation interruption, as a partial means of protecting valuable equipment and contents, when the cost of design for immediate occupancy is excessive.

Life Safety Structural Performance Level (LS) (S-3)

Structural Performance Level S-3, Life Safety, means the post-earthquake damage state in which significant damage to the structure has occurred, but some margin against either partial or total structural collapse remains. Some structural elements and components are severely damaged. Injuries may occur during the earthquake; however, the overall risk of life-threatening injury as a result of

structural damage is expected to be low. It should be possible to repair the structure; however, for economic reasons this may not be practical. While the damaged structure is not an imminent collapse risk, it would be prudent to implement structural repairs or install temporary bracing prior to reoccupancy.

Limited Safety Structural Performance Range (S-4)

Structural Performance Range S-4, Limited Safety, shall be defined as the continuous range of damage states between the Life Safety Structural Performance Level (S-3) and the Collapse Prevention Structural Performance Level (S-5).

Collapse Prevention Structural Performance Level(CP) (S-5)

Structural Performance Level S-5, Collapse Prevention, means the post-earthquake damage state in which the building is on the verge of partial or total collapse. Substantial damage to the structure has occurred, potentially including significant degradation in the stiffness and strength of the lateral-forceresisting system, large permanent lateral deformation of the structure, and—to a more limited extent—degradation in vertical-load-carrying capacity. However, all significant components of the gravityload- resisting system must continue to carry their gravity load demands. The structure may not be technically practical to repair and is not safe for reoccupancy, as aftershock activity could induce collapse.

Structural Performance Not Considered (S-6)

This performance level is related to non-structural rehabitilation and, therefore, is not related to the research topic of this thesis.

4.2 Failure Criteria of CBFs

In CBF, braces are counted on to provide the ductile response by responding in-elastically under the effect of the applied lateral loads. Meanwhile, columns and beams are supposed to remain able to carry applied loads elastically. As such, it is essential to allow for the formation of plastic hinges in the braces under certain level of loading. In the meantime, columns and beams are not assigned such plastic hinges. The following failure criteria for CBF are utilized in the current thesis:

- **Storey Collapse Mechanism**: occurs when plastic hinges form in all the braces at particular level or if a plastic hinge forms in any column at any level of the structure, whichever occurs first. In either case, it is considered that the lateral load resisting system is significantly damaged and the frame capacity has decreased dramatically. In the current study, such plastic hinges were assumed to take place once the level of deformations in any member reached the level of damage corresponding to the Life Safety Performance level (S-3). As discussed earlier, at this particular performance level, the damaged structure is repairable along with a low probability of life-threatening injury.

- **Building Collapse Mechanism**: is the point where the entire structure loses its stability and collapses. This mechanism takes place when the building becomes unable to withstand any additional lateral load during the pushover process.

The structural performance level adopted in the current study is Life Safety. This particular level was selected since it represents an intermediate level between Immediate Occupancy (where the structural elements are over conservatively

designed to ensure minor post-earthquake structural damage) and the Collapse Prevention level (in which the structure experiences substantial damage and is on the verge of collapse).

The basic behavior of a typical plastic hinge in a bracing element is shown in Fig. 4.3 (FEMA 356, 2000)**.** The figure shows the generalized force-deformation relation under tension or compression. The rapid loss of load carrying capacity under compressive load is attributed to buckling failure of the brace element. The correlation between the hinge behavior and the various structural performance levels is also provided in Fig. 4.3.
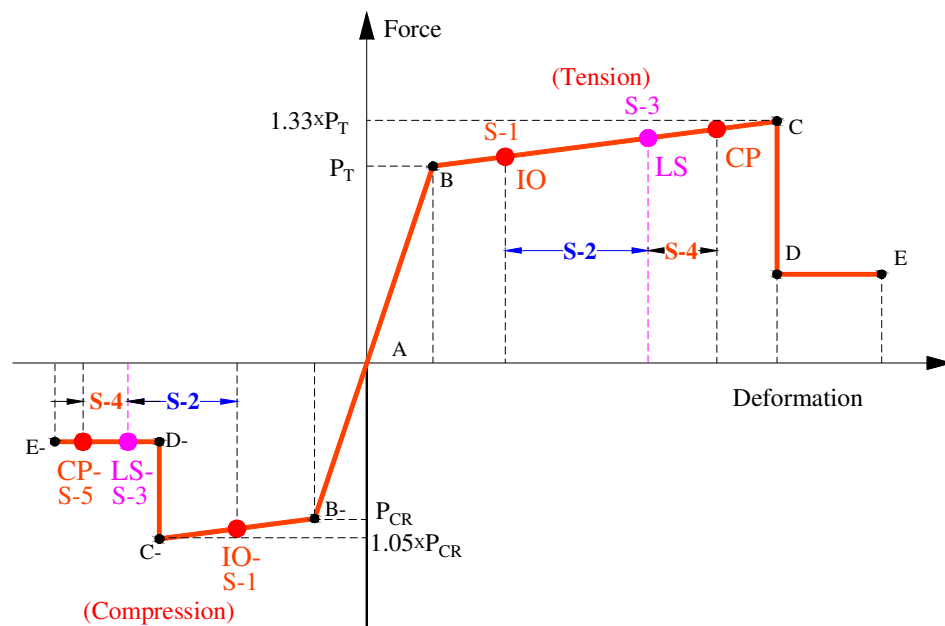
Figure 4.3: Structural Performance Levels

4.3 Finite Element Modeling

Analytical prediction of the behavior of CBFs is carried out using the SeismoStruct 2012 Software. SeismoStruct adopts the Finite Element approach in

predicting the large displacement response of structures under static or dynamic loading, taking into consideration both geometric nonlinearities and material inelasticity.

In SeismoStruct (2012), use is made of the fiber approach to model the cross-section behavior, where each fiber is associated with a uniaxial stress-strain relationship. A main characteristic of this software is its ability to model the spread of inelasticity along the member length and across the section depth to allow for accurate estimation of damage accumulation and distribution. In addition, the program possesses the ability to automatically subdivide the loading increment, whenever convergence problems arise. The level of subdivision depends on the convergence difficulties encountered. When convergence difficulties are overcome, the program automatically increases the loading increment back to its original value. An Inelastic beam-column frame element was used to represent the behavior of all CBFs members. This element type accounts for both geometric and material non-linearity. In such an element, the sectional stress-strain state is obtained through the integration of the nonlinear uniaxial stress-strain response of the individual fibers in which the section has been subdivided. For the frame members, 200 section fibers were employed along with 5 integration sections (SeismoStruct, 2012). Bracing members were modeled using the inelastic beam-column frame element with the introduction of link elements at both ends of the member to mimic the behavior of braces in tension and compression. Besides, this modeling technique enables modeling the post-buckling behavior of the braces under compressive loads. The link element connects two initially coincident structural nodes and performs based on a pre-defined force-displacement (or moment-rotation) response curve for each of its

local six translation and rotation degrees-of-freedom (F1, F2, F3, M1, M2, M3) as shown in Fig. 4.4.
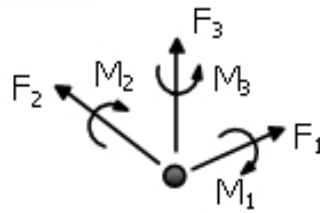
Figure 4.4: Translation and Rotation Degrees-of-Freedom of Link Element

In the current study, the asymmetric bilinear link was used since it allows for different axial behavior of the element when subjected to tensile or compressive force effects. Six parameters need to be defined in order to fully characterize the asymmetric bilinear curve as depicted in Fig. 4.5:

Initial stiffness in positive region (k_o^+).

Yield force in positive region (F_y^+).

Post-yield hardening ratio in positive region (r^+).

Initial stiffness in negative region (k_o^-).

Yield force in negative region (F_y^-).

Post-yield hardening ratio in negative region (r^-).
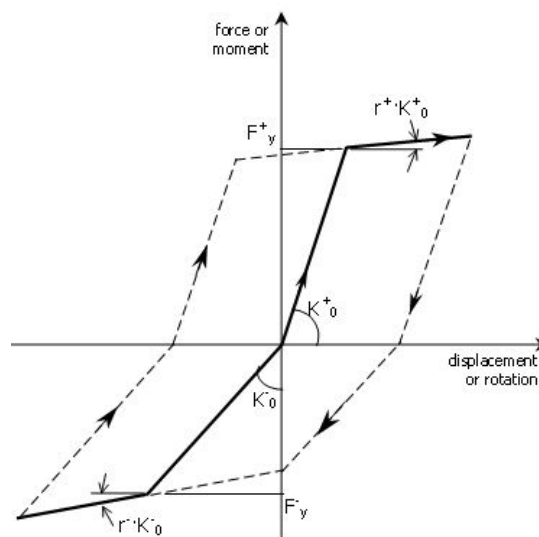
Figure 4.5: Bilinear Asymetric Link Response Curve (SeismoStruct, 2012)

4.4 Model Validation for Pushover Analysis

The accuracy of SeismoStruct (2012) in performing pushover analysis and the effectiveness of the employed brace modelling technique (as described in section 4.3) are verified in this section by comparing the numerical predictions with relevant experimental measurements reported in the literature. The experimental results of one storey-one bay concentrically braced steel frames carried out at Kyoto University by Wakabayashi et al. (1974) are used to verify the performance of the developed SeismoStruct model. The test was conducted on large-scale specimens of braced portal steel frames, Fig. 4.6, subjected to horizontal load that was monotonically applied to the top left joint of the tested frames. Frames were manufactured by welding H-shape members made of SS41 steel.
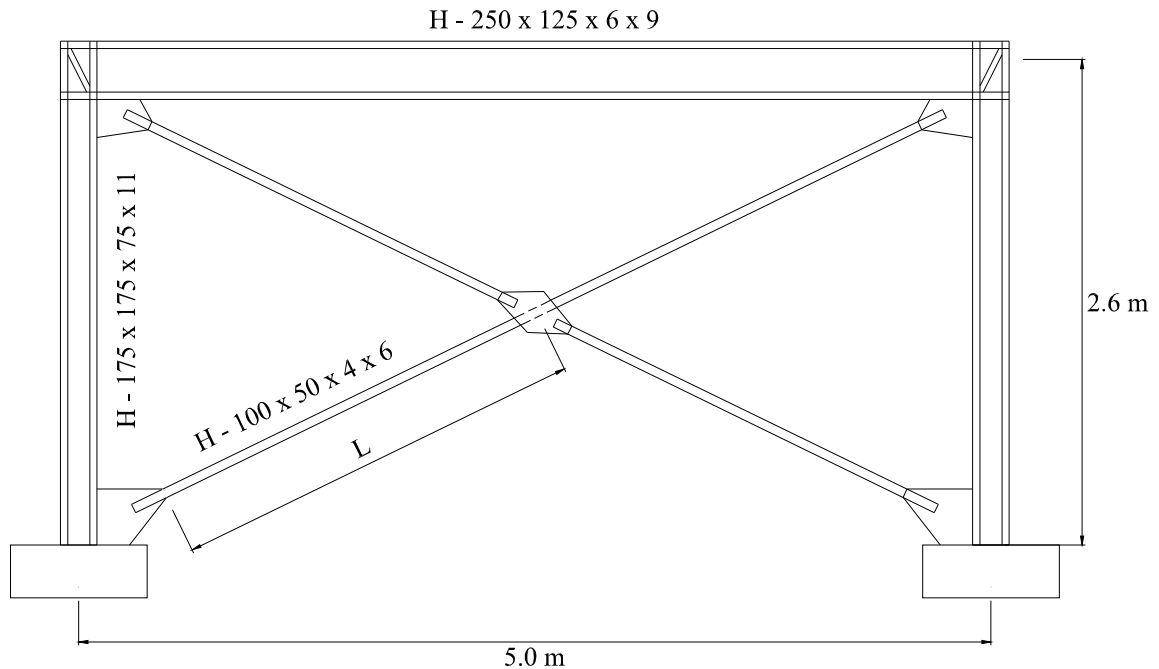
Figure 4.6: Typical Steel Braced Frame Tested by Wakabayashi et al. (1974)

Detailed information on the properties of used sections and material mechanical properties can be found in Wakabayashi et al. (1974). For verification purposes, a typical specimen of the tested braced frames was modeled using the technique described in section 4.3. A bilinear material model was utilized for steel with a modulus of Elasticity (E = 210 GPa) and a kinematic strain hardening ratio of 1.4% for columns, 1.3% for braces and 1.1% for beams. Yield stress values (F_y) of 248.2 MPa, 269.8 MPa and 287.4 MPa were assigned for columns, beams and brace elements, respectively, to match the main mechanical properties reported by Wakabayashi et al. (1974). The developed finite element model includes dimensionless link elements with asymmetric bilinear behavior to simulate the global response of brace members. Yield strength is used to represent the response of the brace in tension in compliance with the AISC Provisions for Structural Steel Buildings (ANSI/AISC 360-10, 2010). The estimated yield force in positive region was $F_y^+ = 290$ kN with an initial stiffness K_o^+ of 151 kN/mm. An assumed post-yield hardening ratio ($r^+ = 1.3\%$) was assumed in the positive response zone. Meanwhile, post-buckling strength is used to represent the response of the brace in compression as per current design practice based on the AISC Seismic Design Provisions (ANSI/AISC 341-10, 2010). The yield force in negative zone of the response curve $F_y^- = 104$ kN was estimated based on the residual strength of the brace member after buckling as per the AISC Provisions for Structural Steel Buildings (ANSI/AISC 360-10, 2010). The initial stiffness K_o^- and post-yield hardening ratio (r^-) were kept the same as in the positive response zone. Detailed calculations of bilinear link parameters are provided in Appendix C. Fig. 4.7 shows the comparison between the experimental and numerical response curves of the braced frame. The figure indicates the significant matching in the general response trend as obtained

experimentally and numerically. The comparison between the experimental results
and numerical predictions shown in Fig. 4.7 implies a variation in the yield load and
peak load of 1.4% and 0.6%, respectively. The kink in the experimental response
curve at 150 kN was reported by Wakabayashi et al. (1974) to be resulting from
onset of buckling of the compression bracing. Although this kink doesn't explicitly
appear in the analytical curve, a reduction in the system stiffness is clearly shown in
the analytical curve as evident by the reduced system stiffness between 160 and 180
kN.
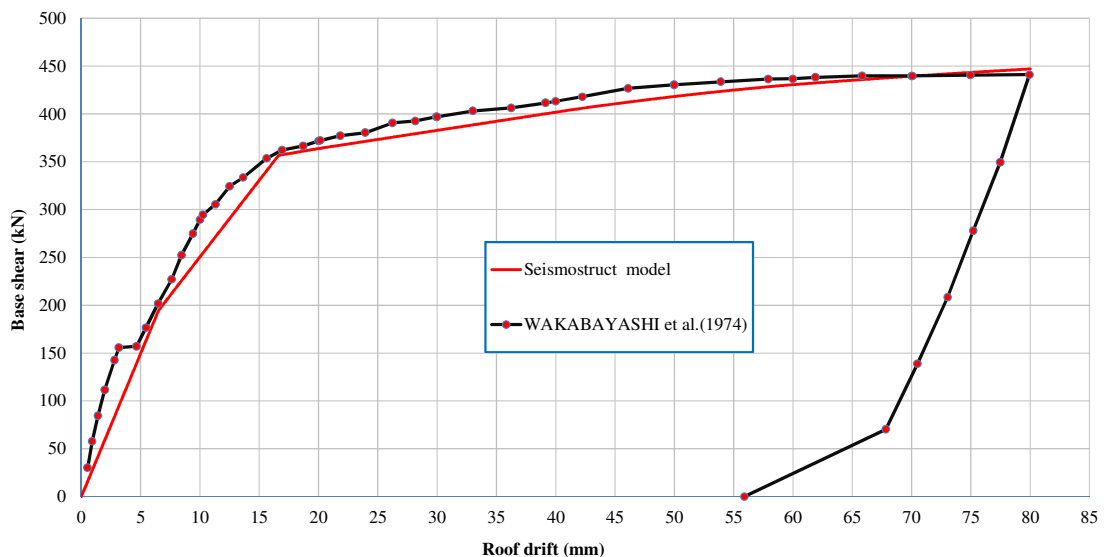
Figure 4.7: Experimental and Analytical Response Curves of Steel Braced Frame

4.5 Pushover Analysis of the Model Buildings

The office building layout shown in Fig. 3.3 represents the typical floor plan
of the buildings analyzed in this study. As a result of the symmetry in geometry and
structural system, two-dimensional models were developed using the non-linear
finite element program SeismoStruct (2012) following the procedure described in
section 4.3. A series of six-, nine- and fifteen-storey buildings is considered as
presented in Fig. 3.4. A bilinear material model for steel was employed with a

kinematic strain hardening parameter of 3%, a yield stress of 345 MPa and a modulus of elasticity of 200 GPa. Inelastic beam-column frame elements were used to represent the behavior of all structural members in the developed models. Asymmetric bilinear link elements were employed to connect all bracing members to adjacent elements to simulate the ideal pin-joint behavior at the end of bracing members. For each building height, the bracing system was designed twice based on the Ordinary Concentrically Braced Frames (OCBF) strength requirements and Special Concentrically Braced Frames (SCBF) ductility requirements and capacity procedures of the ANSI/AISC 341-10 (2010) as was explained in details in section 3.2. The corresponding link parameters are summarized in Tables 4.1, 4.2 and 4.3 for the six-storey, nine-storey and fifteen-storey buildings, respectively. Inelastic pushover analyses were then performed for all six model buildings.

Table 4.1a: Bilinear Link Parameters for the Six-Storey OCBF Model

OCBF – Six-storey			
Storey 1-3		Storey 4-6	
Tension		Tension	
K_0^+ (kN/mm)	490.22	K_0^+ (kN/mm)	368.24
F_Y^+ (kN)	2275.34	F_Y^+ (kN)	1709.15
r^+ (%)	3.0	r^+ (%)	3.0
Compression		Compression	
K_0^- (kN/mm)	490.22	K_0^- (kN/mm)	368.24
F_Y^- (kN)	491.26	F_Y^- (kN)	368.90
r^- (%)	1.2	r^- (%)	1.2

Table 4.1b: Bilinear Link Parameters for the Six-Storey SCBF Model

SCBF – Six-storey			
Storey 1-3		Storey 4-6	
Tension		Tension	
K_0^+ (kN/mm)	414.30	K_0^+ (kN/mm)	381.38
F_Y^+ (kN)	1922.95	F_Y^+ (kN)	1770.16
r^+ (%)	3.0	r^+ (%)	3.0
Compression		Compression	
K_0^- (kN/mm)	414.23	K_0^- (kN/mm)	381.38
F_Y^- (kN)	325.07	F_Y^- (kN)	256.09
r^- (%)	1.2	r^- (%)	1.2

Table 4.2a: Bilinear Link Parameters for the Nine-Storey OCBF Model

OCBF – Nine-storey					
Storey 1-3		Storey 4-6		Storey 7-9	
Tension		Tension		Tension	
K_0^+ (kN/mm)	525.81	K_0^+ (kN/mm)	525.81	K_0^+ (kN/mm)	525.81
F_Y^+ (kN)	2440.51	F_Y^+ (kN)	2440.51	F_Y^+ (kN)	2440.51
r^+ (%)	3.0	r^+ (%)	3.0	r^+ (%)	3.0
Compression		Compression		Compression	
K_0^- (kN/mm)	525.81	K_0^- (kN/mm)	525.81	K_0^- (kN/mm)	525.81
F_Y^- (kN)	570.94	F_Y^- (kN)	570.94	F_Y^- (kN)	570.94
r^- (%)	1.2	r^- (%)	1.2	r^- (%)	1.2

Table 4.2b: Bilinear Link Parameters for the Nine-Storey SCBF Model

SCBF – Nine-storey					
Storey 1-3		Storey 4-6		Storey 7-9	
Tension		Tension		Tension	
K_0^+ (kN/mm)	460.56	K_0^+ (kN/mm)	460.56	K_0^+ (kN/mm)	380.49
F_Y^+ (kN)	2137.69	F_Y^+ (kN)	2137.69	F_Y^+ (kN)	1766.04
r^+ (%)	3.0	r^+ (%)	3.0	r^+ (%)	3.0
Compression		Compression		Compression	
K_0^- (kN/mm)	460.56	K_0^- (kN/mm)	460.56	K_0^- (kN/mm)	380.49
F_Y^- (kN)	425.45	F_Y^- (kN)	425.45	F_Y^- (kN)	254.32
r^- (%)	1.2	r^- (%)	1.2	r^- (%)	1.2

Table 4.3a: Bilinear Link Parameters for the Fifteen-Storey OCBF Model

OCBF – Fifteen-storey					
Storey 1-3 & 4-6		**Storey 7-9 & 10-12**		**Storey 13-15**	
Tension		**Tension**		**Tension**	
K_0^+ (kN/mm)	611.81	K_0^+ (kN/mm)	528.77	K_0^+ (kN/mm)	460.56
F_Y^+ (kN)	2839.70	F_Y^+ (kN)	2454.28	F_Y^+ (kN)	2137.69
r^+ (%)	3.0	r^+ (%)	3.0	r^+ (%)	3.0
Compression		**Compression**		**Compression**	
K_0^- (kN/mm)	611.81	K_0^- (kN/mm)	528.77	K_0^- (kN/mm)	460.56
F_Y^- (kN)	763.91	F_Y^- (kN)	577.60	F_Y^- (kN)	425.45
r^- (%)	1.2	r^- (%)	1.2	r^- (%)	1.2

Table 4.3b: Bilinear Link Parameters for the Fifteen-Storey SCBF Model

SCBF – Fifteen-storey							
Storey 1-3		**Storey 4-6 & 7-9**		**Storey 10-12**		**Storey 13-15**	
Tension		**Tension**		**Tension**		**Tension**	
K_0^+ (kN/mm)	611.81	K_0^+ (kN/mm)	528.77	K_0^+ (kN/mm)	460.56	K_0^+ (kN/mm)	413.11
F_Y^+ (kN)	2839.7	F_Y^+ (kN)	2454.28	F_Y^+ (kN)	2137.69	F_Y^+ (kN)	1917.45
r^+ (%)	3.0	r^+ (%)	3.0	r^+ (%)	3.0	r^+ (%)	3.0
Compression		**Compression**		**Compression**		**Compression**	
K_0^- (kN/mm)	611.81	K_0^- (kN/mm)	528.77	K_0^- (kN/mm)	460.56	K_0^- (kN/mm)	413.11
F_Y^- (kN)	763.91	F_Y^- (kN)	577.60	F_Y^- (kN)	425.45	F_Y^- (kN)	322.55
r^- (%)	1.2	r^- (%)	1.2	r^- (%)	1.2	r^- (%)	1.2

The vertical distribution of the lateral loads was taken to be similar to the distribution used in the design that follows the IBC (2012) provisions (i.e., trapezoidal distribution). These loads are summarized in Tables 4.4, 4.5 and 4.6 for the six-storey, nine-storey and fifteen-storey buildings, respectively.

Table 4.4a: Vertical Distribution of Lateral Earthquake Loads on Six-Storey OCBF

OCBF – Six-storey		
Level (i)	Height from base to level i h_x (m)	Lateral force induced at level i F_x (kN)
1	3.6	118.761
2	7.2	257.364
3	10.8	404.596
4	14.4	557.727
5	18.0	715.399
6	21.6	876.788

Table 4.4b: Vertical Distribution of Lateral Earthquake Loads on Six-Storey SCBF

SCBF – Six-storey		
Level (i)	Height from base to level i h_x (m)	Lateral force induced at level i F_x (kN)
1	3.6	64.329
2	7.2	139.406
3	10.8	219.156
4	14.4	302.102
5	18.0	387.508
6	21.6	474.927

Table 4.5a: Vertical Distribution of Earthquake Loads on the Nine-Storey OCBF

OCBF – Nine-storey		
Level (i)	Height from base to level i h_x (m)	Lateral force induced at level i F_x (kN)
1	3.6	45.801
2	7.2	108.612
3	10.8	179.986
4	14.4	257.561
5	18.0	340.098
6	21.6	426.819
7	25.2	517.180
8	28.8	610.779
9	32.4	707.304

Table 4.5b: Vertical Distribution of Earthquake Loads on the Nine-Storey SCBF

SCBF – Nine Storey		
Level (i)	Height from base to level i h_x (m)	Lateral force induced at level i F_x (kN)
1	3.6	25.190
2	7.2	59.736
3	10.8	98.993
4	14.4	141.659
5	18.0	187.054
6	21.6	234.750
7	25.2	284.449
8	28.8	335.928
9	32.4	389.017

Table 4.6a: Vertical Distribution of Earthquake Loads on the Fifteen-Storey OCBF

OCBF – Fifteen-Storey		
Level (i)	Height from base to level i h_x (m)	Lateral force induced at level i F_x (kN)
1	3.6	10.758
2	7.2	29.699
3	10.8	53.792
4	14.4	81.988
5	18.0	113.691
6	21.6	148.499
7	25.2	186.124
8	28.8	226.339
9	32.4	268.967
10	36.0	313.858
11	39.6	360.889
12	43.2	409.953
13	46.8	460.957
14	50.4	513.820
15	54.0	568.469
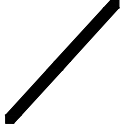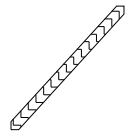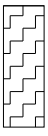
Table 4.6b: Vertical Distribution of Lateral Earthquake Loads on Fifteen-Storey
SCBF

SCBF – Fifteen-Storey		
Level (i)	Height from base to level i h_x (m)	Lateral force induced at level i F_x (kN)
1	3.6	5.827
2	7.2	16.087
3	10.8	29.137
4	14.4	44.410
5	18.0	61.582
6	21.6	80.437
7	25.2	100.817
8	28.8	122.601
9	32.4	145.690
10	36.0	170.006
11	39.6	195.482
12	43.2	222.058
13	46.8	249.685
14	50.4	278.319
15	54.0	307.921

Meanwhile, the gravity loads were held constant during carrying out the pushover process. The analysis was conducted in a response- controlled scheme where a large target drift was defined. The building was pushed laterally in an incremental fashion until the displacement corresponding to collapse was reached (i.e. the building becomes unable to withstand any additional lateral load during the pushover process). As a result, the ultimate lateral capacity and associated failure (yielding/buckling) were determined.

4.6 Failure Sequence of the Analyzed CBFs

This section discusses the results of the inelastic pushover analysis by showing the order and distribution of formation of plastic hinges in the six-, nine- and fifteen-storey OCBFs and SCBFs. The type of failure is presented on the pushover capacity curves and on the studied CBF elevation by symbols and notations, respectively, as shown in Fig. 4.8.

Notations for structural members		
Yielded brace will be filled with solid hatch.	Buckled brace will be filled with zigzag hatch.	Buckled column will be filled with zigzag hatch.

Symbols used in P.Curves		
○	△	✕
Buckled brace will be presented as Triangle	Yielded brace will be presented as Circle	Buckled column will be presented as X

Figure 4.8: Notations and Symbols used to Describe Failure Sequence

Meanwhile, the sequence of failure of various elements is depicted by the number indicated next to each symbol/notation. The order and distribution of plasticity or buckling/yielding depend, to a large extent, on the brace sizes and the slenderness ratio. If the brace sizes are uniform along the height of the building and the braces have the same slenderness ratio, buckling is most likely to be initiated at braces of lower storeys where compressive forces are at their maximum values.

4.6.1 Six-Storey OCBF and SCBF Buildings

As discussed in Chapter 3, the OCBFs were designed only to satisfy the strength design requirements and drift limits. Meanwhile, SCBFs were dimensioned in accordance with the capacity design approach provided by ANSI/AISC 341-10 (2010). Figure 4.9 shows the response curves resulting from pushover analyses of the six-storey OCB and SCB frames.
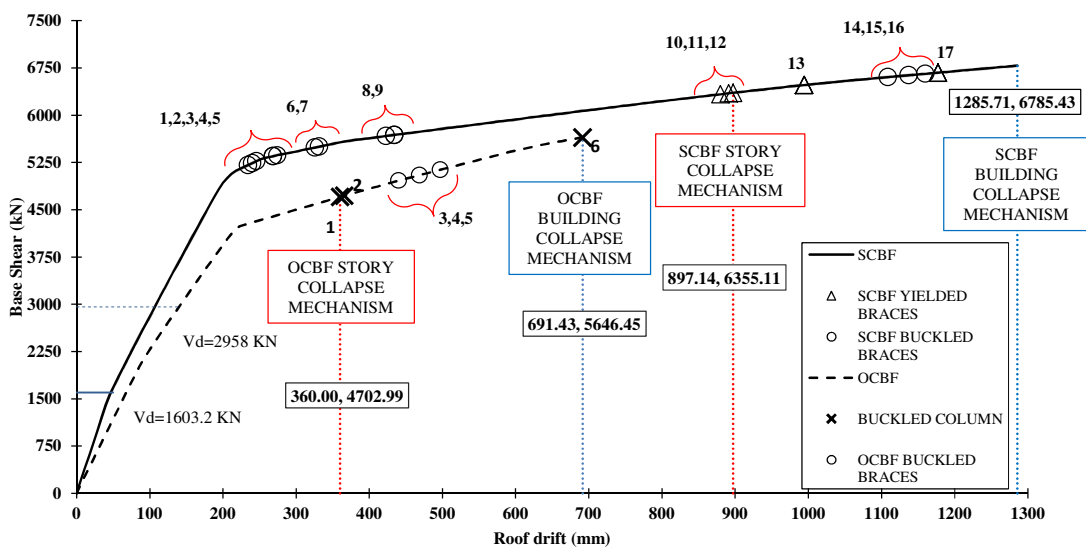
Figure 4.9: Pushover Response of Six-Storey OCBF and SCBF

The order and distribution of failed elements that lead to the formation of a storey collapse mechanism is shown in Figs. 4.10(a) and 4.10(b) for OCB and SCB frames, respectively. Similarly, the failure sequence until a building collapse mechanism was reached is depicted in Figs. 4.11(a) and 4.11(b) for OCBFs and SCBFs, respectively.

(a) OCBF   (b) SCBF
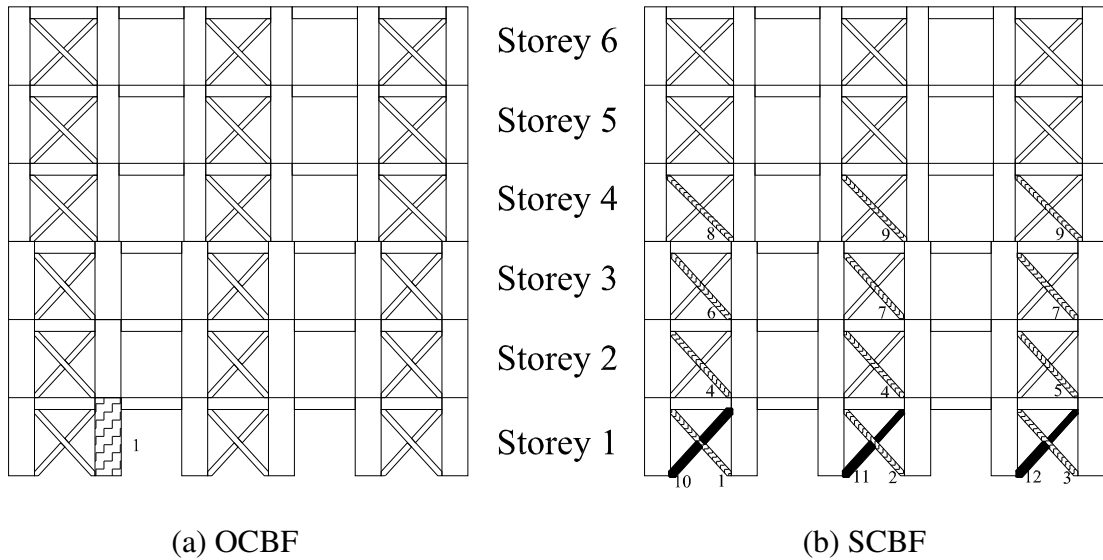
Figure 4.10: Failure Sequence of the Six-Storey OCBF and SCBF Pushed to the Storey Collapse Limit

(a) OCBF   (b) SCBF
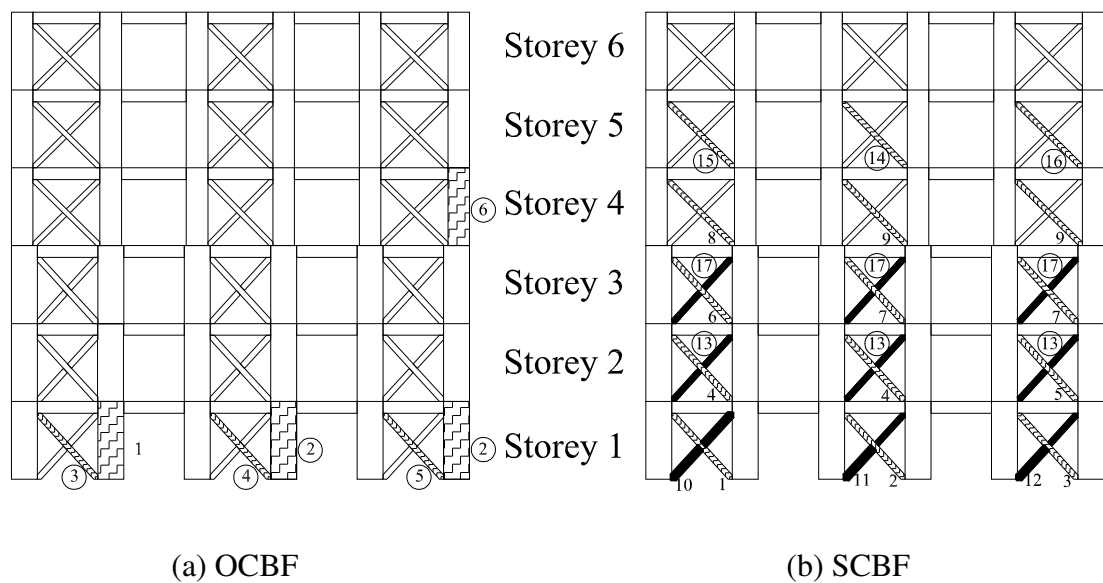
Figure 4.11: Failure Sequence of the Six-Storey OCBF and SCBF Pushed to the Building Collapse Limit

In these figures, members having the same numbers shown next to them are expected to buckle/yield simultaneously. The storey and building collapse mechanisms were identified in details in section 4.2. From Figs. 4.9 and 4.10(a) it can be observed that OCBF reached the storey collapse mechanism due to the buckling of a ground floor column (marked 1) before any buckling or yielding

initiation in the braces. This is due to the fact that columns were not sized for capacity design requirements which made the columns susceptible to fail for any additional forces in the braces beyond the strength design values. This indicates that there is no optimum usage of the OCBF members as the storey capacity limit was reached due to failure of one member only (column 1) while all other frame members were at the safe stage without any sign of progressive buckling or yielding of braces as part of the OCBF failure mechanism. On the other hand, the six-storey SCBF (Figs. 4.9 and 4.10(b)) showed a much better performance when subjected to pushover analysis. This is evident by the distribution of progressive buckling and yielding of braces along the SBF height. The storey failure mechanism took place at storey (1) by buckling and yielding of all storey braces with no failure in the gravity load supporting system in place. This enhancement in the structural response, relative to the OCBF, resulted from using stronger columns' sections to comply with the ductility design requirements as explained in Chapter (3). The failure sequence in Fig. 4.9 and Fig. 4.10(b) started by sequential buckling of three braces at storey (1) (1, 2 and 3), followed by buckling of three braces at storey (2) (4, 4 and 5) and buckling of three braces at storey (3) (6, 6 and 7), followed by buckling of three braces at storey (4) (8, 8 and 9) and finally yielding of three braces at storey (1) (10, 11 and 12). As a result, the failure mechanism was formed at storey (1) because all its braces have either buckled or yielded.

Pushover analyses were continued by pushing the six-storey OCBF and SCBF beyond the storey collapse limit till complete failure (building collapse limit) was reached. In view of Fig. 4.9 and Fig. 4.11(a), the OCBFs failure sequence continued by simultaneous buckling of two columns at storey (1) (2 and 2), followed

by buckling of three braces at the same storey (3, 4 and 5), followed by buckling of an edge column at storey (4) (marked as 6) in Fig. 4.11(a). Likewise, the SCBF (Fig. 4.9 and Fig. 4.11(b)) continued the systematic manner in failure sequence along its height. Three braces yielded at storey (2) (marked as 13), followed by buckling of three braces at storey (5) (14, 15 and 16), followed by simultaneous yielding of three braces at storey (3) (denoted as 17). At that point, the building failure limit was reached as the system was unable to withstand any additional lateral loads. The results obtained in this section implied the unfavorable behavior of OCBFs where the structure collapsed as a result of failure in its gravity system. In an earthquake event, a properly designed system should maintain the integrity of its gravity load resisting system before buckling/yielding of its brace members. On the contrary, the SCBF proved to be more reliable than OCBF as none of its gravity load resisting elements failed while the building collapse took place after all braces of the first three storeys yielded or buckled. Additionally, collapse happened after a good distribution of energy dissipation all over the five storeys out of the six storeys.

The inter-storey drift ratio (IDR) at the storey collapse limit for OCBF and SCBF are shown in Figs. 4.12(a) and 4.12(b), respectively. Shown also in these figures are the IDR limits related to Immediate Occupancy (IO = 0.5%) and Life Safety (LS = 1.5%) as recommended by FEMA 356 (2000). For the six-storey OCBF (Fig. 4.12 (a)), the IDR of all storeys exceeded the IO and LS FEMA 356 (2000) limits with the exception of storey (1) that reached the LS limit. This is attributed to the premature formation of storey collapse mechanism due to failure of one of columns in storey (1) before spread of yielding/buckling along the height of six-storey OCBF. On the contrary, the IDR profile of the six-storey SCBF showed a

typical variation with the maximum IDR taking place at the storey (1) with a decreasing trend towards the top of the building.

(a) OCBF

(b) SCBF
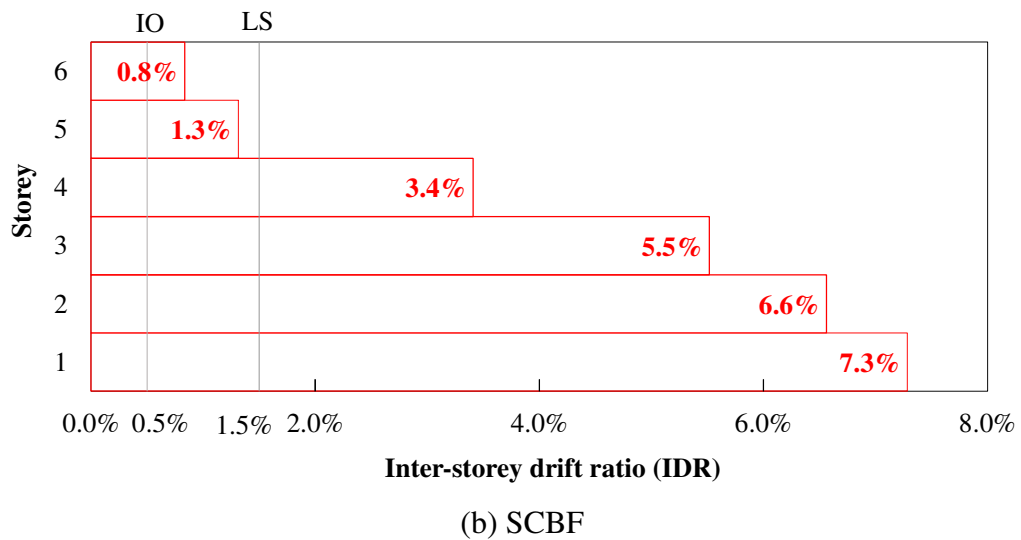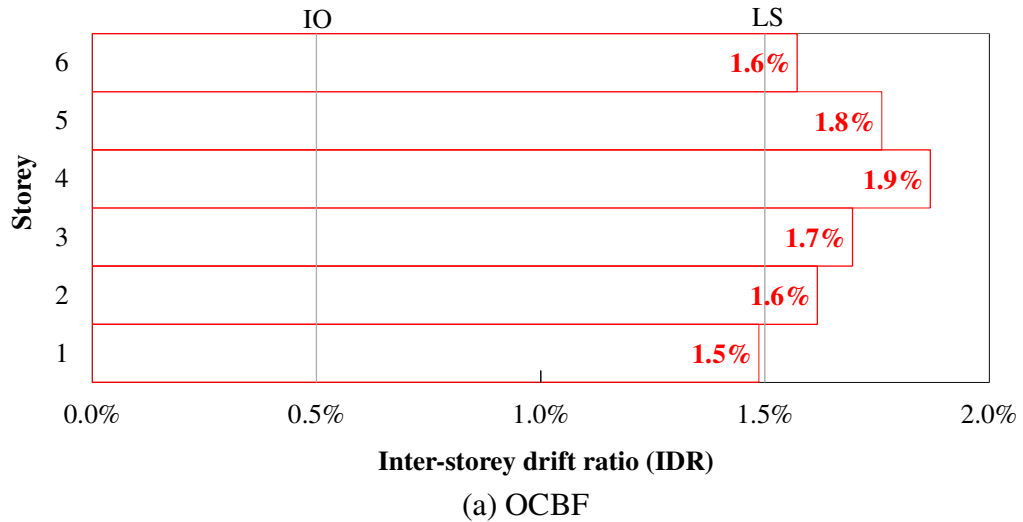
Figure 4.12: Inter-Storey Drift Ratio of Six-Storey OCBF and SCBF at Storey Collapse Limit

4.6.2 Nine-Storey OCBF and SCBF Buildings

Unlike the six-storey OCBF discussed in section 4.6.1, the drift control starts to influence the section sizes of the nine-storey OCBF as strength-based sections did not satisfy the storey drift code limits. Thus, in order to reduce the ID to code limits

level, the section of some columns was increased beyond the strength fulfillment level to reduce the ID. This increase of some section sizes beyond the strength level improved the OCBF ductility to some extent. The SCBF continues in the same trend of the six-storey SCBF with the spread of buckling through the SCBF height without failure in the gravity load-resisting elements. As depicted by Figs. 4.13 and 4.14(a), it can be observed that the OCBF reached the storey collapse mechanism due to the buckling of a ground floor column following spread of brace buckling in the first three storeys which shows an improved ductile behavior compared to the six-storey OCBF. The failure sequence started by buckling of three braces at storey (1) (1, 2 and 3) followed by buckling of three braces at storey (2) (4, 5 and 5) and followed by buckling of three braces at storey (3) (6, 7 and 7). Finally, buckling of an internal column at storey (1) (marked as 8) took place leading to the formation of a storey collapse mechanism.

The nine-storey SCBF behaves in a similar way to the six-storey one where the failure sequence presented in Fig. 4.13 and Fig. 4.14(b) started by buckling of three braces at storey (1), (1, 1 and 2), followed by buckling of two braces at storey (2) (3 and 3) followed by buckling of one brace at storey (3) (marked as 4), followed by simultaneous buckling of three braces, one at storey (2) and two at storey (4) (all denoted as 5), followed by buckling of three braces at storey (4) (6, 6 and7), followed by buckling of three braces at storey (5) (8, 8 and 9), followed by buckling of three braces at storey (6) (10, 11 and 12). Finally, yielding of the remaining three braces at storey (1) (13, 14 and 15) leading to formation of failure mechanism at storey (1) because all storey braces have either buckled or yielded. By pushing the nine-storey OCBF and SCBF beyond the storey collapse limit till complete failure,

building collapse limit is reached. In view of Figs. 4.13 and 4.15(a), the OCBFs

failure sequence continued by simultaneous buckling of two columns at storey (1)

(denoted 9), followed by buckling of three braces at storey (4) (10, 11 and 12),

followed by yielding of three braces at storey (1) (13, 14 and 15), followed by

yielding of three braces at storey (2) (16, 17 and 18), followed by buckling of two

columns at storey (4) (19 and 20), followed by yielding of two braces at storey (3)

(21 and 22). Meanwhile, the SCBF in Figs. 4.13 and 4.15(b) responded in a similar

manner to its six-storey counterpart where failure scheme was distributed along the

SCBF height. Three braces buckled at storey (7) (16, 17 and 18), followed by

yielding of three braces at storey (2) (19, 19 and 20), followed by yielding of three

braces at storey (3) (21, 21 and 22), followed by yielding of three braces at storey (4)

(23, 24 and 24). At this stage, the building collapse limit was reached and a building

failure mechanism took place.
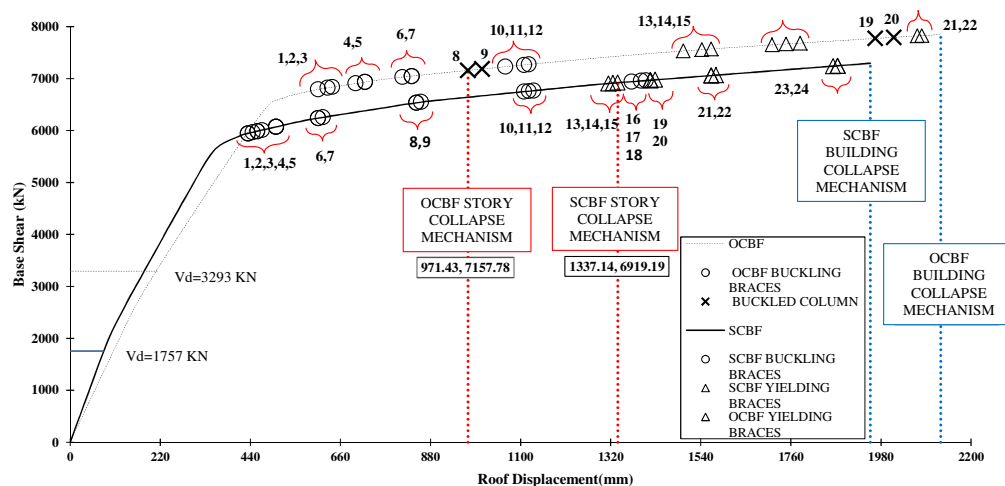
Figure 4.13: Pushover Response Curves for Nine-Storey OCBF and SCBF

(a) OCBF   (b) SCBF
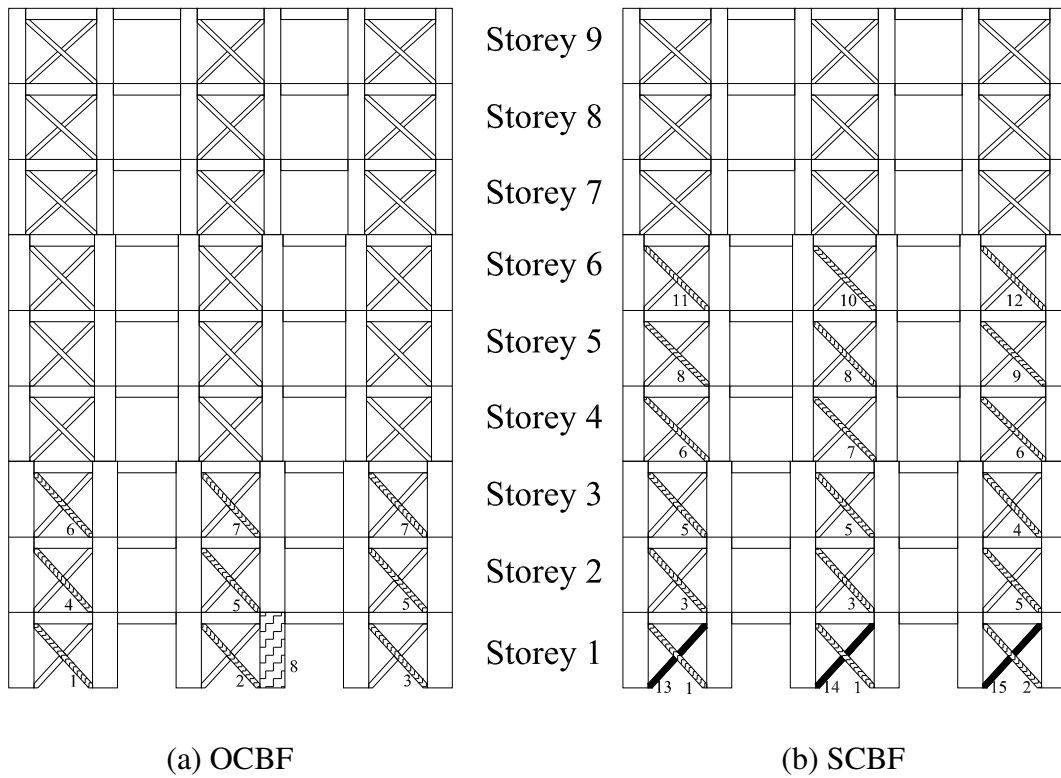
Figure 4.14: Failure Sequence of the Nine-Storey OCBF and SCBF Pushed to the Storey Collapse Limit

(a) OCBF   (b) SCBF

Figure 4.15: Failure Sequence of the Nine-Storey OCBF and SCBF Pushed to the Building Collapse Limit

The inter-storey drift ratios (IDR) for the nine-storey OCBF and SCBF are presented in Fig. 4.16 (a) and Fig. 4.16 (b) respectively.

(a) OCBF
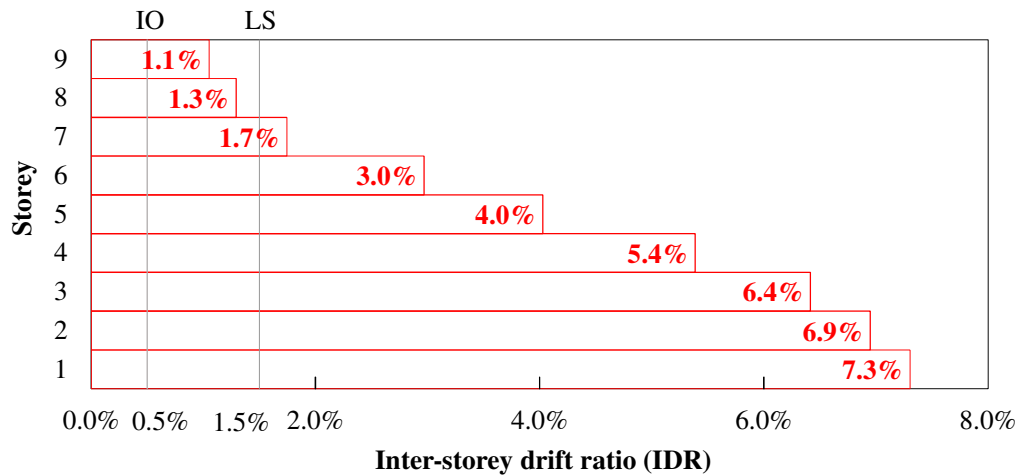
(b) SCBF

Figure 4.16: Inter-Storey Drift Ratio of Nine-Storey OCBF and SCBF at Storey Collapse Limit

Figure 4.16 (a) shows the variation of the IDR along the height of the nine-storey OCBF. It can be observed that the IDR of all storeys exceeded the IO and LS limits of FEMA 356 (2000) with a typical variation along the height with the maximum IDR of 4.75% at storey (1) and the minimum IDR of 2.01% at the top. Comparison between Fig. 4.16(a) and Fig. 4.12(a) reveals the improvement in the

performance of the nine-storey OCBF compared to its six-storey counterpart. The more ductile response of the nine-storey OCBF could be explained in view of the need to increase the members' sizes to satisfy the IDR limits as part of the strength design procedure. Meanwhile, the IDR profile for the nine-storey SCBF, shown in Fig. 4.16 (b), shows a typical profile with the highest IDR (7.3%) at the storey (1) where storey collapse limit was reached. This difference in maximum IDR values between OCBF (4.75%) and SCBF (7.3%) reflects the higher level of ductility attained by the SCBFs compared to OCBs of the same height.

4.6.3 Fifteen-Storey OCBF and SCBF Buildings

Inter-storey drift control governed the design of the fifteen-storey OCBF (54.0 m high) as at the strength design level, the ID values were significantly higher than the allowable code limits. As a result, almost all columns and braces sections were increased to satisfy the code's drift limit values. This considerable increase in columns and brace sections resulted in final OCBF design that is close to the capacity design of the SCBF. Thus, ductility of the OCBF was improved and similar failure sequence and mechanism to those of the SCBF may be expected. Starting with the OCBF, the failure sequence in Fig. 4.17 and Fig. 4.18(a) involved buckling of the brace elements in all braced bays starting at storey (1) until reaching storey (10) of the building (failing members were denoted 1 through 23). Finally, the three remaining braces at storey (1) yielded (24, 25 and 26) leading to the formation of storey collapse mechanism due to yielding/buckling of all braced bays at storey (1). A similar failure mechanism was observed for the SCBF where buckling of braces spread along the building height starting at storey (4) as depicted by the failure sequence shown in Figs. 4.17 and 4.18(b).

Following buckling of brace members marked (1 to 18), two elements (19 and 19), one yielded at storey (1) and the other buckled at storey (11), then another brace (20) buckled at storey (11), followed by yielding of two braces (21 and 22) at storey (1) which resulted in a storey collapse mechanism to take place. By pushing the fifteen-storey OCBF beyond the storey collapse limit, sequential brace yielding occurred (27 to 36) followed by buckling of three brace members (37, 38 and 39) at storey (11) as presented in Figs. 4.17 and 4.19(a). At this stage, the structure was unable to carry any additional lateral load and the building collapse mechanism was reached. Similarly, when the pushover process was continued on the fifteen-storey SCBF, one brace (23) buckled at storey (11) followed by yielding of eighteen brace members (24 to 36) at storeys (2) to (7) as shown in Figs. 4.17 and 4.19(b). The buckling of two braces (37 and 38) at storey (12) rendered the structure into a building collapse failure.
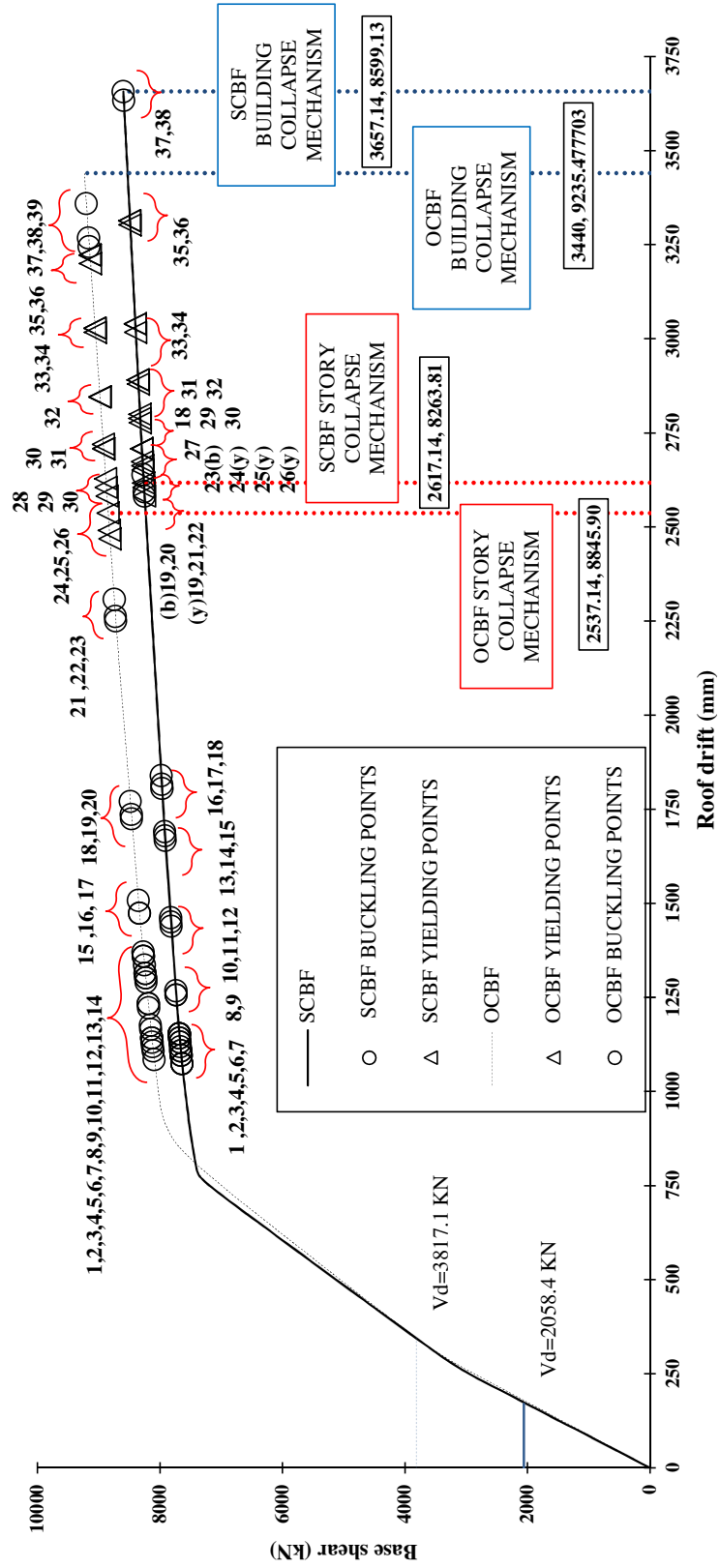
Figure 4.17: Pushover response curves for fifteen storey OCBF and SCBF

| | (a) OCBF | (b) SCBF |
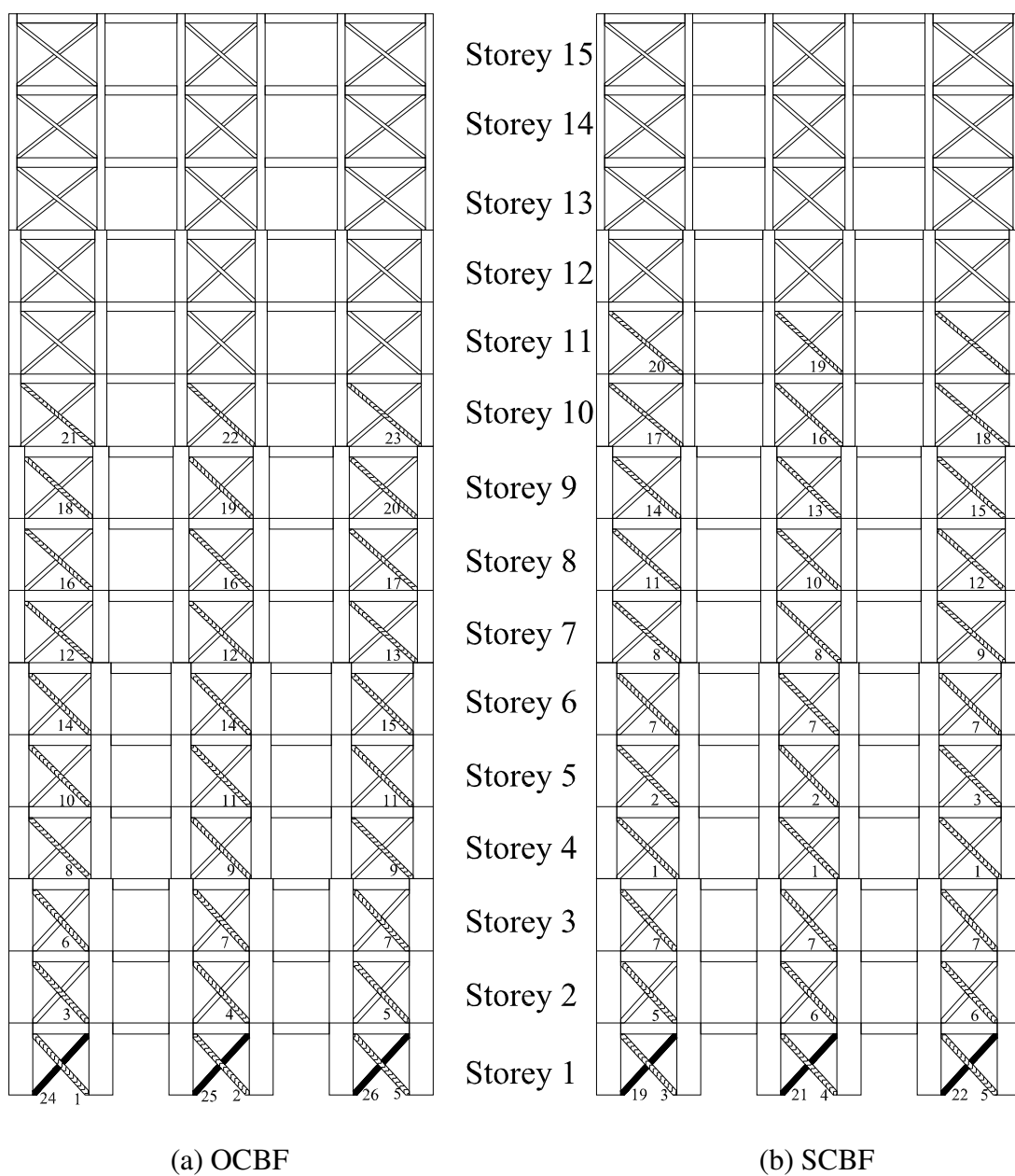
Figure 4.18: Failure Sequence of the Fifteen-Storey OCBF and SCBF Pushed to the Storey Collapse Limit
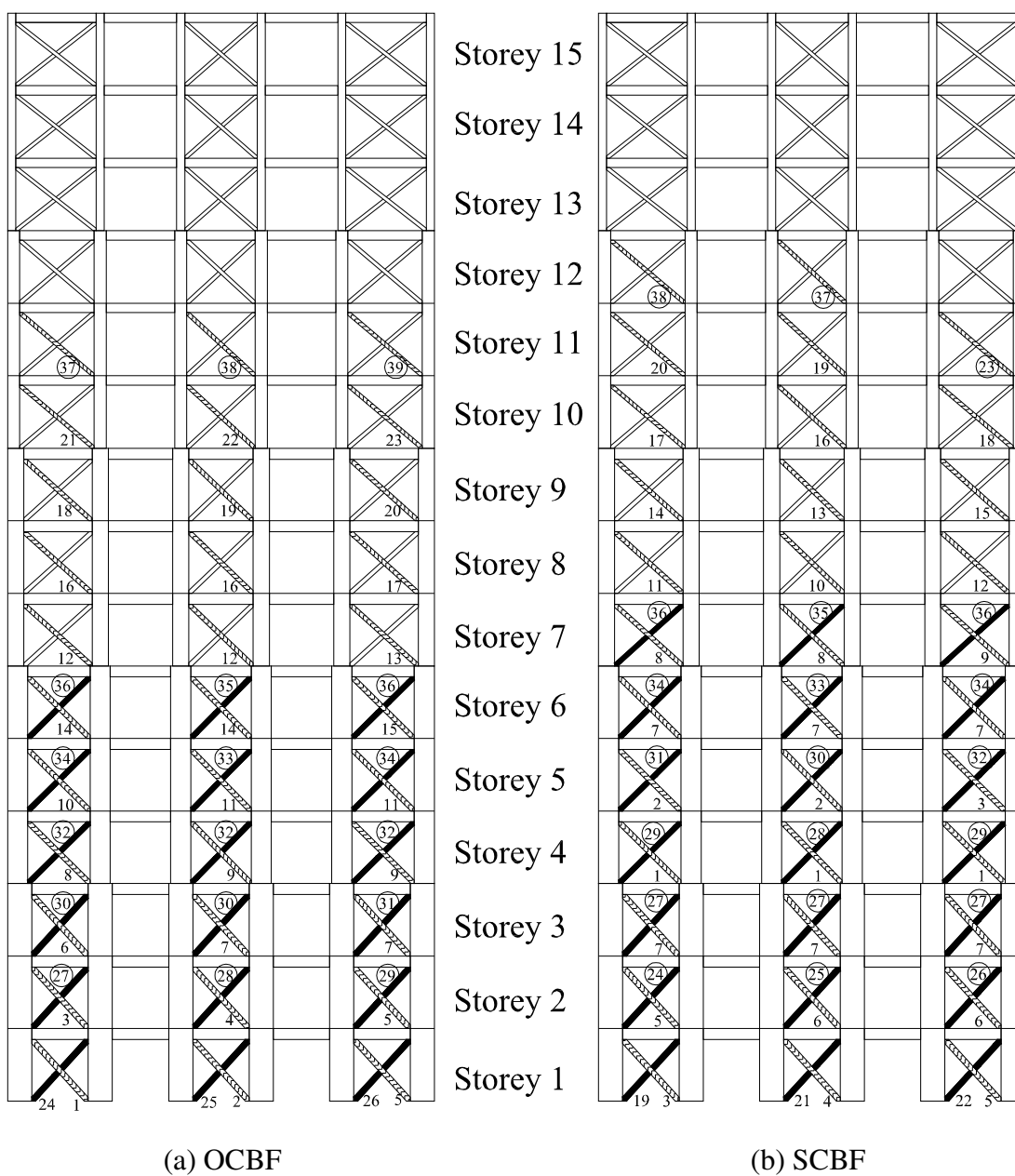
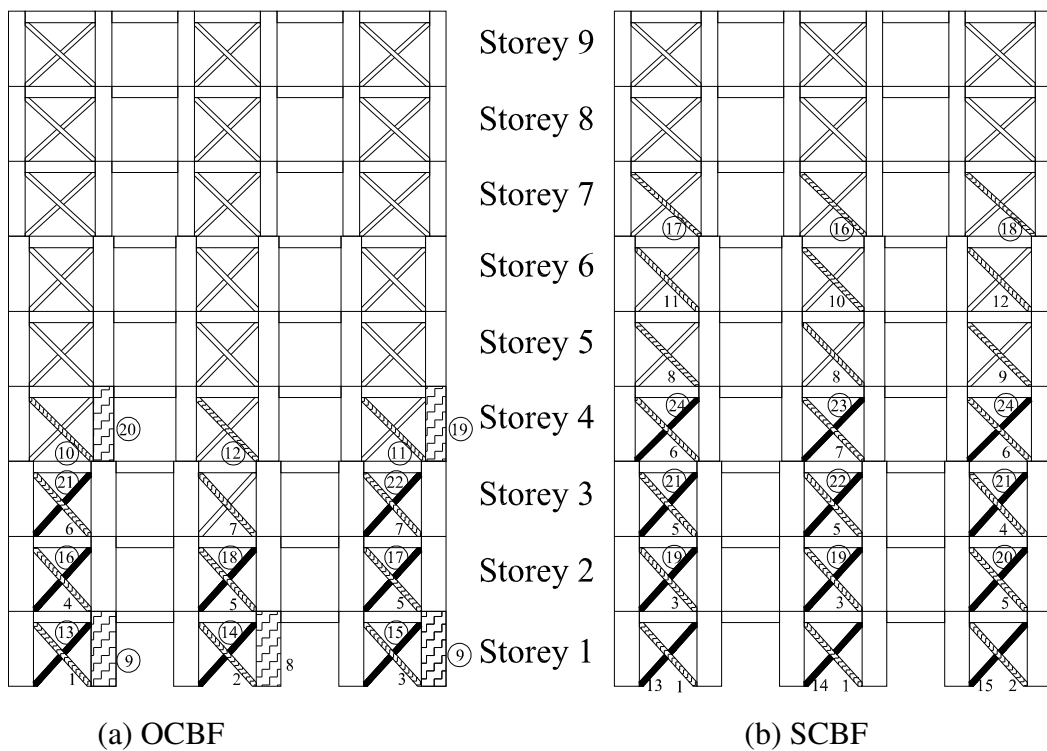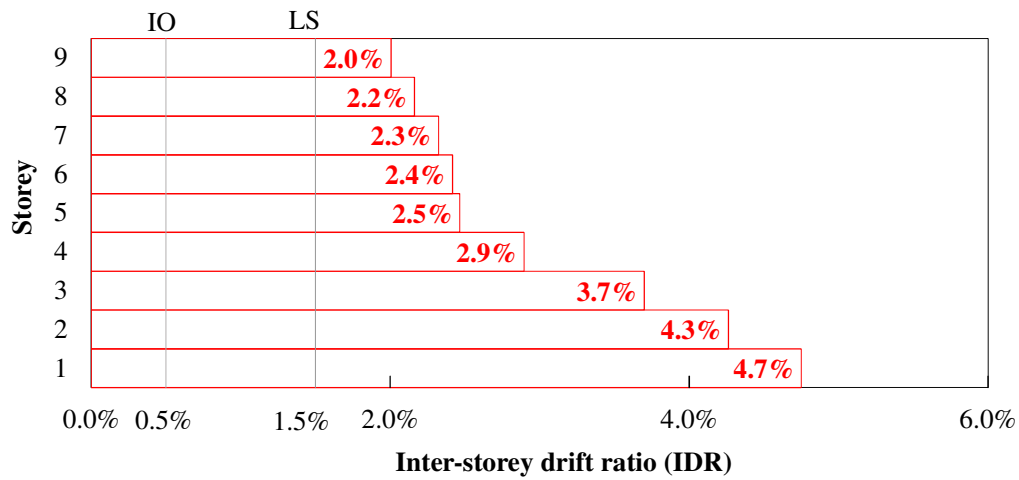(a) OCBF   (b) SCBF

Figure 4.19: Failure Sequence of the Fifteen-Storey OCBF and SCBF Pushed to the Building Collapse Limit

The inter-storey drift ratios (IDR) for the fifteen-storey OCBF and SCBF are presented in Fig. 4.20 (a) and Fig. 4.20 (b) respectively.
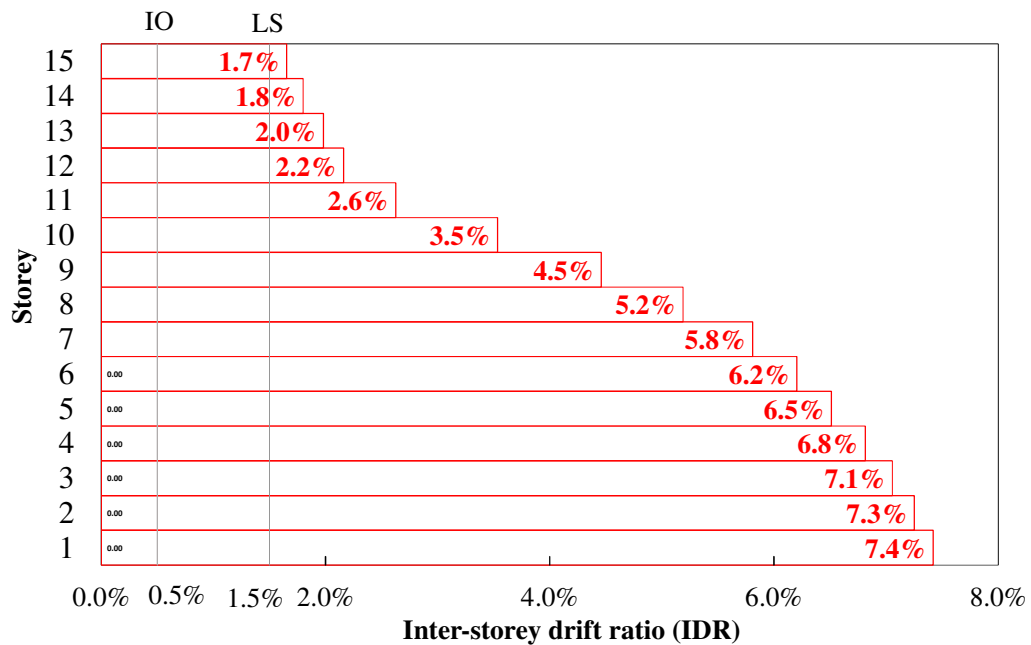
(a) OCBF
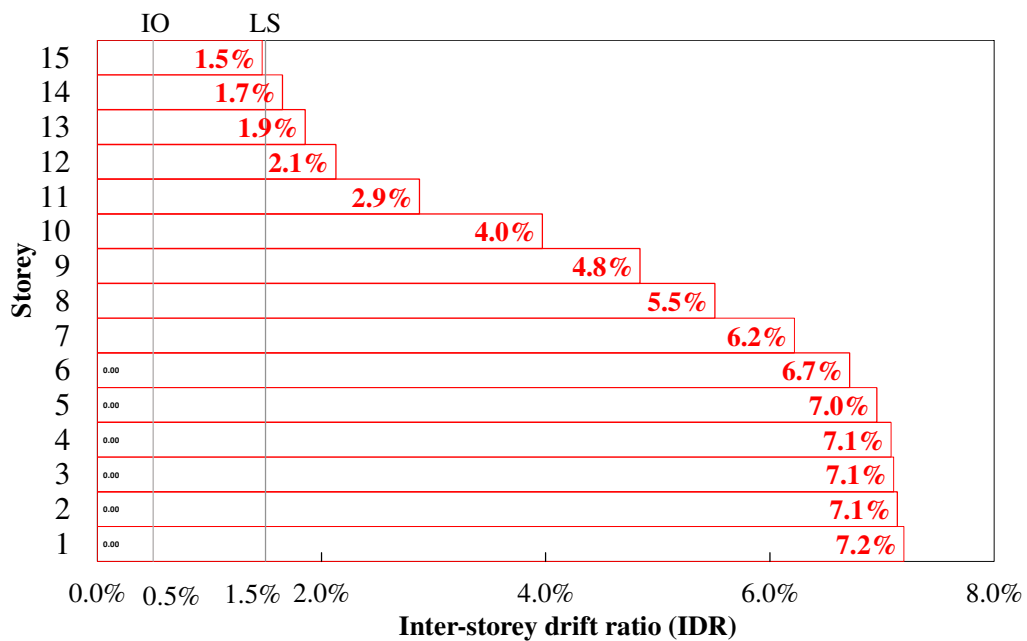
(b) SCBF

Figure 4.20: Inter-Storey Drift Ratio of Nine-Storey OCBF and SCBF at Storey Collapse Limit

Figures 4.20 (a) and (b) show similar IDR profiles with close values for the OCBF and SCBF, respectively. Both maximum IDR for OCBF (7.42%) and SCBF (7.19%) took place at storey (1) where the storey collapse limit was reached. As

discussed in section 4.6.2, the drift control requirements implemented during strength design of the OCBF improved its ductile behavior. The higher drift values associated with the increase in building height (fifteen-storey as compared to nine-storey in section 4.6.2) resulted in a considerable increase in the members sizes to satisfy the drift limits requirements. Thus, similar IDR profiles and values are obtained.

4.7 System Overstrength and Ductility of Steel CBFs

4.7.1 Overstrength of CBFs

The reserve strength in the structural system depends on several factors including the sizing of the structural members, structural redundancy, strain hardening of the construction material and participation of nonstructural elements. For all types of structural system, critical members are designed for worst case loading combinations. However, common construction practice necessitates that the resulting sections be used for other non-critical members in the system to reduce the variety of section sizes used in the project. In braced frame systems, overstrength evolves when compression braces buckle while additional forces are still needed to induce yielding in tension braces. Such redistribution of internal forces due to redundancy of the system leads to its overstrength. For a typical structural capacity curve (Fig. 4.21), an estimate of the overall structural overstrength Ω_o can be obtained as follows:

$$\Omega_o = V_m/V_d \tag{4.6}$$

V_m is the base shear carried by the system at a particular mechanism (storey or building)

V_d is the design base shear

Another method to estimate the overstrength Ω_o is the FEMA P695 (2009). It outlines a procedural methodology for reliably quantifying seismic performance factors, including the response modification coefficient (R), the system overstrength factor (Ω_o), and the deflection amplification factor (C_d). Proper implementation of this methodology in the seismic design process results in equivalent safety against collapse in an earthquake, comparable to the inherent safety against collapse intended by current seismic codes, for buildings with different seismic-force-resisting systems. Implementation of the methodology involves uncertainty, judgment, and potential for variation. The FEMA P695 (2009) methodology is intended for use with model building codes and standards to set minimum acceptable design criteria for code-approved seismic-force-resisting systems when linear design methods are applied. It also provides a basis for evaluation of current code-approved systems and their ability to meet the seismic performance intent of the code (NEHRP, 2010). Application of this methodology is beyond the scope of this thesis.
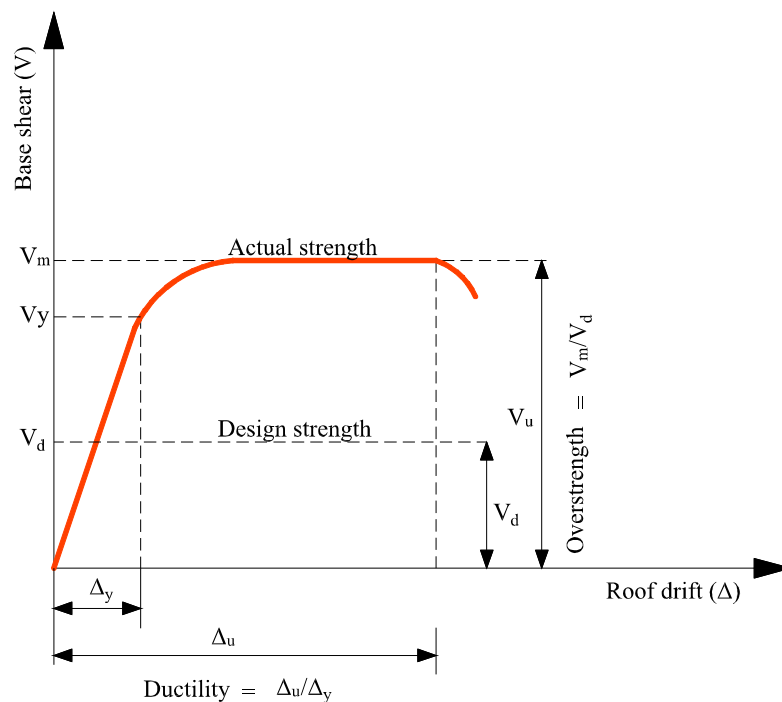
Figure 4.21: Typical Structural Response Envelope

Figures 4.9, 4.12 and 4.15 indicate that, for all six building models considered in this study, the base shear that corresponds to the first buckling of a column or a compression brace member is always higher than the design base shear, V_d, which results in overstrength factor greater than 1.0. Previous experimental investigations implied an overstrength factor of the order of 2.4 – 2.8 for six-storey braced steel frame (Uang and Bertero, 1986; Whitaker et al., 1989). Besides, a numerical study reported the overstrength factor due to internal force redistribution to be in the range of 1.5 to 2.1 for ten-storey braced steel frame (Rahgozar and Humar, 1998). It can be noted also that, for the particular case of six-storey frames, the capacity curve of the OCBF is significantly different from that of the SCBF. This difference becomes much less apparent with the increase in building height (i.e., for nine- and fifteen-storey buildings). This observation is due to the considerable similarity in cross sections sizes of the majority of the members constituting the nine- and fifteen-storey frames. This similarity arose from the need to resize most of the members of the nine- and fifteen-storey OCBFs to satisfy the drift limitation, which was not needed in the six-storey OCBF. The pushover capacity curves (Figs. 4.9, 4.13 and 4.17) were then used to estimate the overstrength factor Ω_o for each of the analyzed frames. Table 4.7 summarizes the calculated overstrength factors for the three heights of OCBFs and SCBFs.

Table 4.7: Overstrength Factors of Analyzed OCBFs and SCBFs

Number of Storeys	Overstrength Factor (Ω_o) associated with Storey Mechanism		Overstrength Factor (Ω_o) associated with Building Collapse Mechanism	
	OCBF	SCBF	OCBF	SCBF
6	1.59	3.96	1.91	4.23
9	2.17	3.94	2.38	4.15
15	2.32	4.01	2.42	4.18

For each frame, two overstrength factors were calculated corresponding to the storey mechanism and the building mechanism. The overstrength factor was obtained based on the ratio of the ultimate load (either at the formation of storey or building mechanism) to the design base shear value.

The results indicate that for OCBFs, triggering storey mechanism required lateral forces that are about 60 – 130% greater than those considered during design. The overstrength factors for the six-, nine-, and fifteen-storey are respectively 1.59, 2.17 and 2.32 implying the increase in overstrength with the increase in height of OCBFs. Meanwhile, forces 91 – 142% greater than design base shear are necessary to develop overall failure of the analyzed OCB frames. The corresponding overstrength factors for the six-, nine-, and fifteen-storey are respectively 1.91, 2.38 and 2.42 as shown in Table 4.7. All obtained values for the nine- and fifteen storey buildings exceed the system overstrength factor of 2.0 recommended by ASCE7-10 standards for OCBFs. Meanwhile, the ACSE7-10 requirements do not seem to be satisfactory for the six-storey OCBFs considered in the current study. The significant increase in the reserve strength when height increased from six to nine and fifteen storey could be attributed to the fact that sizing of the six storey building sections was solely based on strength design requirements. On the contrary, member sizes for the nine and fifteen storey frames were increased to satisfy drift limits as with increased height of buildings, the inter-storey drift values increased considerably and originally designed section sizes were found insufficient to satisfy the code drift limits. As a result, brace and column sections in the nine-storey and fifteen-storey CBFs were enlarged to reduce the drift values within acceptable limits. Such an increase in the members' size led to higher reserve strength in those frames. This conclusion is in agreement with the observations by Rahgozar and

Humar (1998) that the height of ductile CBFs contributes very little or nothing at all to the frame's reserve strength.

Obtained results of SCBFs, Table 4.7, show the need for lateral forces about 400% greater than design forces to cause storey mechanism in SCBFs, while a slightly higher ratio (not exceeding 423%) was needed to trigger the overall building collapse mechanism. The close values of reserve strength calculated for all heights of SCBFs was expected since the capacity design requirements necessitated increasing the sizes of the members in the SCBFs, irrespective of the frame height, from the original strength designed sizes. The considerable increase in the members' sizes led to an estimated reserve strength values that exceed twice as much the system overstrength factor of 2.0 specified by ASCE7-10 (2010) standards for SCBFs. Thus, the use of $\Omega_o = 2.0$ given by ASCE7-10 (2010) is expected to result in conservative design of SCBFs. It should be noted that the assessment of overstrength being conducted in this study is not intended to reestablish the overstrength factor that is addressed by FEMA P695 (2009).

4.7.2 Ductility of CBFs

The level of ductility is assessed by calculating the structural ductility factor μ defined by the ratio of the ultimate structural drift (Δ_u) to the displacement corresponding to the yield strength (Δ_y) using the relationship:

$$\mu = \Delta_u/\Delta_y \tag{4.7}$$

Values for Δ_u and Δ_y can be readily obtained from the pushover capacity curve. The yield displacement (Δ_y) is obtained by approximating the actual structural capacity curve to an idealized bilinear elasto-plastic curve. Two values are adopted to represent the ultimate drift (Δ_u) to represent the failure mode under

consideration. In other words, Δ_u is taken either as the drift value at which a storey mechanism is formed or that value associated with the building collapse event.

The pushover capacity curves presented in Figs. 4.9, 4.13 and 4.17 show that SCBFs yield before OCBFs since the cross sections sizes of SCBFs braces are always smaller than those of OCBFs having the same height. Table 4.8 reports the estimated ductility factors for the six-, nine- and fifteen-storey OCBFs and SCBFs.

Table 4.8: Structural Ductility of Analyzed OCBFs and SCBFs

Number of Storeys	Ductility Factor (μ) associated with Storey Mechanism		Ductility Factor (μ) associated with Building Collapse Mechanism	
	OCBF	SCBF	OCBF	SCBF
6	1.85	4.27	3.55	6.12
9	2.16	4.05	4.72	5.83
15	2.95	3.58	4.00	5.01

For the ductility associated with the formation of storey mechanism, tabulated results imply that the fifteen-storey OCBF shows more ductile behavior, followed by the nine-storey and then the six-storey frame. The relatively low ductility of the six-storey OCBF could be attributed to the rapid formation of storey collapse mechanism due to failure of an exterior column in the first storey shortly after the yielding of the system took place. For the fifteen-storey, drift control mandated increasing the size of several sections, which caused storey mechanism to occur at relatively higher load and displacement values. As a result, its ductility factor is higher than that of the six-storey OCBF. The response of the nine-storey OCBF lies in-between those of the six-storey and fifteen-storey buildings.

Unlike the case of OCBFs, ductility design provisions applied to SCBFs resulted in smaller brace sections than those utilized in OCBFs. As a result, a

decrease in the yield displacement with increasing building height took place leading to higher values of ductility factors for SCBFs than those of OCBFs. A similar behavior is observed for the ductility factors associated with the building failure mechanism of SCBFs where, for buildings with the same height, ductility factor of SCBF is higher than that of OCBF. Meanwhile, the ductility factor decreases with the increase in the number of storeys of SCBFs.

For the ductility of OCBFs associated with the building collapse mechanism, the relative values of yielding drift and global maximum drift depend on the type and location of the members their sections were enlarged to control the drift values at acceptable limits. Another controlling factor is the relative distribution of the brace member's sizes along the height of the building.

In general, the tabulated values indicate a significantly higher ductility factors, at the building collapse mechanism, of SCBFs compared to OCBFs of the same height. While this increase in ductility reaches 72% for six-storey frames, it is limited to about 24-25% for both nine- and fifteen-storey frames, respectively. This trend is more pronounced at the storey collapse mechanism where the ductility of the six-storey SCBFs is about 131% higher than its OCBF counterpart. This ratio becomes 88% for the nine-storey SCBF compared to OCBF of the same height. The ductility increase reaches only 21% for fifteen-storey SCBF relative to the building with OCBF.

4.8 Conclusions

This chapter focused on using non-linear static pushover analysis technique to explore the influence of changing the lateral load resisting system on the response

of steel braced frames having different heights. Two braced frame systems were considered in the study; namely OCBFs and SCBFs. Three buildings' heights were modeled and analyzed including six-, nine- and fifteen-storey steel braced frames. For each frame, two failure criteria were considered to represent potential levels of damage that could be induced in structural systems during earthquake events of various strength. Storey Collapse Mechanism was utilized to represent the state of a damaged structure that is repairable with a low probability of life-threatening injury as per FEMA Life Safety Performance Level (S-3). A more severe damage scenario was represented by the Building Collapse Mechanism that represents the ultimate state at which the entire structure loses its stability and becomes unable to withstand any additional loads. A finite element model was developed to simulate the behavior of the three building heights mentioned above when OCBF and SCBF are used as the lateral load resisting system of each building leading to a total of six model buildings to be considered. The accuracy of the finite element model was validated by comparing its predictions to relevant experimental measurements reported in the literature. Results of the pushover analyses reveal that SCBFs reach yield before their OCBFs counterparts due to the smaller brace sections used in SCBFs relative to those employed in OCBFs. Pushover capacity curves of six-storey buildings indicate considerably different response of OCBFs and SCBFs of these short buildings. This difference becomes less apparent in medium height (nine-storey and fifteen-storey) buildings. This observation was attributed to the relative similarity in section sizes of OCBFs and SCBFs in medium height buildings due to the need to enlarge the strength designed sections of OCBFs to satisfy drift limits requirements.

Estimated overstrength factors of analyzed models indicate the increase in overstrength with increasing the height of OCBFs. The overstrength factors associated with the storey mechanism of the six-, nine-, and fifteen-storey OCBF buildings are 1.59, 2.17 and 2.32, respectively. Higher values (1.91, 2.38 and 2.42, respectively) are found to correspond to overall building collapse. The considerable increase in the estimated reserve strength when height increased from six to fifteen storey is attributed to the fact that sizing of the six-storey building sections was solely based on strength design requirements, while those of the nine- and fifteen-storey frames were enlarged to meet the drift limits. The obtained reserve strength values for nine- and fifteen-storey buildings satisfy the ASCE7-10 recommended overstrength value of 2.0 for OCBFs. However, this recommendation may not lead to safe designs of six-storey OCBFs.

Overstrength factors of SCBFs had a narrow range of variation for different heights (3.96 to 4.01) to reach a storey mechanism and (4.15 to 4.23) to trigger an overall building collapse mechanism. The close values of reserve strength calculated for all heights of SCBFs were expected since the capacity design requirements led to increasing the sizes of the members in the SCBFs from their original strength-design sizes irrespective of the frame height. The estimated reserve strength factors are more than double the system overstrength factor of 2.0 specified by ASCE7-10 standards for SCBFs indicating the conservative approach adopted by the ASCE7-10 for designing SCBFs.

The level of ductility shown by all analyzed models was also explored in the current investigation. The results imply that the level of ductility achieved by SCBF is significantly higher than that of OCBF of the same height. For short buildings

(six-storey model), the ductility of SCBF is about 131% and 72% higher than that of the OCBF at the storey and building collapse mechanisms, respectively. For medium height buildings (nine-storey model), the ductility of SCBF is about 88% and 24% higher than that of the OCBF at the storey and building collapse mechanisms, respectively. Meanwhile, for tall buildings (fifteen-storey model), the ductility of SCBF reached around 21% and 25% higher than that of the OCBF at the storey and building collapse mechanisms, respectively. These comparisons indicate that the influence of changing the lateral load resisting system from OCBF to SCBF on the level of ductility is less pronounced as the height of the building increases. At the meantime, the ductility of building with SCBFs is always higher than that of buildings with OCBFs. This observation confirms the importance of adopting the ductility design provisions provided by the code for SCBFs to attain lateral load resisting systems with high level of ductility.

The inter-storey drift ratio (IDR), at the storey collapse limit, of the six-storey OCBF exceeded the IO (Immediate Occupancy) and LS (Life Safety) limits recommended by FEMA 356 (2000) with the exception of storey (1) that did not exceed the LS limit. This behavior is attributed to the formation of storey collapse mechanism due to failure of one of columns in storey (1). Meanwhile, the IDR of the six-storey SCBF showed a typical profile in which the maximum IDR taking place at the storey (1) with a decreasing trend towards the top of the building. For the nine-storey OCBF, the IDR of all storeys exceeded the IO and LS limits of FEMA 356 (2000) with a typical variation along the height with the maximum IDR of 4.75% at storey (1) and the minimum IDR of 2.01% at the storey (9). The drift control requirements implemented during strength design of the OCBF improved its ductile

behavior compared to the six-storey OCBF. A similar IDR profile is obtained for the nine-storey SCBF with a more ductile behavior relative to its OCBF counterpart as evident by the higher IDR value of 7.3% at the top of the nine-storey SCBF. Almost identical IDR profiles are observed for the fifteen-storey OCB and SCB frames. Both maximum IDR for OCBF (7.42%) and SCBF (7.19%) took place at storey (1) where the storey collapse limit was reached. Similar to the nine-storey OCBF, the drift control requirements improved the ductile behavior of the OCBF. The higher drift values associated with the fifteen-storey as compared to the nine-storey OCBF led to a significant increase in the members' sizes to satisfy the drift limits requirements. As such, similar IDR profiles and values are obtained for the fifteen-storey OCBF and SCBF.

Chapter 5: Time History Analysis of Steel Concentrically Braced Frames (CBFs)

5.1 Introduction

The seismic response of a structural system depends on the system type and details and the dynamic characteristics of the applied ground motion. For the latter, the frequency content and magnitude of the earthquake have significant impact on the level of seismic damage induced in the system. As a result, it is crucial to simulate not only the structural system configuration, but also the main characteristics of the applied excitation to correctly predict the seismic performance and response of the analyzed system. Incorporating the variability and randomness inherent in many of these factors in the analysis is a challenging task, especially when the anticipated response is largely inelastic. Dynamic time history analysis is an efficient and reliable approach for assessing the seismic capacity of structures. The time history analysis technique relies on subjecting the structure to a specific record of earthquake ground motion to determine its response (such as: drift, base shear, internal forces and deformations) as a function of time. Estimating the response with sufficient accuracy requires careful incorporation of inelastic characteristics such as energy dissipation and strength degradation. In modern design codes, building systems are expected to deform well into the inelastic region under severe earthquakes. The braced frames used in this chapter will be the SCBFs as Chapter 4 showed that the SCBFs are more ductile, have better overstrength and offer more flexibility for use in seismic design category (SDC) D. Additionally, there is strict limitations on the use of OCBFs in SDC D for building height that exceeds 35 ft.

5.2 Structural Damping

Damping is the dissipation of energy from an oscillating system, primarily through friction. All structures have their own unique ways of dissipating kinetic energy, and in certain designs, mechanical systems known as dampers can be installed to increase the overall damping rate of the structure. There are several sources of damping in structures (Lindeburg and Mcmullin, 2011; Chopra 2012), including:

Hysteretic damping represents the energy dissipated internally during cyclic straining that takes place when the structure yields during reversals of the load.

Body-friction damping (Coulomb damping) is a non-hysteretic damping that results from friction between two dry surfaces such as members in contact or various elements constituting a structural joint. Friction between structural members and non-structural elements (such as masonry walls or partitions) is also considered as body-friction damping.

Radiation damping occurs as a structure vibrates and becomes a source of energy itself. Some of the energy is reradiated through the foundation back into the ground.

Viscous damping is the mode of energy dissipation arising from the thermal effect of repeated elastic straining of the material and from the internal friction when a solid element is deformed. The corresponding damping force is linearly related to the velocity. Although this particular damping mode is not a major damping mechanism in structures, it is used to express the overall structural damping due to its simple mathematical form. Therefore, the structural damping resulting from several energy dissipating mechanisms is referred to as equivalent viscous damping. According to

this idealization, the total damping force experienced by the structure (f_D) can be readily calculated by multiplying the equivalent viscous damping coefficient (c) by the corresponding velocity ($\dot{x}$) as shown in Eq. (5.1)

$$f_{D=}c\dot{x} \tag{5.1}$$

The particular value of the equivalent viscous damping coefficient (c) that brings the system to equilibrium in a minimum time without oscillation is referred to as the critical damping coefficient ($c_{critical}$). The ratio of the actual damping coefficient to the critical damping coefficient is known as the damping ratio and is given by:

$$\zeta = \frac{c}{c_{critical}} \tag{5.2}$$

In the SeismoStruct software (2012), hysteretic damping is implicitly included within the nonlinear fiber model formulation of the inelastic elements. The average estimate of this damping source is about (0.5%) for Steel structures. Meanwhile, the non-hysteretic damping from all other dissipation sources is modeled using the traditional Rayleigh damping model proportional to the initial stiffness matrix. A damping ratio of (1.5%) is utilized in the current study to represent the damping exerted by the non-hysteretic sources (Clough and Penzien, 2003; Tedesco, 1999)

5.3 Selection of Ground Motion Records

The United Arab Emirates is situated in the Arabian plate, which is classified as a stable region with low seismic activity (Fenton et al., 2006). Corresponding earthquakes are classified as near-fault moderate ground motions with a short distance from the epicenter. On the other hand, the Arabian plate is surrounded by many active tectonic faults that cause the major seismic hazard in the UAE. These

active boundaries include Zagros and Zindan-Minab faults and Makran subduction zone (Kaviani et al., 2007; Rajendran et al., 2013). The presence of these surrounding active fault lines is associated with far-field severe events with a long distance from the epicenter. These two distinct scenarios are taken into consideration in the current study by selecting various earthquake records that represent both loading situations. The ASCE7-10 standards (section 16.2.3) state the need for a set of not less than three appropriate ground motions when conducting nonlinear time history analysis. In the current study, eight natural earthquake records are selected to conduct the dynamic analysis (Mwafy et al., 2006; Issa and Mwafy, 2013). The main characteristics of the chosen records are presented in Table 5.1. The first four records represent near-fault local moderate earthquakes with a short distance from the epicenter (not exceeding 25 km). Meanwhile, the last four records correspond to far-field severe events with a long distance from the epicenter (more than 50 km). This scenario is most likely to occur as a result of regional strong earthquakes.

Another factor that is considered in classification of the records selected in this study is the ratio of peak ground acceleration to peak ground velocity (a/v). The first four sets of records correspond to high (a/v > 1·2 g/(m/s)) while the last four events have low (a/v < 0·8 g/(m/s)) (Zhu et al., 1988). It should be noted that the (a/v) ratio accounts for many seismo-tectonic and site characteristics of earthquake ground motion records. For instance, low (a/v) ratios correspond to earthquakes with long periods, long epicentral distances, long duration and medium-to-high magnitudes. On the contrary, high (a/v) ratios represent short periods, short epicentral distance, shorter durations and small-medium magnitudes (Sawada et al., 1992).

Table 5.1: The Eight Ground Motions Considered in the Current Study

Designation.	Earthquake	Station	Comp.	Date	Magnitude (M_w)	Site Class	Epicentre Distance (km)	Duration (Sec.)	PGA (m/s^2)	A/V (g/(m/sec))
EQ1	Basso Tirreno, Italy	Naso	NS	15-04-1978	6.10	v. dense	18	34	1.47	1.87
EQ2	Preveza, Greece	OTE building-NS	NS	10-03-1981	5.45	v. dense	28	20	1.41	1.60
EQ3	Lazio Abruzzo, Italy	Cassino-Sant Elia	EW	07-05-1984	5.93	stiff	16	30	1.12	1.59
EQ4	Umbria Marchigiano, Italy.	Castelnuovo-Assisi	NE	26-09-1997	6.04	stiff	22	45	1.60	1.25
EQ5	Chi-Chi, Taiwan	TAP017	E	20-09-1999	7.62	stiff	148	151	1.12	0.53
EQ6	Chi-Chi, Taiwan	ILA030	E	20-09-1999	7.62	stiff	136	90	1.16	0.43
EQ7	Loma Prieta, USA	Emeryville	260	18-10-1989	6.93	v. dense	96.5	39	2.45	0.57
EQ8	Loma Prieta, USA	Oakland	0	18-10-1989	6.93	stiff	94	40	2.75	0.67

As depicted by Table 5.1, the selected near-fault records have a magnitude (M_w) that ranges from 5.45 to 6.10, stiff and very dense soil classes, a PGA ranging from 1.12 to 1.60 m/s^2 with high a/v ratio. Meanwhile, for far-field records, a magnitude (M_w) range of 6.93 to 7.62, stiff and very dense soil classes, a PGA range of 1.12 to 2.75 m/s^2 with low a/v ratio are considered.

In seismic design codes, the design earthquake load is usually defined based on a 10% probability of exceedance in 50 years (i.e., 0.002 probability of a single exceedance per year), which corresponds to a 475 years return period. Most of the available studies focused on assessing the seismic hazard of Dubai and reported estimates of Peak Ground Acceleration PGA (related to a return period of 475 years) as summarized in Table 5.2.

Table 5.2: PGA Values Reported by Research Studies for Dubai

Study	PGA
Grunthel et al. (1999)	0.32g
Abdalla and Al-Homoud (2004)	0.15g
Sigbjornsson and Elnashai (2006)	0.16g
Mwafy et al. (2006)	0.16g
Peiris et al. (2006)	0.06g
Aldama-Bustos et al. (2009)	0.05g
Shama (2011)	0.17g
Khan et al. (2013)	0.047g

It should be noted that studies that reported low PGA values (0.047g to 0.06g) either did not consider the effect of the surface soil strata or disregarded some local sources of earthquakes, which could underestimate the seismic hazard of the studied area leading to un-conservative evaluation of the structural response. These

factors were not omitted in the studies that recommended very close estimates of PGA (0.15g to 0.17g). On the contrary, the PGA value of 0.32g provided by Grunthel et al. (1999) could be overestimated since it was reckoned and extrapolated from the calculated hazard at Dead Sea and Zagros area without performing actual seismic hazard analysis for sites in the UAE. Meanwhile, few published studies estimated the seismic hazard of Abu Dhabi. The available estimates of PGA for Abu Dhabi (for 475 years return period) are presented in Table 5.3.

Table 5.3: PGA Values Reported by Research Studies for Abu Dhabi

Study	PGA
Grunthel et al. (1999)	0.24g
Abdalla and Al-Homoud (2004)	0.10g
Peiris et al. (2006)	0.05g
Aldama-Bustos et al. (2009)	0.04g
Khan et al. (2013)	0.035g

In view of the previous discussion related to seismicity of Dubai, the last three recommended PGA values (0.035g to 0.05g) are not considered in the current study as they could lead to un-conservative evaluation of the structural response. A reliable estimate, based on consistency of values for Dubai, could be the PGA = 0.10g reported by Abdalla and Al-Homoud (2004). To ensure a higher level of conservatism in the outcomes of the current study, a higher PGA value will be adopted by averaging the 0.10g with the 0.24g recommended by Grunthel et al. (1999). Hence, a representative PGA value of 0.17g, corresponding to a 10% probability of exceedance in 50 years, is employed in the current study as a conservative measure of seismic activity in Abu Dhabi. The selected records (Table

5.1) are scaled to a PGA level of 0.17g before being applied to the model buildings. Figures 5.1 and 5.2 show the acceleration histories of the scaled near-fault and far-field records, respectively.

(a) Basso Tirreno (EQ1)

(b) Preveza (EQ2)

(c) Lazio Abruzzo (EQ3)

(d) Umbria Marchigiano (EQ4)
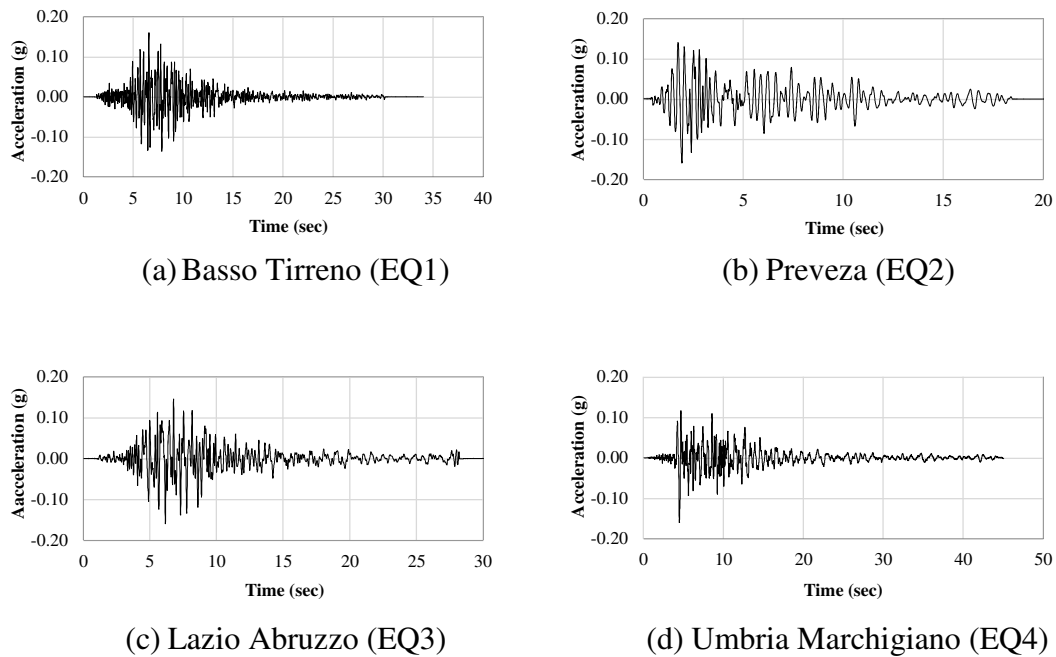
Figure 5.1: Scaled acceleration histories of near-fault records

(a) Chi-Chi TAP017 (EQ5)

(b) Chi-Chi ILA030 (EQ6)

(c) Loma Prieta (Emeryville) (EQ7)

(d) Loma Prieta (Oakland) (EQ8)
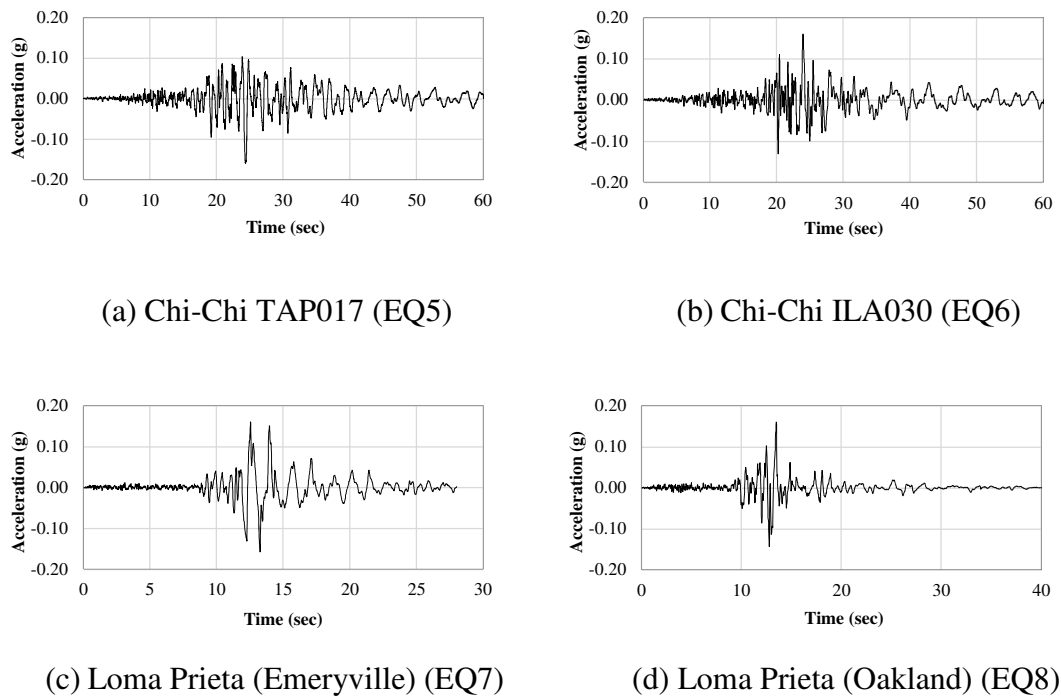
Figure 5.2: Scaled Acceleration Histories of Far-Field Records

The corresponding spectral accelerations for the scaled near-fault earthquake records are shown in Fig. 5.3 along with Abu Dhabi and Dubai design response spectra for seismic design categories (SDC) C and D. The comparison indicates that the near-fault records match the IBC (2012) response spectrum in the short period range. Similarly, a comparison between the spectral accelerations for the scaled far-field input ground motions and Abu Dhabi and Dubai design response spectra (SDC C and D) is presented in Fig. 5.4. It is evident from the comparison that the far-field records match the long period segment of the IBC (2012) response spectrum.
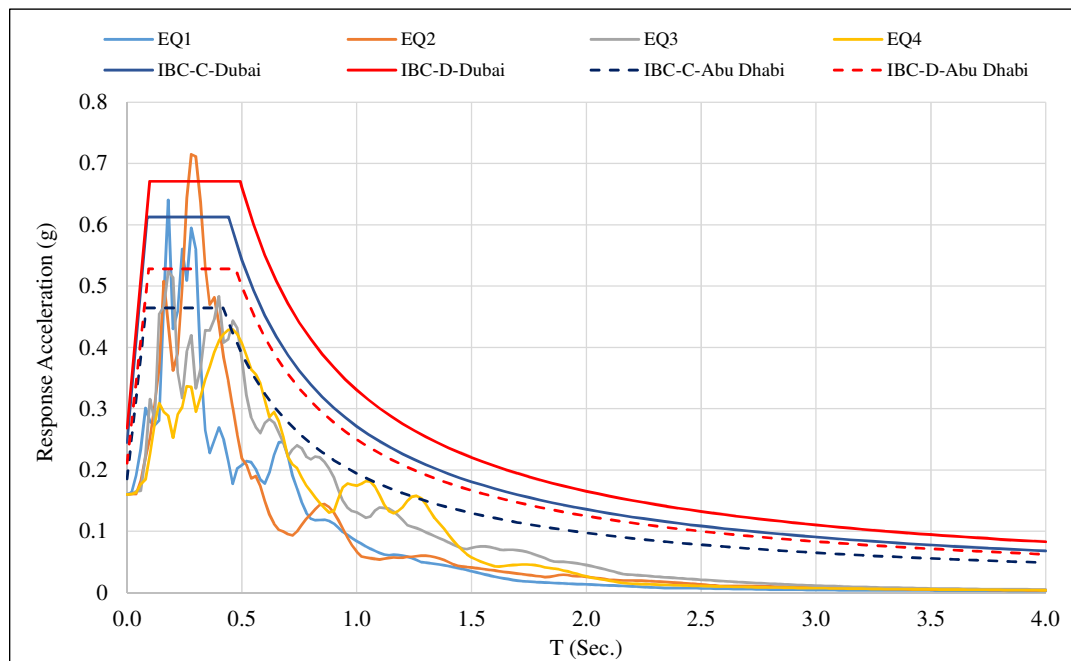
Figure 5.3: Response Spectra of Near-Fault Earthquake Records and the Current Design Spectra for Abu Dubai and Dubai (SDC C and D)
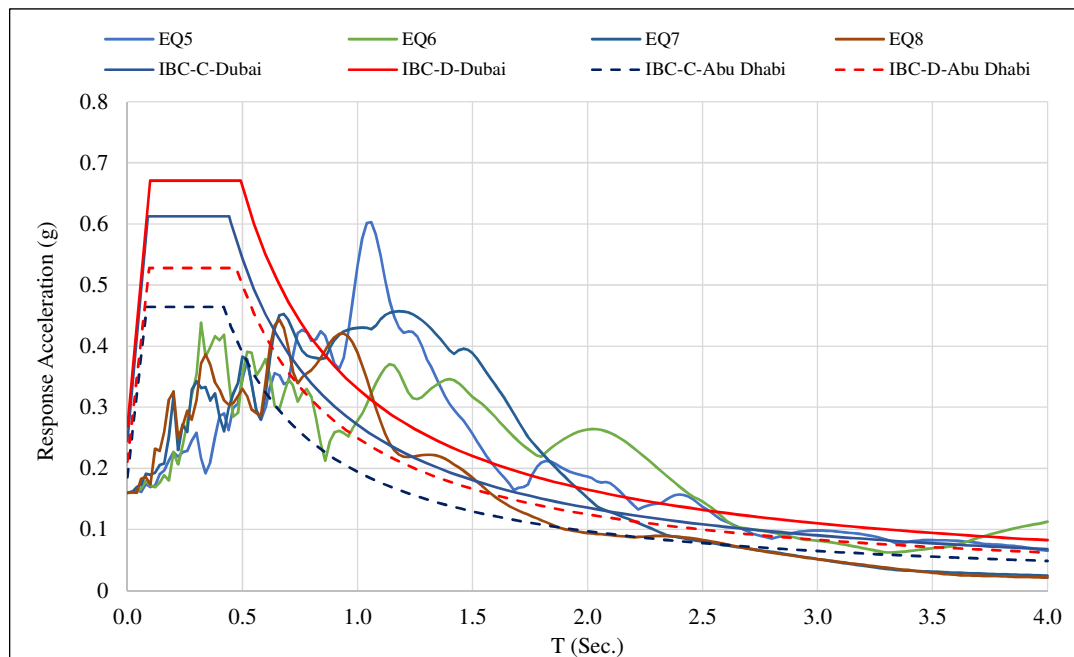
Figure 5.4: Response Spectra of Far-Field Earthquake Records and the Current Design Spectra for Abu Dubai and Dubai (SDC C and D)

5.4 Dynamic Response History of SCBF's

The finite element software SeismoStruct (2012) is used to conduct time history analysis of the six-, nine- and fifteen-storey SCBFs introduced in Chapter 4. Three basic sets of information need to be defined to enable obtaining the dynamic response history namely; the earthquake ground motion records, the CBF's natural periods and the damping ratio. In this study, the Hilber-Hughes-Taylor integration scheme is employed along with a time step size of 0.01 second in order to solve the system of equations of motion. A series of Eigenvalue (modal) analyses are conducted for the six-, nine- and fifteen-storey SCBF's to find the natural frequencies and the associated mode shapes. Results of the free vibration analyses reveal that the dynamic response of these frames is dominated by their fundamental mode of vibration with slight contribution from higher modes. This is evident by the mass participation ratios and frequencies of the first, second and third mode of

vibration summarized in Table 5.4. The mode shapes associated with the first three

modes of vibration of all analyzed SCBFs are shown in Fig. 5.5.

Table 5.4: Results of Eigenvalue Analyses

Building/Mode		Period (sec.)	Mass Participation Ratio (%)
Six-Storey Frame	Mode 1	0.784	80.60 %
	Mode 2	0.260	14.06 %
	Mode 3	0.142	3.34 %
Nine-Storey Frame	Mode 1	1.176	76.01 %
	Mode 2	0.388	16.16 %
	Mode 3	0.205	4.00 %
Fifteen-Storey Frame	Mode 1	1.957	70.70%
	Mode 2	0.618	18.49%
	Mode 3	0.316	4.96%

| 6 ST. SCBF | T1=0.784 sec | T2=0.260 sec | T3=0.142 sec |
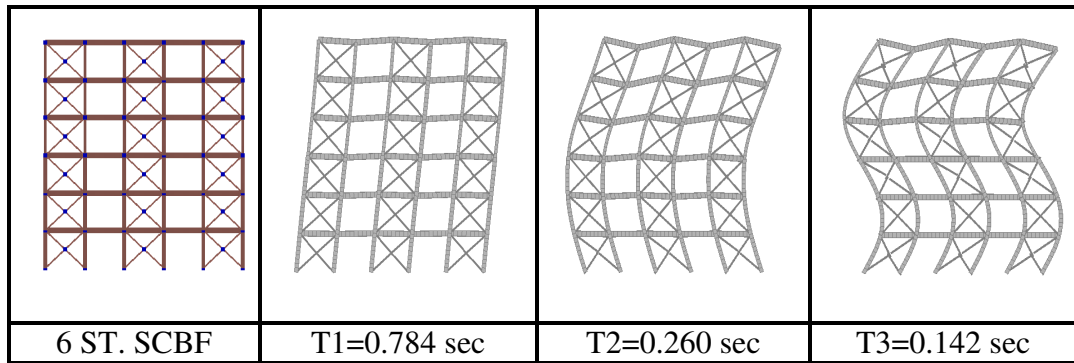
(a) Three fundamental mode shapes of the six-storey SCBF

| 9 ST. SCBF | T1=1.176 sec | T2=0.388 sec | T3=0.205 sec |
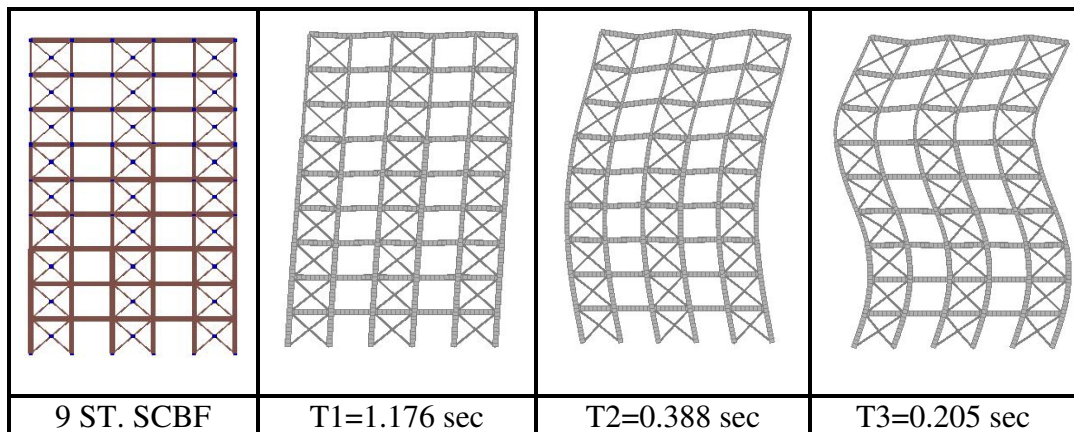
(b) Three fundamental mode shapes of the nine-storey SCBF

| 15 ST. SCBF | T1=1.957 sec | T2=0.618 sec | T3=0.316 sec |
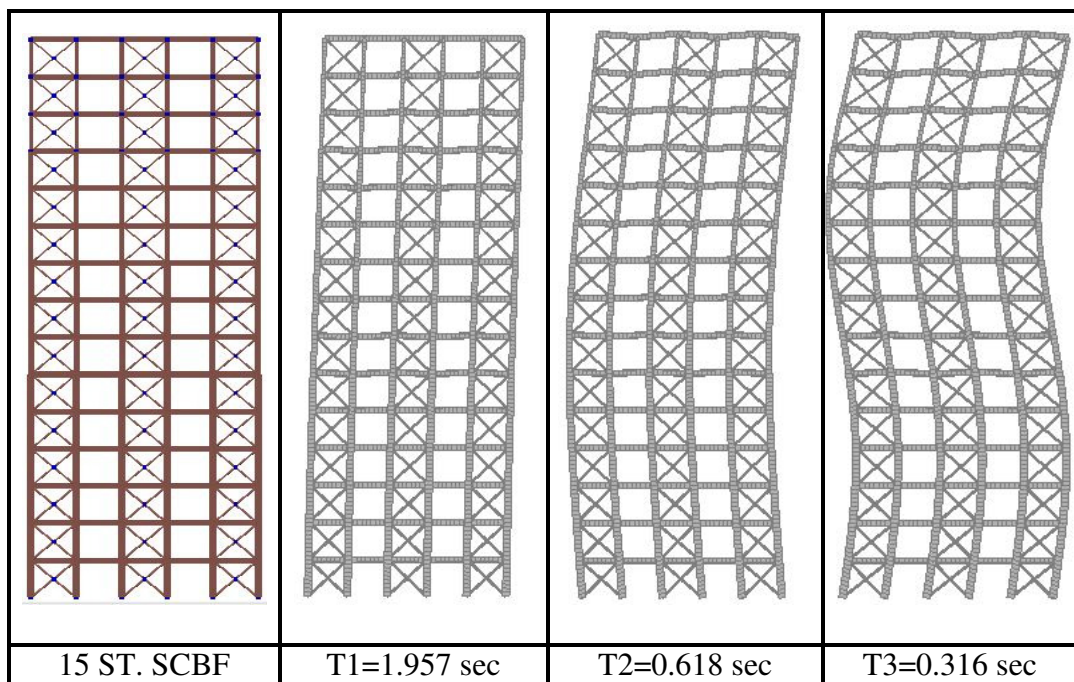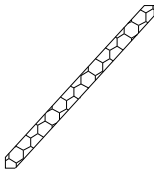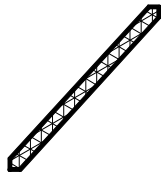
(c) Three fundamental mode shapes of the fifteen-storey SCBF

Figure 5.5: Modal Analyses Results for the Six-, Nine- and Fifteen-Storey SCBFs

5.5 Damage Schemes of the Analyzed SCBFs

This section discusses the results of the time history analyses by presenting the sequence of spreading of damage and reporting the sequence of maximum deformation in affected members in the six-, nine- and fifteen-storey SCBFs for the scaled ground motion records. The type of damage is presented on the elevation of each of the analyzed SCBFs using symbols and notations as shown in Fig. 5.6.

Notations for Structural members	
*MDT's figure : Compression damaged brace will be filled with honey combs hatch.	*MD's figure : Compression damaged brace will be filled with net hatch.

* Refer to Section 5.6.1 for detailed explanation of MDT and MD indicators.

Figure 5.6: Damage Symbols for Braces

5.5.1 Six-Storey SCBF Building

A series of time history analyses was conducted for the six-storey SCBF under the effect of the eight scaled ground motion records summarized in Table 5.1. Figures 5.7 and 5.8 show the recorded response (base shear and roof drift measured relative to the building base) under the eight ground motion records.
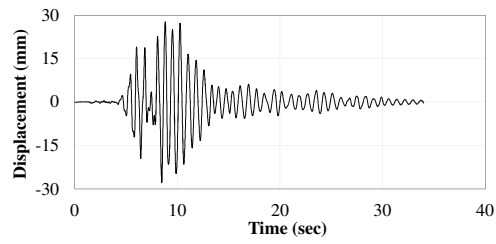
(a) Roof drift (EQ1)
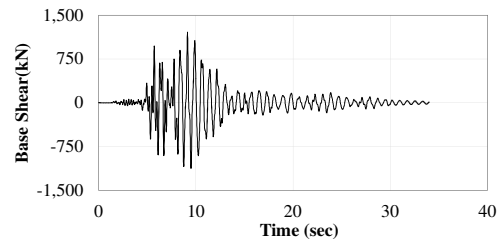
(b) Base shear (EQ1)
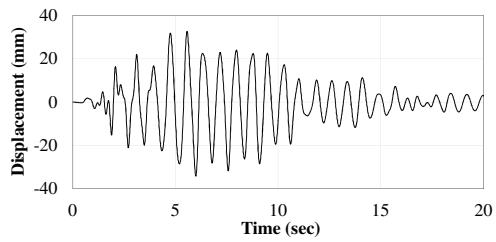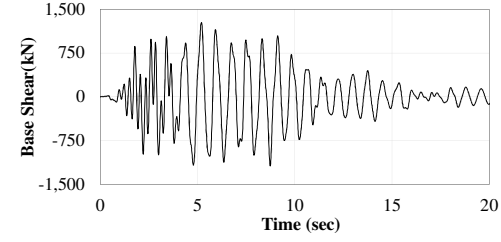
(c) Roof drift (EQ2)
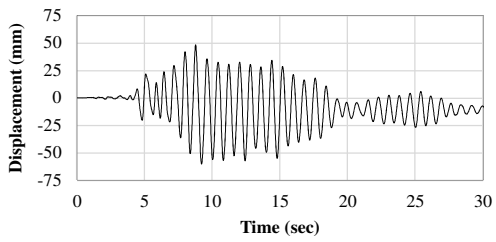
(d) Base shear (EQ2)
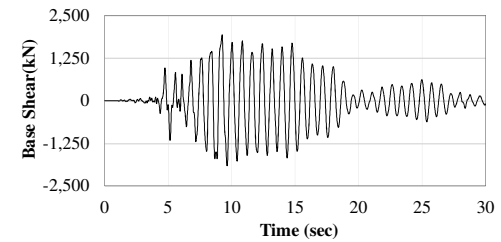
(e) Roof drift (EQ3)
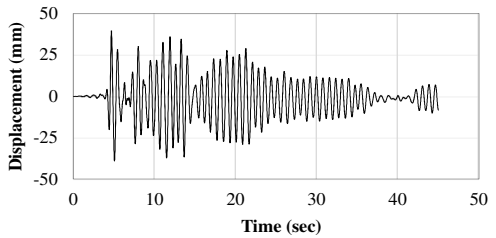
(f) Base shear (EQ3)

(g) Roof drift (EQ4)
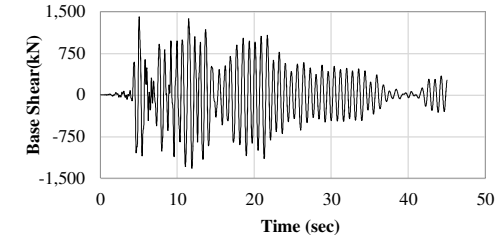
(h) Base shear (EQ4)

Figure 5.7: Response of the Six-Storey SCBF to Near-Fault Records

(a) Roof drift (EQ5) (b) Base shear (EQ5)

(c) Roof drift (EQ6) (d) Base shear (EQ6)

(e) Roof drift (EQ7) (f) Base shear (EQ7)

(g) Roof drift (EQ8) (h) Base shear (EQ8)
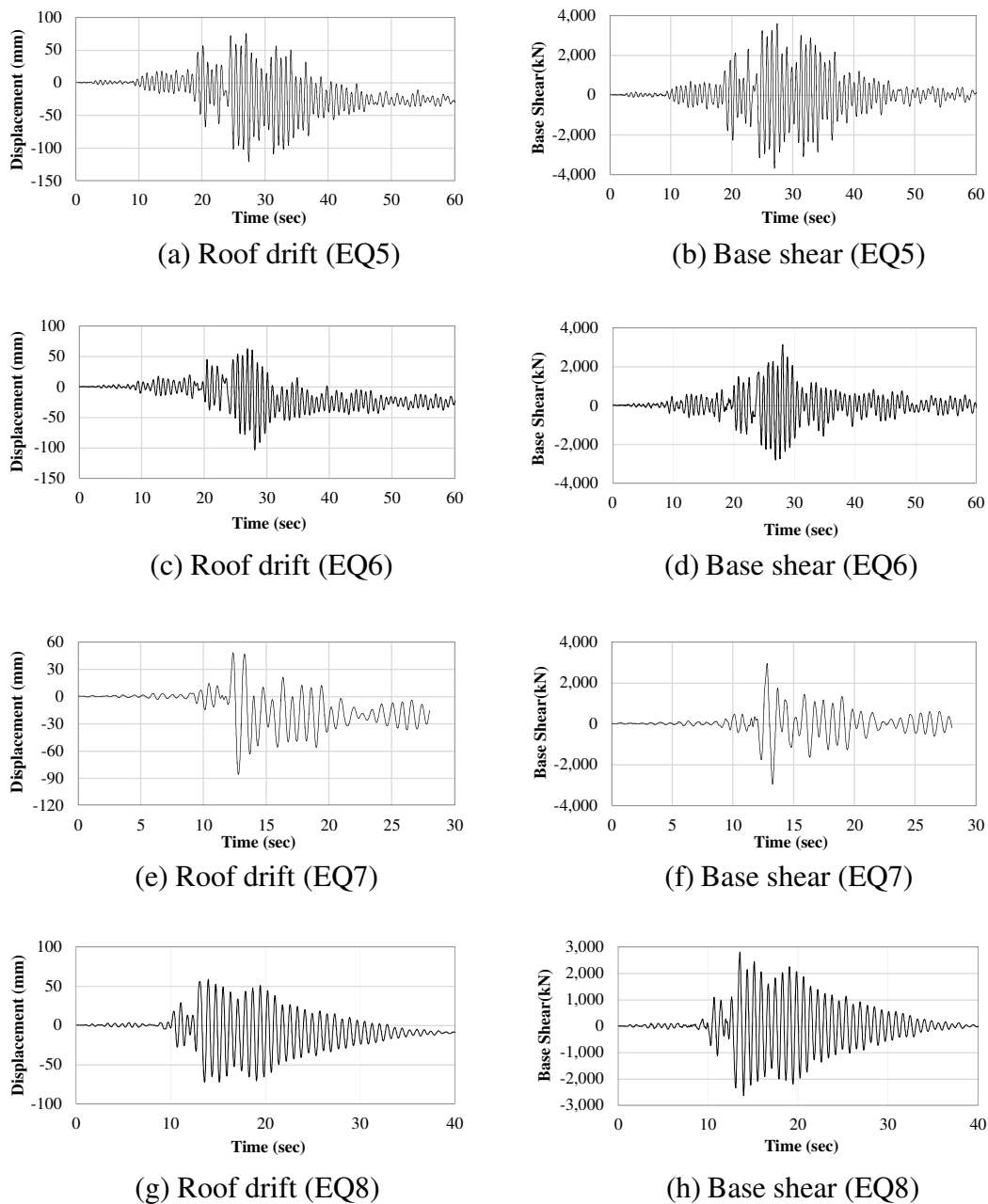
Figure 5.8: Response of the Six-Storey SCBF to Far-Field Records

In general, the level of damage experienced by the six-storey building was relatively low as it was always below the life safety performance level. Only five of the scaled records; (Lazio Abruzzo (EQ3), Chi-Chi-TAP017 (EQ5), Chi-Chi-ILA030 (EQ6), Loma Prieta-Emeryville (EQ7), and Loma Prieta-Oakland (EQ8), caused the deformations in the braces to reach the damage control structural performance range

(S-2). All damage was due to relatively high compressive deformations in brace members while tensile deformations were always below this performance level.

For these particular records listed above, two damage indicators are used to imply the time sequence of damage occurrence and the level of damage incurred by the affected brace elements. The first indicator is referred to as (MDT) and is used to provide the time sequence through which brace members, whose internal deformations exceed the Immediate Occupancy level and reach the damage control structural performance range (S-2), attain their maximum deformations. A schematic presentation of the six-storey MDT indicator is depicted in Figs. 5.9(a), (c), (e), (g) and (k) under the effect of EQ3, EQ5, EQ6, EQ7 and EQ8, respectively. For the MDT sequence, a member labeled as (1) means that this is the first member that reached its maximum deformation under a certain earthquake excitation. Consequently, a member labeled (2) is expected to reach its maximum deformation after the member labeled (1). Members having the same numbers shown next to them are expected to reach their maximum deformation simultaneously.

The second damage indicator (MD) classifies critical elements according to the level of deformation induced in each element. The MD results for the six-storey SCBF is shown in Figs. 5.9(b), (d), (f), (h) and (l) due to excitation records EQ3, EQ5, EQ6, EQ7 and EQ8, respectively.
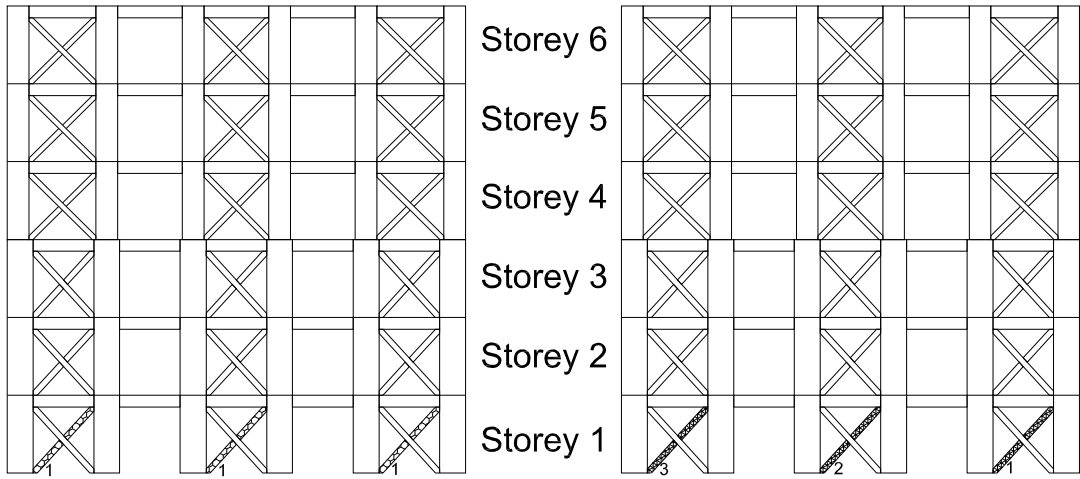
(a) MDT (EQ3) (b) MD (EQ3)
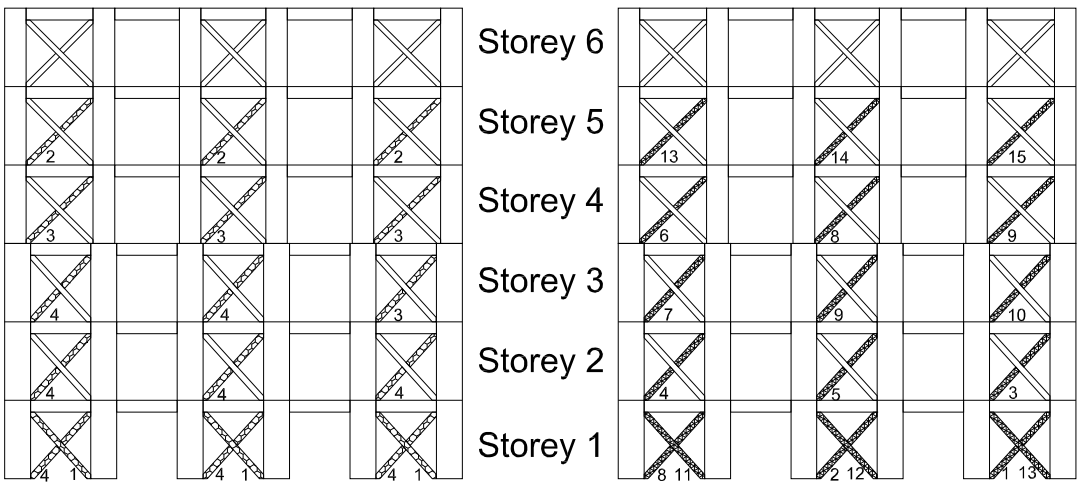
(c) MDT (EQ5) (d) MD (EQ5)
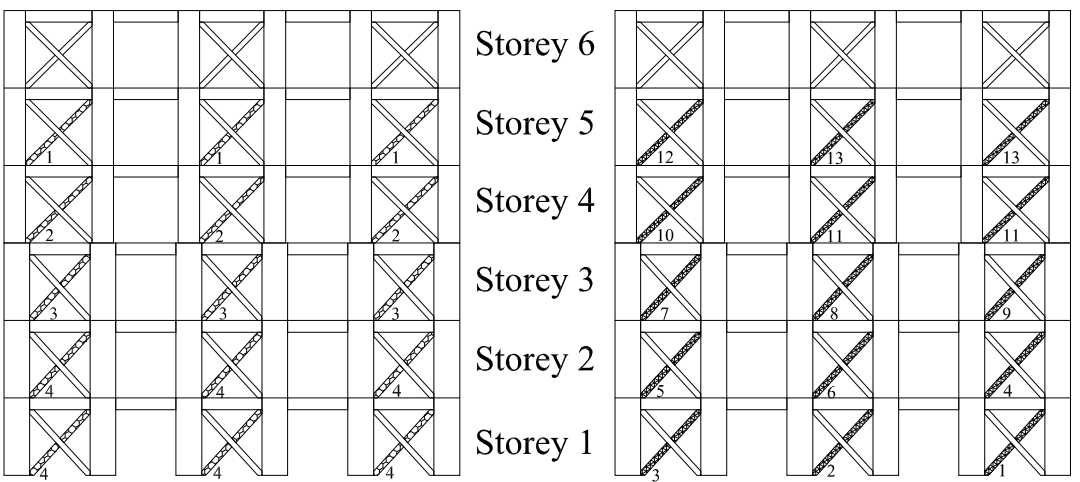
(e) MDT (EQ6) (f) MD (EQ6)

Figure 5.9: MDT and MD of the Six-Storey SCBF
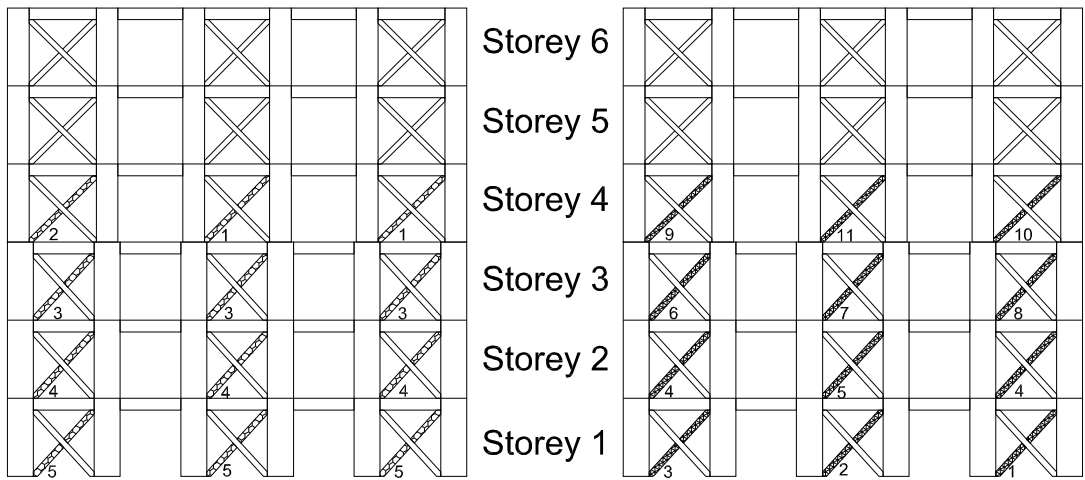
(g) MDT (EQ7)   (h) MD (EQ7)
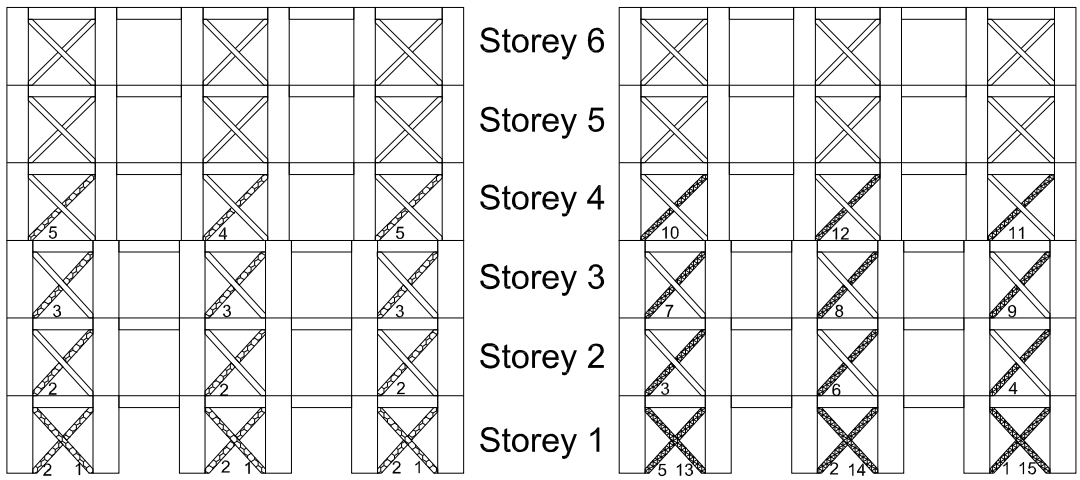
(k) MDT (EQ8)   (l) MD (EQ8)

Figure 5.9: MDT and MD of the Six-Storey SCBF (Cont'd)

Unlike MDT, a member that is marked as (1) in the MD classification system is ought to have the maximum level of deformation (i.e.; damage) relative to all other critical members in the structure. As such, a member that is assigned a label (2) should have less deformation than the one labeled (1). Members that are assigned the same number are expected to have reached the same level of maximum deformations. For instance, the input ground motion (EQ3) caused three members at storey (1) to reach their maximum deformations at the same point of time. Therefore, all three members are assigned a MDT indicator of (1) as shown in Fig. 5.9(a). Meanwhile, the MD indicator implies that the brace member at the rightmost braced bay experiences the highest damage (MD = 1) corresponding to a deformation of 2.78 mm, followed by the member in the middle bay (MD = 2) and finally, the least level of damage is induced in the brace member at the leftmost bay (MD = 3) as explained in Fig. 5.9(b).

The input ground motion (EQ5) caused eighteen brace members to reach their maximum deformation at different points of time as shown in Figs. 5.9(c) and (d). Three members are located at storey (1) with MDT = 1, three members at storey (5) with MDT = 2, three members at storey (4) and one member at storey (3) with MDT = 3 and finally, eight members (three at storey (1), three at storey (2) and two at storey (3)) with all of them having MDT = 4 as explained in Fig. 5.9(c). Furthermore Fig. 5.10(d) shows that at storey (1), the brace member at the rightmost braced bay experiences the highest damage (MD = 1) corresponding to a deformation of 5.34 mm while at storey (5), the brace member at the rightmost bay experiences the lowest damage (MD = 15). The level of deformation induced in the remaining sixteen critical brace members are assigned MD indicators that vary between (2) and (14) as presented in Fig. 5.9(d).

The input ground motion (EQ6) caused fifteen brace members to reach their maximum deformation at different points of time as shown in Figs. 5.9(e) and (f). Three brace members are located at storey (5) with MDT = 1, three members at storey (4) with MDT = 2, three members at storey (3) with MDT = 3 and finally, six brace members (three at storey (2) and three at storey (1)) with all of them having MDT = 4 as explained in Fig. 5.9(e). Furthermore Fig. 5.9(f) shows that at storey (1), the brace member at the rightmost bay experiences the highest damage (MD = 1) corresponding to a deformation of 5.02 mm while at storey (5), the brace members at the middle and rightmost bays experience the lowest damage (MD = 13). The level of deformation induced in the remaining twelve critical brace members are assigned MD indicators that vary between (2) and (12) as presented in Fig. 5.9(f).

The input ground motion (EQ7) caused twelve brace members to reach their maximum deformation at different points of time as shown in Figs. 5.9(g) and (h). Three members are located at storey (4), two of them located at middle and rightmost bays with MDT = 1 and third one located at the leftmost bay with MDT = 2, three members at storey (3) with MDT = 3, three members at storey (2) with MDT = 2, and finally, three members at storey (1) with MDT = 5 as explained in Fig. 5.9(g). Furthermore Fig. 5.9(h) shows that at storey (1), brace member at the rightmost bay experience the highest damage (MD = 1) corresponding to a deformation of 4.73 mm. while at storey (4), the brace member at the middle bay experiences the lowest damage (MD = 11). The level of deformation induced in the remaining ten critical brace members are assigned MD indicators that vary between (2) and (10) as presented in Fig. 5.9(h).

The input ground motion (EQ8) caused fifteen brace members to reach their maximum deformation at different points of time as shown in Figs. 5.9(k) and (l).

Three members are located at storey (1) with MDT = 1, three members at storey (1) and three at storey (2) with MDT = 2, three members at storey (3) with MDT = 3 and finally, three members at storey (4) (the middle with MDT = 4 and the remaining two having MDT = 5 as explained in Fig. 5.9(k). Furthermore Fig. 5.9(l) shows that at storey (1), brace member at the rightmost bay experience the highest damage (MD = 1) corresponding to a deformation of 3.42 mm and at the bay the other brace member experiences the lowest damage (MD = 15). The level of deformation induced in the remaining thirteen critical brace members are assigned MD indicators that vary between (2) and (14) as presented in Fig. 5.9(l).

The above discussion reveals that the four far-field records (EQ5 to EQ8) resulted in a relatively considerable level of damage in a large number of braces (12 to 18) in the six-storey SCBF. On the contrary, only EQ3, among the near-fault earthquakes, caused the same level of damage in 3 bracing members of the six-storey SCBF. The maximum number of affected elements is (18) in five storeys under the influence of EQ5 as presented by Figs. 5.9(c) and (d). This could be attributed to the fact that this particular earthquake has a distinct sharp peak in its response spectrum at 1.06 sec. as shown in Fig. 5.4. This value is very close to the estimated natural period of vibration of the six-storey SCBF of 0.784 sec. provided in Table 5.4. The response spectrum of EQ6 is characterized by multiple peaks in a period range from 0.32 to 1.4 sec. as per Fig. 5.4. This is expected to closely excite about 95% of the mass associated with the first two modes of vibration of the six-storey SCBF (Table 5.4) leading to a considerable impact in 15 of the brace members distributed over 5 storeys as shown in Figs. 5.9(e) and (f). EQ8 has also resulted in considerable deformations in 15 brace members located in 4 storeys only (Figs. 5.9(k) and (l)) as it has two peak responses at 0.66 and 0.92 sec. as can be seen in Fig. 5.4. Given that

the natural period of the structure (0.784 sec.) lies closely within this narrow range, it is highly possible to induce a considerable level of deformations in the bracing system. Meanwhile, EQ7 has caused significant deformations in twelve brace members distributed over four storeys (refer to Figs. 5.9(g) and (h)). EQ7 has two peaks at 0.66 and 1.18 sec. (Fig. 5.4), which could influence the structure due to the closeness of the first peak to the building's natural period of 0.784 sec. The limited damage induced by EQ3 in three bracing members located in storey (1) (Fig. 5.9(a) and (b)) could be attributed to the fact that the main response peak of this record is localized at 0.18 sec. with other less peaks taking place through the period ranging between 0.4 to 0.5 sec. as shown in Fig. 5.3. Although the former is close to the period associated with the third vibrational mode (0.142 sec.), the effective mass participation related to this mode is too low (3.34%) and is not expected to have a significant contribution to the response. The later range could, however, partially excite the first two modes that are associated with about 95% of the effective mass. The combined, but limited, effect of all three modes could explain the limited level of damage incurred by EQ3 to the six-storey SCBF.

Figures 5.10(a), (b), (c), (d) and (e) show the inter-storey drift ratio (IDR) for the six-storey SCBF under the effect of the five influential records EQ3, EQ5, EQ6, EQ7 and EQ8, respectively, at time of occurrence of maximum roof drift. Shown also on these plots are the IDR limits related to Immediate Occupancy (IO = 0.5%) and Life Safety (LS = 1.5%) as recommended by FEMA 356 (2000).

(a) Inter-storey drift ratio (EQ3)

(b) Inter-storey drift ratio (EQ5)

(c) Inter-storey drift ratio (EQ6)

(d) Inter-storey drift ratio (EQ7)

(e) Inter-storey drift ratio (EQ8)
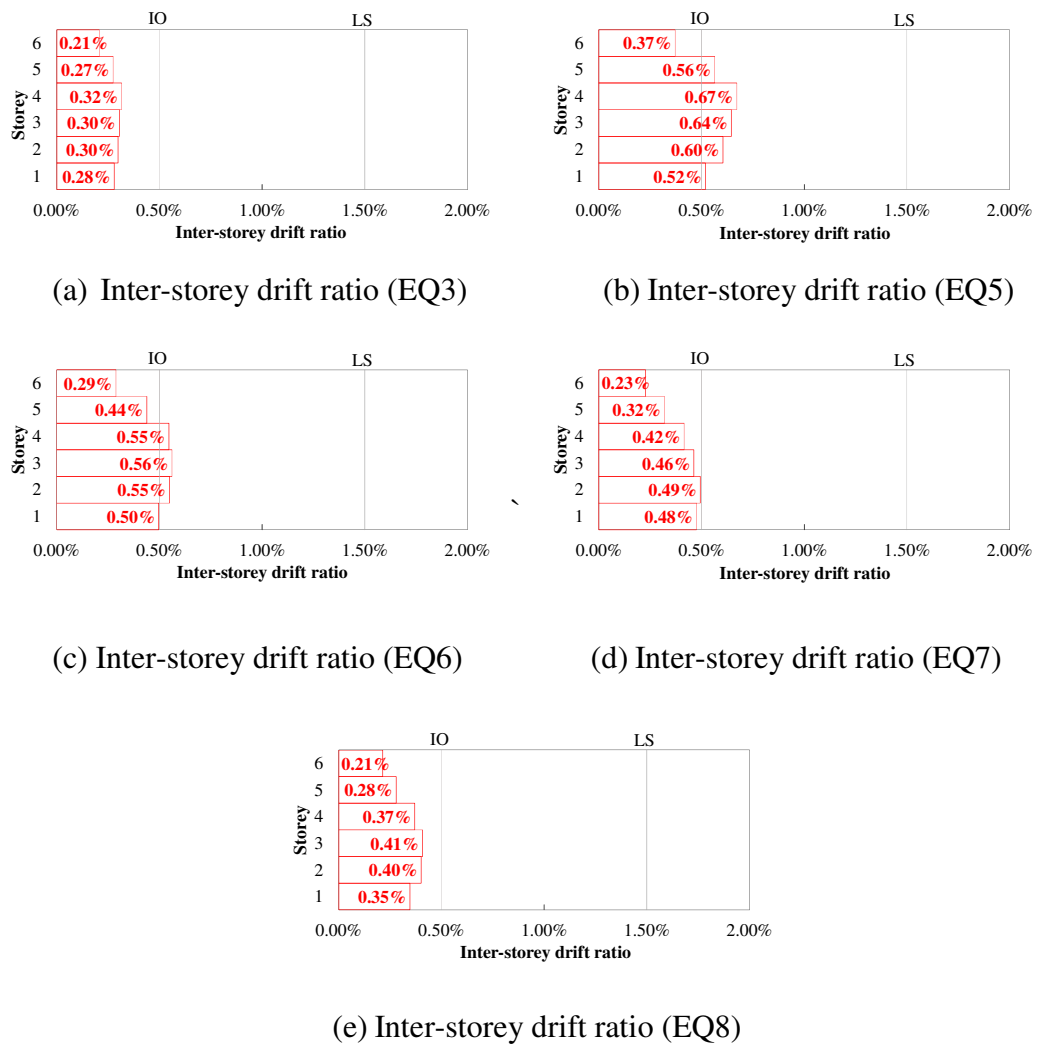
Figure 5.10: Inter-Storey Drift Ratio of the Six-Storey SCBF

It can be seen that the level of maximum IDR under various ground excitations is consistent with the brace damage indicators (MDT) and (MD) summarized in Fig. 5.9 for the same excitations. Figures 5.10(b) and (c) imply that maximum IDR occur under the effect of EQ5 and EQ6, respectively. Under EQ5, the IDRs of the first five storeys exceed the Immediate Occupancy performance limit and reach the Damage Control Structural performance level (S2). Similarly, the IDRs induced by EQ6 indicate that the first four storeys reach the Damage Control Structural performance level (S2). Meanwhile, the IDRs related to EQ7 and EQ8 are

marginally below the Immediate Occupancy performance limit. Consistent with the observation made based on the damage indicators of EQ3 (Figs. 5.9(a) and (b)), the IDRs induced by EQ3 are the least among all five records as they are significantly below the Immediate Occupancy limit which confirms the low level of damage in the brace members. It is worth mentioning that the contribution of the higher modes of vibration to the inter-storey drift profiles is clearly reflected in Figs. 5.10(a) through (e) where, in the vast majority of the cases, the maximum IDRs occur in the mid-height storeys (2, 3 and 4) of the analyzed six-storey SCBFs. Table 5.5 presents a summary of the major results related to time history analysis of the six-storey SCBF. Based on this summary table, it is clear that EQ5 is the most destructive among EQ3, EQ6, EQ7 and EQ8. Furthermore, Table 5.5 introduces a damage severity indicator to sort the records with regards to their damaging effect. Smaller indicator's numbers reflect the highest damaging effect. As a result, the records can be placed in the following order starting with the most destructive record and ending with the least destructive one: EQ5, EQ6, EQ7, EQ8 and EQ3.

Table 5.5: Summary of Major Time History Analysis Results for the Six-Storey SCBF

Ground motion Record	*Damage severity indicator	Number of damaged braces	Maximum brace member deformation (MD indicator= 1)			Maximum roof drift and IDR			
			Maximum brace deformation (mm)	Storey	Time (sec)	Maximum roof drift (mm)	Maximum IDR at time of maximum roof drift (%)	Storey	Time (sec)
EQ3	5	3	2.78	1	9.26	60.53	0.32	4	9.19
EQ5	1	18	5.34	1	27.36	121.5	0.67	4	27.35
EQ6	2	15	5.01	1	28.05	103.68	0.55, 0.56, 0.55	2, 3, 4	28.02
EQ7	3	12	4.73	1	12.79	86.13	0.48, 0.49	1, 2	12.76
EQ8	4	15	3.42	1	13.54	72.6	0.40, 0.41	2, 3	13.56

* Smaller numbers reflect the highest damaging effect

5.5.2 Nine-Storey SCBF Building

Time history analysis was performed to examine the influence of the eight scaled ground motion records (Table 5.1) on the nine-storey SCBF. Figures 5.11 and 5.12 show the recorded response (base shear and roof drift) under the effect of near-fault and far-field records, respectively.

(a) Roof drift (EQ1)

(b) Base shear (EQ1)

(c) Roof drift (EQ2)

(d) Base shear (EQ2)

(e) Roof drift (EQ3)

(f) Base shear (EQ3)

(g) Roof drift (EQ4)

(h) Base shear (EQ4)
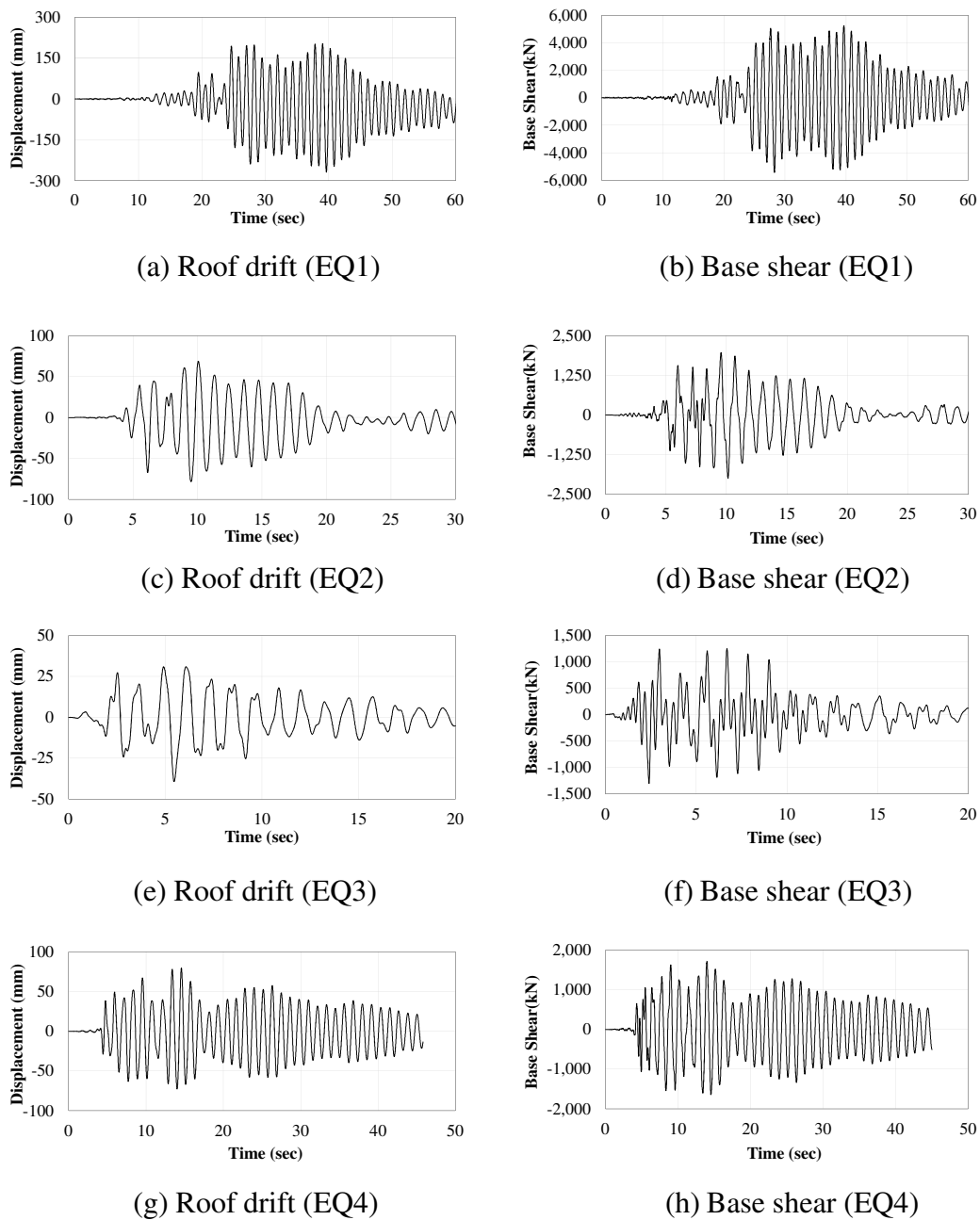
Figure 5.11: Response of the Nine-Storey SCBF to Near-Fault Records

(a) Roof drift (EQ5)

(b) Base shear (EQ5)

(c) Roof drift (EQ6)

(d) Base shear (EQ6)

(e) Roof drift (EQ7)

(f) Base shear (EQ7)

(g) Roof drift (EQ8)

(h) Base shear (EQ8)
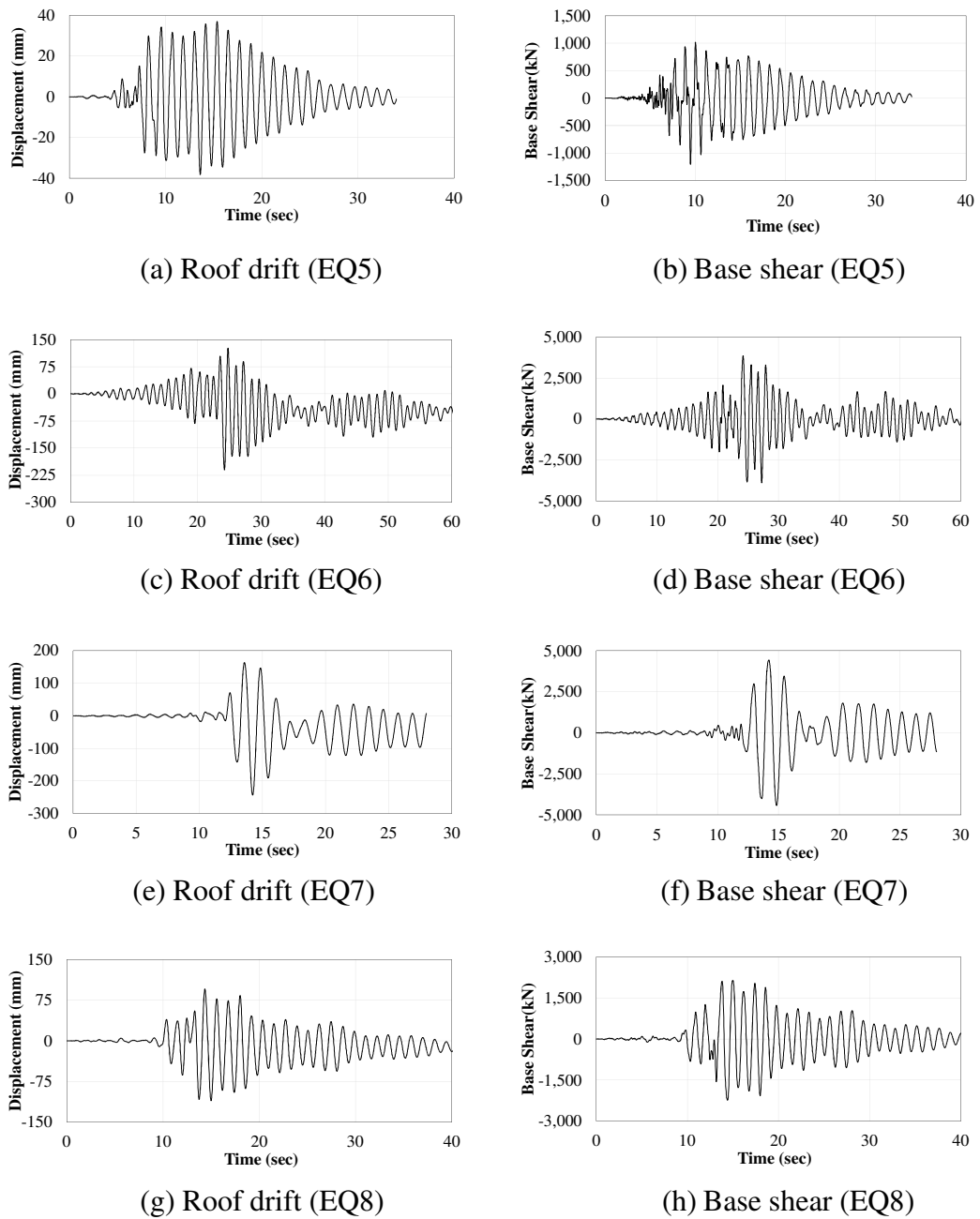
Figure 5.12: Response of the Nine-Storey SCBF to Far-Field Records

In general, the level of damage experienced by the nine-storey building was relatively low as it was always below the life safety performance level. Only three of the scaled records; (Chi-Chi-TAP017 (EQ5), Chi-Chi-ILA030 (EQ6), Loma Prieta-Emeryville (EQ7)), caused the deformations in the braces to reach the damage control structural performance range (S-2). All damage was due to relatively high compressive deformations in brace members while tensile deformations were always below this performance level.

The input ground motion (EQ5) caused thirty-nine brace members, distributed over eight storeys, to reach their maximum deformation at different points of time. The sequence of this damage is presented by the indicator (MDT) as shown in Fig. 5.13(a). This time-dependent sequence starts with three brace members at storey (7) with MDT = 1 and ends with four brace members located at storeys (2) and (3) with MDT = 11. The sequence of damage for the remaining thirty-two members is assigned MDT indicators that vary between (2) and (10). Furthermore, Fig. 5.13(b) shows that at storey (1), the brace member at the rightmost braced bay experiences the highest damage with MD = 1 corresponding to a deformation of 7.56 mm, while at storey (7), the brace member at the rightmost bay experiences the lowest damage with MD = 36. The levels of deformation induced in the remaining thirty-six critical brace members have MD indicators that vary between (2) and (35) as presented in Fig. 5.13(b).

The input ground motion (EQ6) caused twenty-four brace members to reach their maximum deformation at different points of time as shown in Figs. 5.13(c) and (d). The sequence of this damage is presented by the indicator (MDT) as shown in Fig. 5.13(c). This sequence starts with three brace members at storey (1) with MDT = 1 and ends with three brace members located at storeys (8) with MDT = 5. The

sequence of damage for the remaining eighteen brace members is assigned MDT indicators that vary between (2) and (4). Furthermore, Fig. 5.13(d) shows that at storey (1), a brace member at the rightmost braced bay experiences the highest damage with MD = 1 corresponding to a deformation of 6.37 mm, while at storey (8), the brace member at the leftmost bay experiences the lowest damage with MD = 24. The levels of deformation induced in the remaining twenty-two critical brace members are assigned MD indicators that vary between (2) and (23) as presented in Fig. 5.13(d).

The input ground motion (EQ7) caused twenty-five brace members to reach their maximum deformation at different points of time as shown in Figs. 5.13(e) and (f). The sequence of this damage is presented by the indicator (MDT) as shown in Fig. 5.13(c). This time-dependent sequence starts with one brace member at storey (7) in the middle braced bay with MDT = 1 and ends with six brace members located at storeys (4) and (5), distributed all over the three braced bays with MDT = 6. The sequence of damage for the remaining eighteen brace members is assigned MDT indicators that vary between (2) and (5). Furthermore, Fig. 5.13(f) shows that at storey (1), a brace member at the rightmost braced bay experiences the highest damage with MD = 1 corresponding to a deformation of 7.08 mm, while at storey (8), the brace member at the rightmost bay experiences the lowest damage with MD = 23. The levels of deformation induced in the remaining twenty-three critical brace members are assigned MD indicators that vary between (2) and (22) as presented in Fig. 5.13(f).
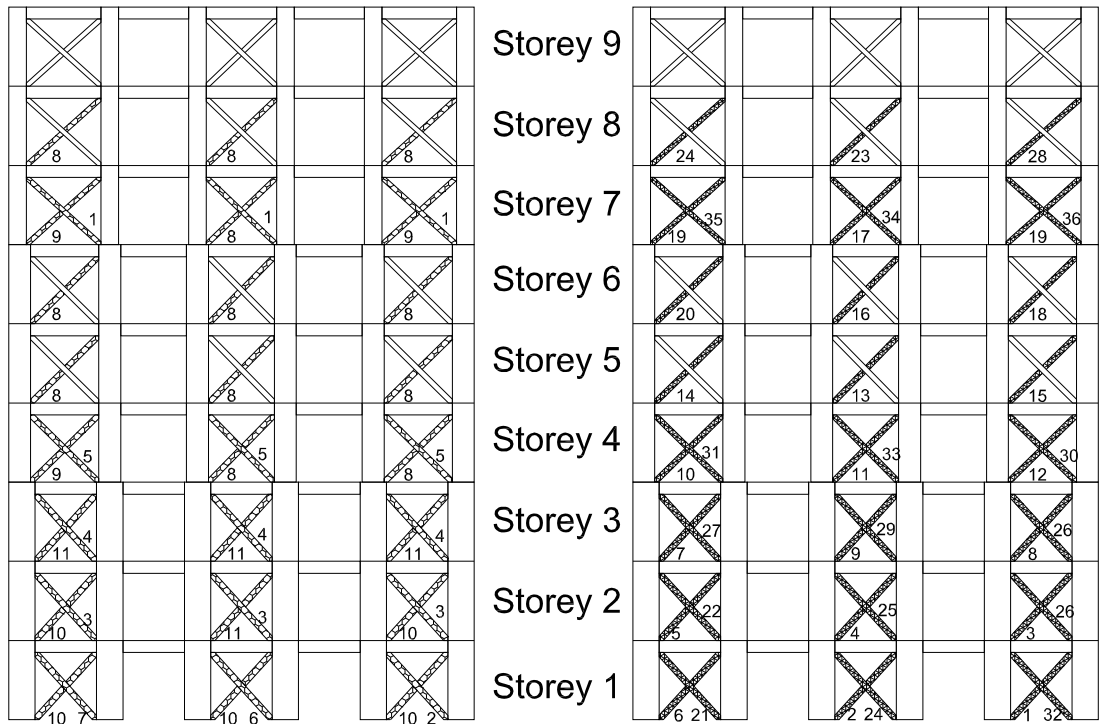
(a) MDT (EQ5)

(b) MD (EQ5)
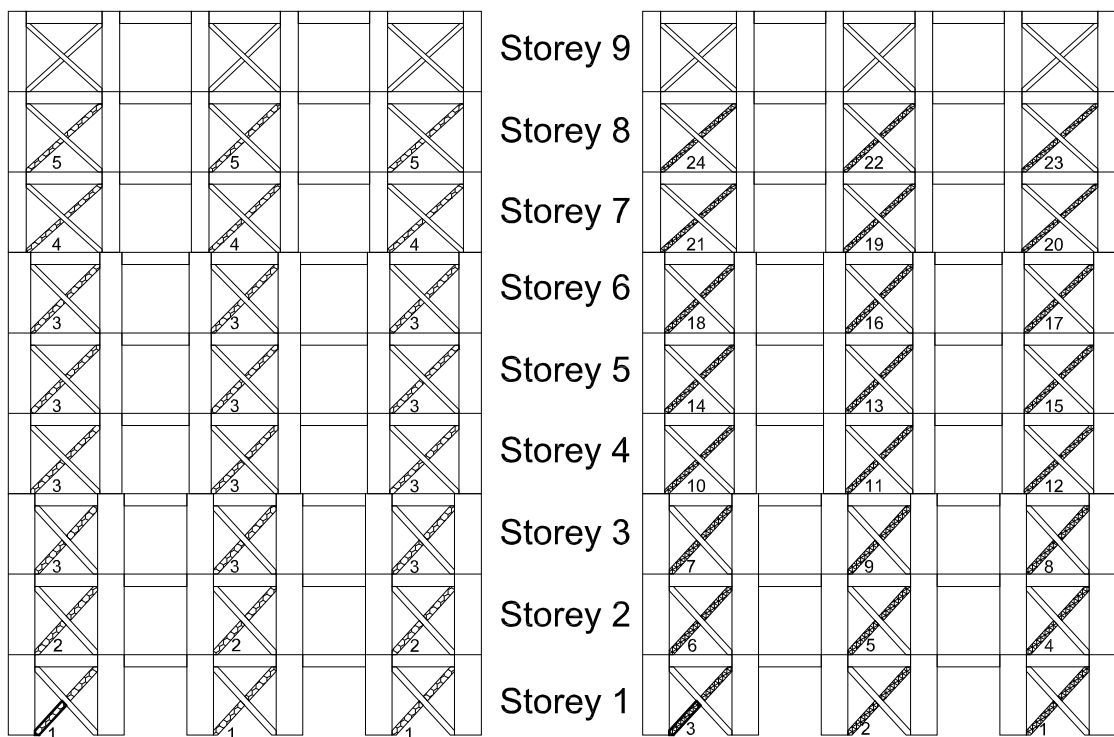
(c) MDT (EQ6)

(d) MD (EQ6)

Figure 5.13: MDT and MD of the Nine-Storey SCBF

(e) MDT (EQ7)   (f) MD (EQ7)
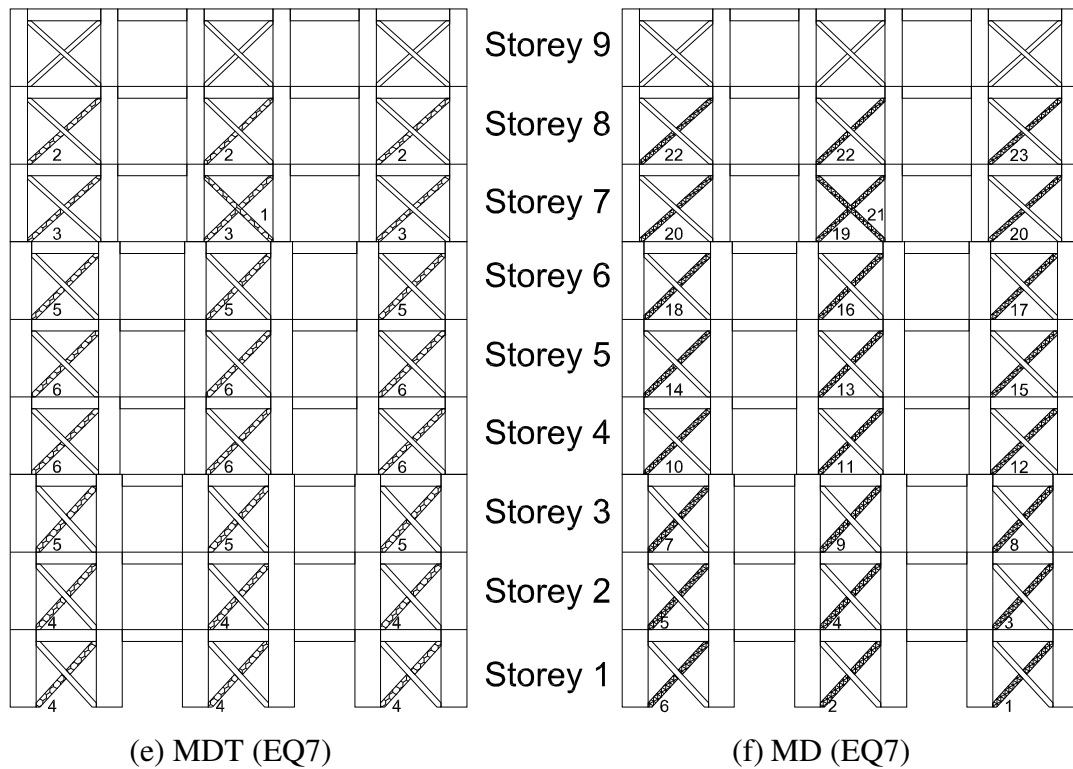
Figure 5.13: MDT and MD of the Nine-Storey SCBF (Cont'd)

The above discussion implies that the three far-field records (EQ5, EQ6 and EQ7) resulted in a relatively considerable level of damage in a large number of braces (24 to 39) in the nine-storey SCBF. The maximum number of affected elements is (39) in eight storeys under the influence of EQ5 as presented by Figs. 5.13(c) and (d). This could be attributed to the fact that this particular earthquake has a distinct sharp peak in its response spectrum at 1.06 sec. as shown in Fig. 5.4. This value is very close to the estimated natural period of vibration of the nine-storey SCBF of 1.176 sec. provided in Table 5.4. The response spectrum of EQ6 is characterized by multiple peaks in a period range from 0.32 to 1.4 sec. as per Fig. 5.4. This is expected to closely excite about 95% of the mass associated with the first two modes of vibration of the nine-storey SCBF having periods of 1.176 sec and 0.388 sec (Table 5.4) leading to a considerable impact in 24 of the brace members

distributed over eight storeys as shown in Figs. 5.13(c) and (d). Meanwhile, EQ7 has caused significant deformations in twenty-five brace members distributed over eight storeys (refer to Figs. 5.13(e) and (f)). EQ7 has two peaks at 0.66 sec and 1.18 sec. (Fig. 5.4), which indicates that the second peak matches the building's natural period of 1.176 sec.

Figures 5.14(a), (b) and (c) show the IDR for the nine-storey SCBF under the effect of the three influential records EQ5, EQ6 and EQ7, respectively, at time of occurrence of maximum roof drift. Shown also on these plots are the inter-storey drift limits related to Immediate Occupancy (IO = 0.5%) and Life Safety (LS = 1.5%) (FEMA 356, 2000). It can be seen that the level of maximum IDRs under various ground excitations are consistent with the brace damage indicators (MDT) and (MD) summarized in Fig. 5.14 for the same earthquake records. Figures 5.14 (a), (b) and (c) imply that the three earthquake records caused drift ratios to fall in the damage control structural performance level S2. The maximum IDRs occur under the effect of EQ5 (0.89%) followed by EQ7 (0.84%) and finally EQ8 (0.74%). Under EQ5 and EQ7, the IDRs of all storeys exceed the Immediate Occupancy performance limit and reach the Damage Control Structural performance level (S2). Meanwhile, the IDR of the ninth storey related to EQ6 is below the immediate occupancy level. It is worth mentioning that the contribution of the higher modes of vibration to the IDR profiles is clearly reflected in Figs. 5.14(a) through (c) where, in the vast majority of the cases, the maximum IDRs occur in the mid-height storeys (between 4 and 7) of the analyzed nine-storey SCBFs. Table 5.6 presents a summary of the major results related to time history analysis of the nine-storey SCBF.
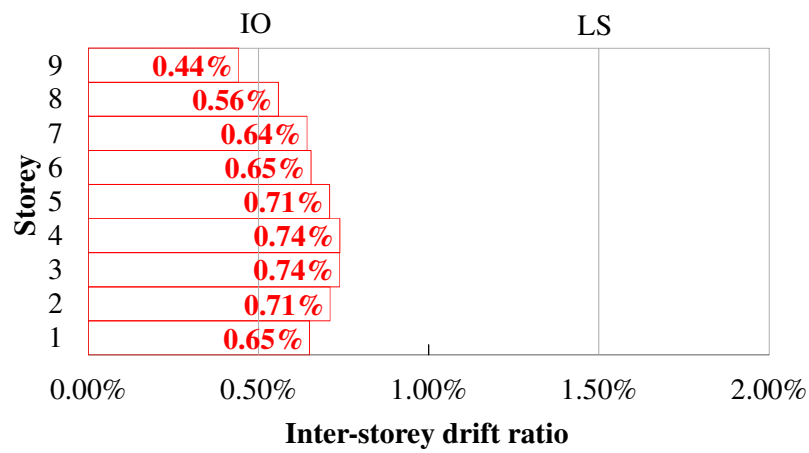
(a) Inter-storey drift ratio (EQ5)
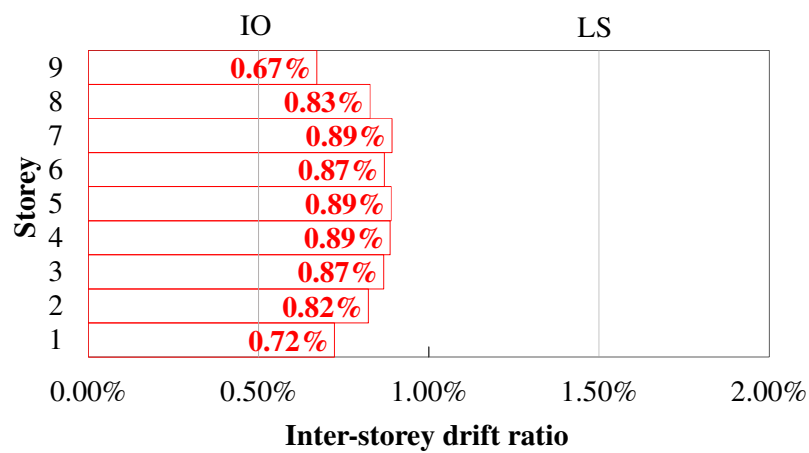
(b) Inter-storey drift ratio (EQ6)
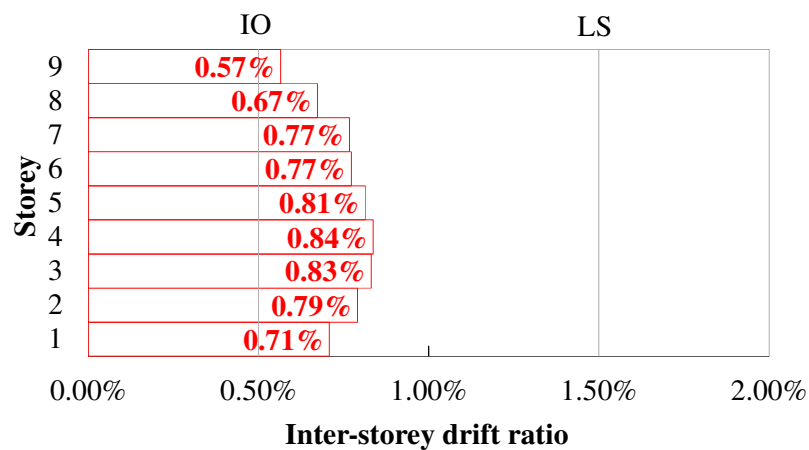
(c) Inter-storey drift ratio (EQ7)

Figure 5.14: Inter-Storey Drift Ratio of the Nine-Storey SCBF

Table 5.6: Summary of Major Time History Analysis Results for the Nine-Storey SCBF

Ground motion Record	*Damage severity indicator	Number of damaged braces	Maximum brace member deformation (MD indicator= 1)			Maximum roof drift and IDR			
			Maximum brace deformation (mm)	Storey	Time (sec)	Maximum roof drift (mm)	Maximum IDR at time of maximum roof drift (%)	Storey #	Time (sec)
EQ5	1	39	7.56	1	39.65	268.2	0.89	4, 5, 7	39.64
EQ6	3	24	6.37	1	24.19	210.42	0.74	3, 4	24.23
EQ7	2	25	7.08	1	14.22	243.31	0.83,0.84	3, 4	14.23

* Smaller numbers reflect the highest damaging effect

Based on the information summarized in Table 5.6, it is clear that EQ5 is the most destructive relative to EQ6 and EQ7. Furthermore, Table 5.6 provides the damage severity indicator that suggests the order of EQ5, EQ7 and EQ6 to reflect the level of impact of these records on the nine-storey SCBF. It is worth mentioning that there is almost a perfect match between the time of maximum brace member deformation reached in the nine-storey SCBF and the time of maximum roof drift (see Table 5.6)

5.5.3 Fifteen-Storey SCBF Building

Figures 5.15 and 5.16 present the response history of the base shear and roof drift of the fifteen-storey SCBF under the effect of near-fault and far-field scaled records respectively. Results reveal that the level of damage experienced by the fifteen-storey building was always below the life safety performance level. Only two of the scaled records; (Chi-Chi-TAP017 (EQ5) and Chi-Chi-ILA030 (EQ6)), caused the deformations in the braces to reach the damage control structural performance range (S-2). All damage was due to relatively high compressive deformations in brace members while tensile deformations were always below this performance level.

(a) Roof drift (EQ1)

(b) Base shear (EQ1)

(c) Roof drift (EQ2)

(d) Base shear (EQ2)

(e) Roof drift (EQ3)

(f) Base shear (EQ3)

(g) Roof drift (EQ4)

(h) Base shear (EQ4)
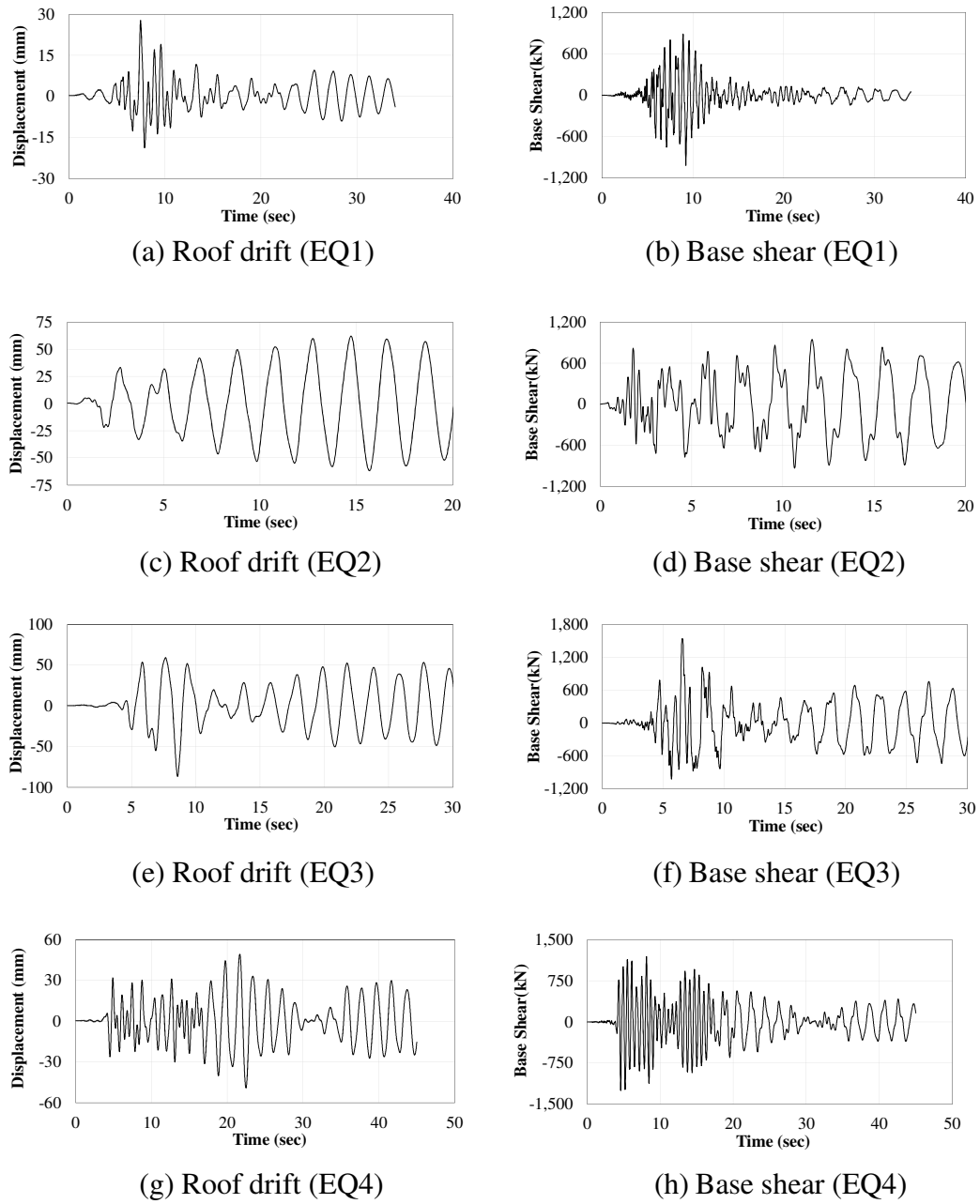
Figure 5.15: Response of the Fifteen-Storey SCBF to Near-Fault Records

(a) Roof drift (EQ5)

(b) Base shear (EQ5)

(c) Roof drift (EQ6)

(d) Base shear (EQ6)

(e) Roof drift (EQ7)

(f) Base shear (EQ7)

(g) Roof drift (EQ8)

(h) Base Shear (EQ8)
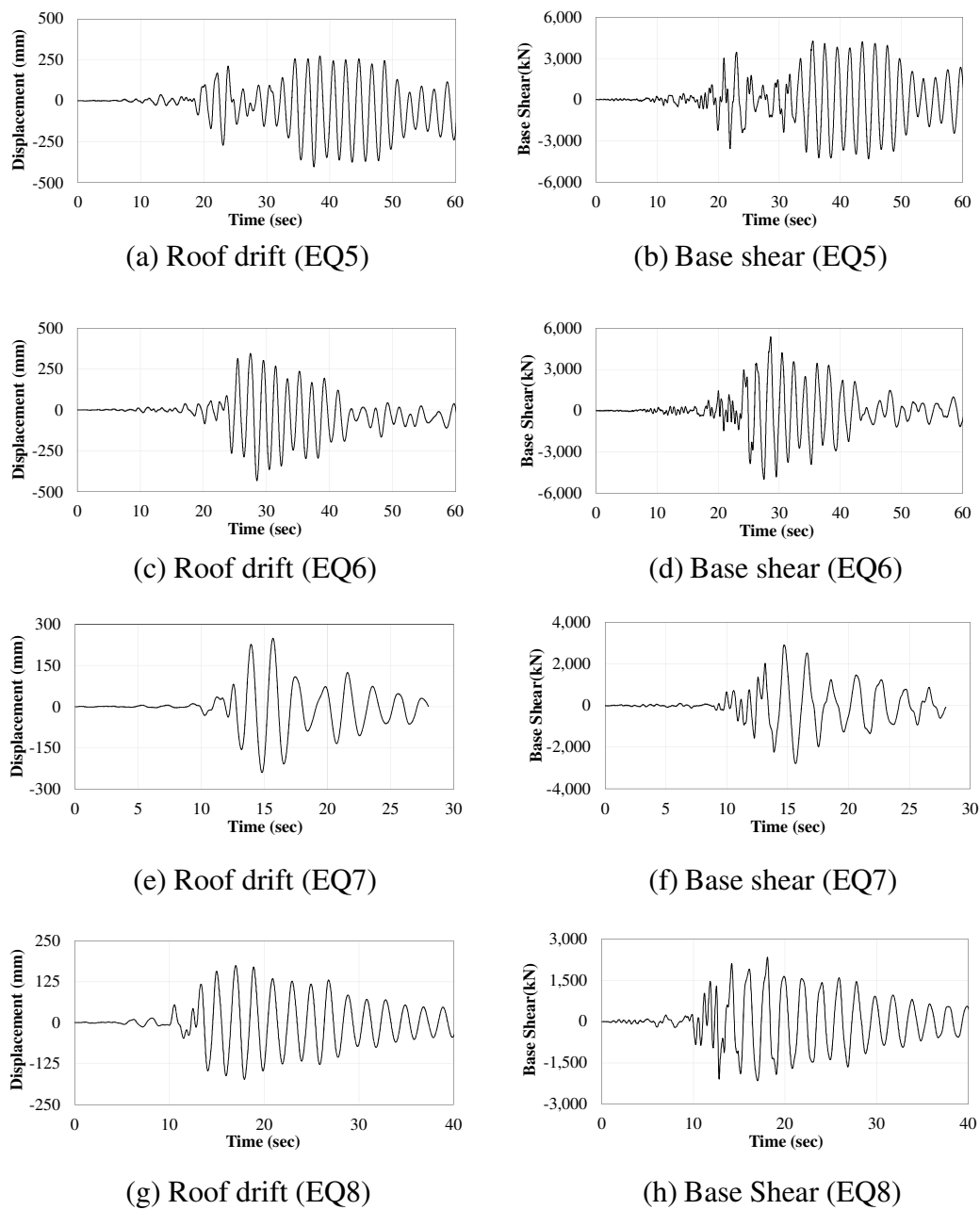
Figure 5.16: Response of the Fifteen-Storey SCBF to Far-Field Records

The input ground motion (EQ5) caused thirty-three brace members distributed over eight storeys to reach their maximum deformation at different points of time. The sequence of this damage is presented by the indicator (MDT) as shown in Fig. 5.17(a). This damage sequence starts with four brace members at storey (1) with MDT = 1 and ends with nine brace members located at storeys (8), (9) and (10)

with all of them having MDT = 8. The sequence of damage for the remaining twenty members is shown by MDT indicators that vary between (2) and (7). Besides, Fig. 5.17(b) shows that at storey (1), two brace members at the rightmost and middle braced bays experience the highest damage with MD = 1 associated with a deformation of 4.43 mm. Meanwhile, at storey (11), the brace member at the leftmost bay experiences the lowest damage with MD = 23. The levels of deformation induced in the remaining twenty-nine critical brace members are assigned MD indicators that vary between (2) and (22) as presented in Fig. 5.17(b).

The input ground motion (EQ6) caused thirty-six brace members to reach their maximum deformation at different points of time as shown in Figs. 5.17(c) and (d). The sequence of this damage is presented by the indicator (MDT) as shown in Fig. 5.17(c). This time-dependent sequence starts with three brace members at storey (12) with MDT = 1 and ends with six brace members located at storeys (1) and (2) with MDT = 11. The sequence of damage for the remaining twenty-seven brace members is assigned MDT indicators that vary between (2) and (10). Furthermore, Fig. 5.17(d) shows that at storey (1), a brace member at the rightmost braced bay experiences the highest damage with MD = 1 corresponding to a deformation of 4.55 mm, while at storey (12), the brace member at the leftmost bay experiences the lowest damage with MD = 26. The levels of deformation induced in the remaining thirty-four critical brace members are assigned MD indicators that vary between (2) and (25) as presented in Fig. 5.17(d).
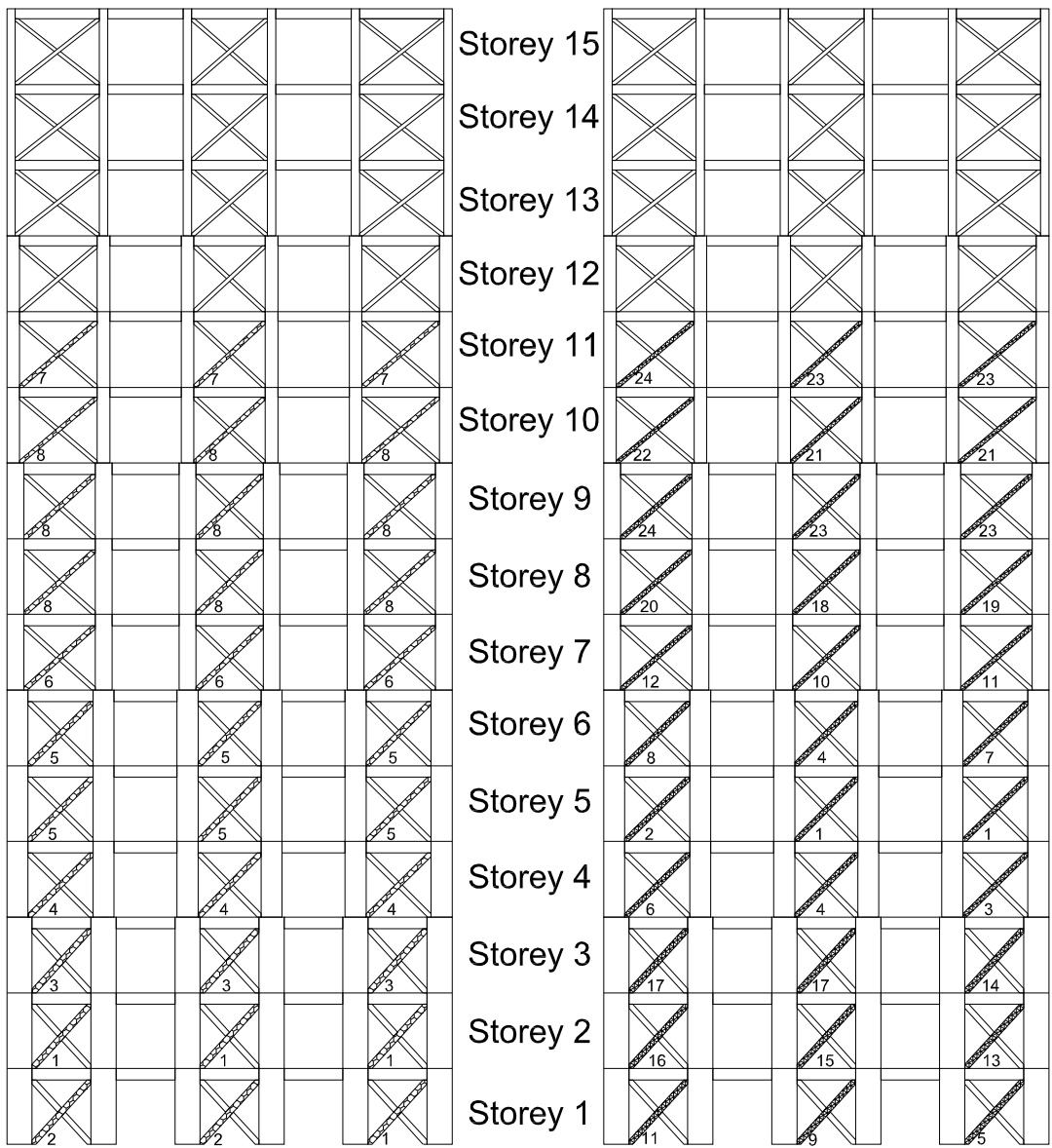
(a) MDT (EQ5)   (b) MD (EQ5)

Figure 5.17: MDT and MD of the Fifteen-Storey SCBF
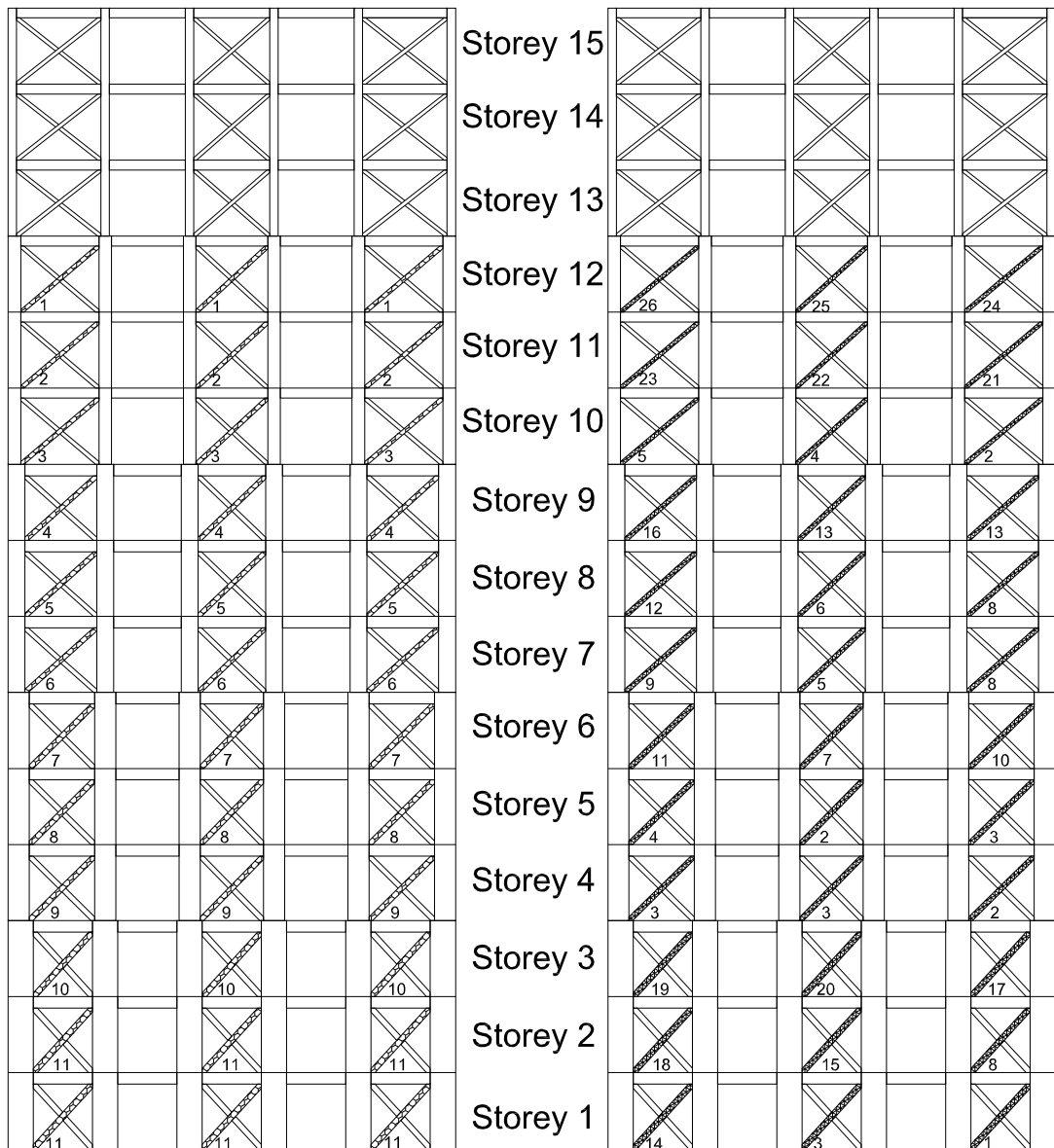
(c) MDT (EQ6)   (d) MD (EQ6)

Figure 5.17: MDT and MD of the Fifteen-Storey SCBF (Cont'd)

The above discussion reveals that only two far-field records (EQ5 and EQ6) led to a relatively considerable level of damage in a large number of braces (33 and 36) in the fifteen-storey SCBF. The maximum number of affected elements is (36) in twelve storeys under the influence of EQ6 as presented by Figs. 5.17(c) and (d). The response spectrum of EQ6 is characterized by multiple peaks in a period range from 0.32 to 2.0 sec. as per Fig. 5.4. This is expected to closely excite about 95% of the mass associated with the first three modes of vibration of the fifteen-storey SCBF whose corresponding periods range from 0.316 to 1.957 sec. as shown in Table 5.4. Meanwhile, EQ5 has caused deformations in thirty-three brace members distributed over eleven storeys as shown in Figs. 5.17(c) and (d)). EQ5 has four peaks at 0.30, 0.72, 1.06 and 1.82 sec. as shown in Fig. 5.4. The peak of 1.82 sec. is close to the first mode's period 1.957 sec. but the acceleration related to this peak is small (0.21 g) and as result it will have limited effect on the braces damage. The first two peaks (0.32 and 0.72 sec.) are expected to excite about 20% of the mass associated with the second and third mode of vibration of the fifteen-storey SCBF (Table 5.4) leading to a moderate impact on SCBFs brace members). This explains the low damage level caused by EQ5 compared to EQ6.

Figures 5.18(a), and (b) show the IDR for the fifteen-storey SCBF under the effect of the two influential records EQ5 and EQ6, respectively, at time of occurrence of maximum roof drift. It can be seen that the level of maximum IDRs under various ground excitations are consistent with the brace damage indicators (MDT) and (MD) summarized in Fig. 5.18 for the same earthquake records. Table 5.7 presents a summary of the major results related to time history analysis of the fifteen-storey SCBF.
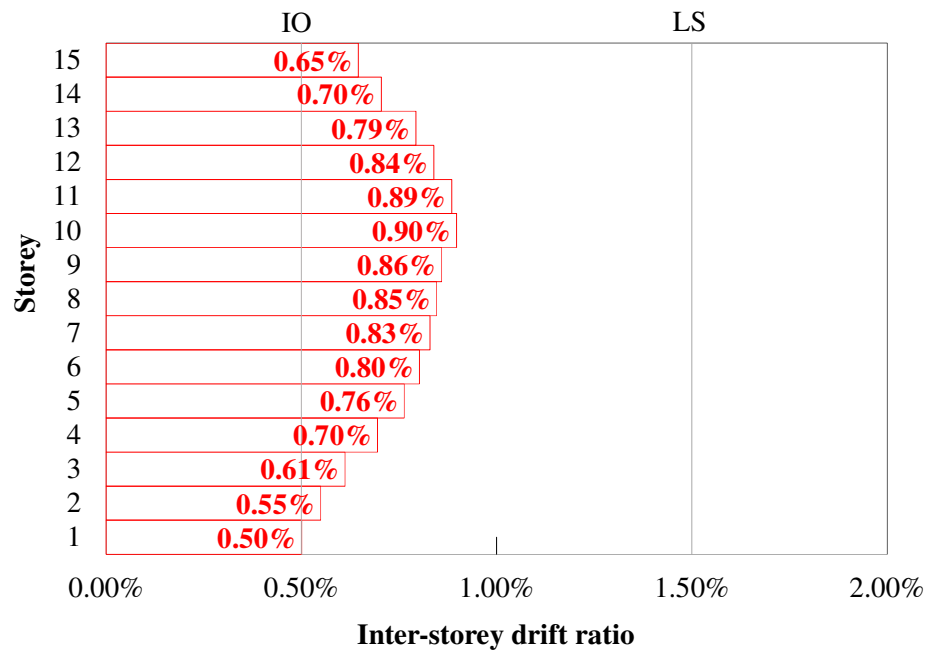
(a) Inter-storey drift ratio (EQ5)
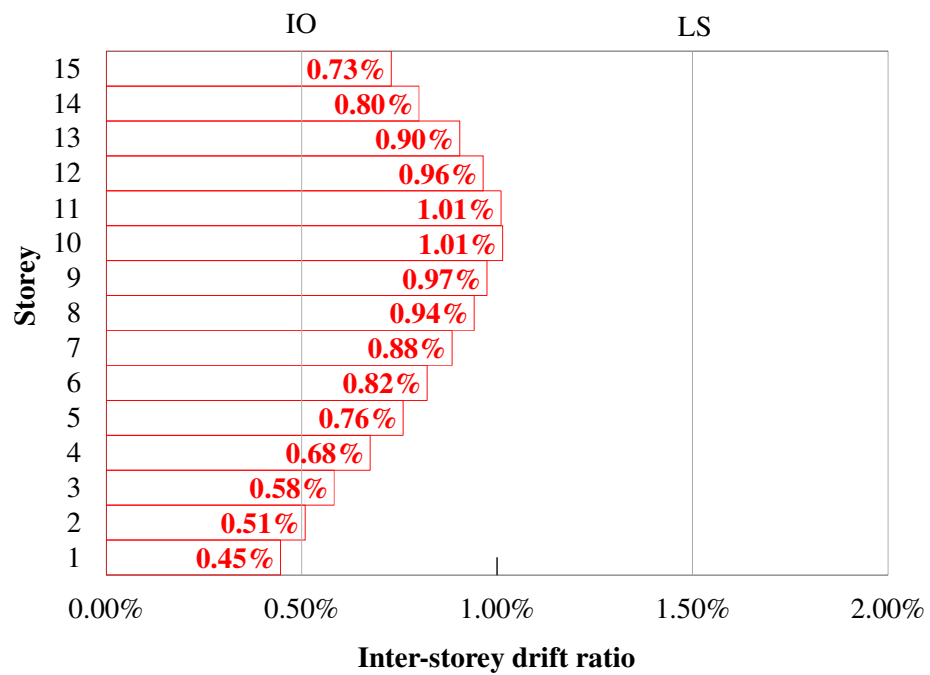
(b) Inter-storey drift ratio (EQ6)

Figure 5.18: Inter-Storey Drift Ratio of the Fifteen-Storey SCBF

Table 5.7: Summary of Major Time History Analysis Results for the Fifteen-Storey SCBF

Ground motion Record	*Damage severity indicator	Number of damaged braces	Maximum brace member deformation (MD indicator= 1)			Maximum roof drift and IDR			
			Maximum brace deformation (mm)	Storey	Time (sec)	Maximum roof drift (mm)	Maximum IDR at time of maximum roof drift (%)	Storey #	Time (sec)
EQ5	2	33	4.43	5	37.48	404.03	0.9	10	37.49
EQ6	1	36	4.55	1	28.6	432.58	1.01	10, 11	28.47

* Smaller numbers reflect the highest damaging effect

Figures 5.18(a) and (b) imply that the two earthquake records caused IDRs to fall in the damage control structural performance level S2. The maximum IDRs occurred under the effect of EQ6 (1.01%) followed by EQ5 (0.9 %) as seen in Fig. 5.18. Under EQ5 and EQ6, the IDRs of the all storeys exceed the Immediate Occupancy performance limit and reach the Damage Control Structural performance level (S2) at the exception of storey (1) for EQ6, the corresponding drift is lower than the immediate occupancy level. It is worth mentioning that the contribution of the higher modes of vibration to the IDR profiles is clearly reflected in Figs. 5.18(a) and (b) where the maximum IDRs occur at the (10 and 11) storeys of the analyzed fifteen-storey SCBFs. Based on the information summarized in Table 5.7, it is evident that EQ6 is more destructive than EQ5. Additionally, a significant match between the time of occurrence of the maximum brace member deformation and the time of maximum roof drift of the fifteen-storey SCBF (see Table 5.7).

5.6 Use of Pushover Analysis Technique as a Simplified Tool to Predict the Damage Scheme

5.6.1 Six-Storey SCBF

For the six-storey SCBF, the record EQ5 caused the highest response among all eight ground motions leading to roof drift (121.5 mm) and base shear (3688.78 kN) as shown in Figs 5.19 and 5.20, respectively. Static pushover analysis applied to the same SCBF, as provided in chapter 4, yielded a roof drift of 897.14 mm and a base shear of 6355.11 kN at the storey collapse limit (refer to Figs. 5.19 and 5.20, respectively).

Figure 5.19: Maximum Roof Drift of the Six-Storey SCBF Resulting from Time
History Analysis using the Eight Selected Ground Motion Records

Figure 5.20: Maximum Base Shear of the Six-Storey SCBF Resulting from Time
History Analysis using the Eight Selected Ground Motion Records

For a global assessment of the performance of the SCBF under the most influencing ground motion record, the hysteretic curve for EQ5 was plotted against the capacity curve obtained from pushover analysis, as depicted in Fig. 5.21, where it can be noticed that hysteretic response is enclosed within the limits of the capacity curve.

Figure 5.21: Hysteretic Curve (EQ5) versus Pushover Capacity Curve for the Six-Storey SCBF

As a conclusion, none of the eight ground motion records that are scaled to represent Abu Dhabi seismicity lead to the formation of storey or building collapse mechanism of the six-storey SCBF. It is important to note that the five ground motions EQ5, EQ6, EQ7, EQ8 and EQ3 that caused considerable deformation in the braces resulted in a base shear greater than the design base shear (V_d) as shown in Fig. 5.20. In fact, the low-level repairable damage experienced by the SCBF is attributed to applying the capacity and ductility design provisions to the SCBF. It is also important to observe the difference between the IDR profiles shown in Fig. 5.10 and those of pushover analysis of the six-storey SCBF shown in Fig. 4.12. This

difference is due to the fact that the adopted pushover analysis assumes domination of the response by the first mode of vibration. Meanwhile, in time history analysis, all mode shapes contribute to the overall response of the SCBF. This becomes more significant with the increase in SCBF height where the contribution of higher modes to the mass participation becomes more considerable as discussed in sections 5.6.2 and 5.6.3.

5.6.2 Nine-Storey SCBF

Similar to the six-storey SCBF, the maximum seismic response experienced by the nine-storey SCBF resulted from EQ5. Under this particular earthquake record, the maximum roof drift observed was 268.2 mm and the associated base shear was 5429.25 kN as shown in Figs. 5.22 and 5.23, respectively. Static pushover analysis of the nine-storey SCBF resulted in a roof drift of 897.14 mm and a base shear of 6919.19 kN at the storey collapse limit (refer to Figs. 5.22 and 5.23, respectively). For a global assessment of the performance of the SCBF under the most influencing ground motion record, the hysteretic curve for EQ5 was plotted against the capacity curve obtained from pushover analysis as depicted in Fig. 5.24, where it can be noticed that hysteretic response is enclosed within the limits of the capacity curve.
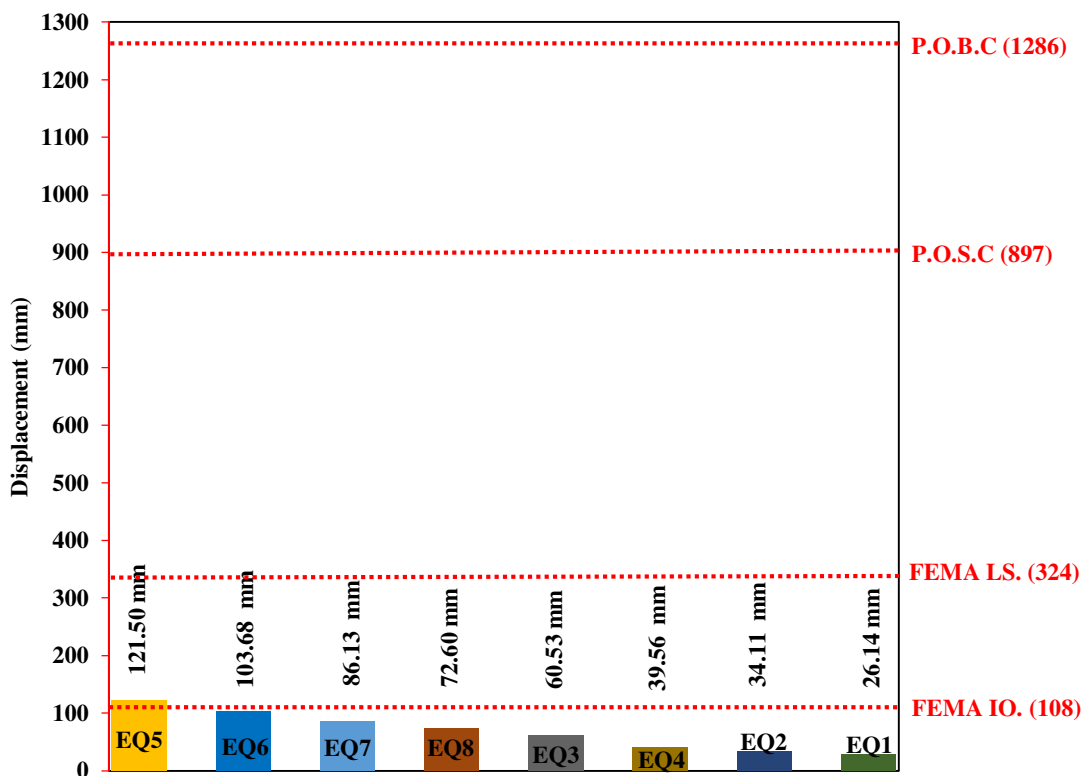
Figure 5.22: Maximum Roof Drift of the Nine-Storey SCBF Resulting from Time History Analysis using the Eight Selected Ground Motion Records
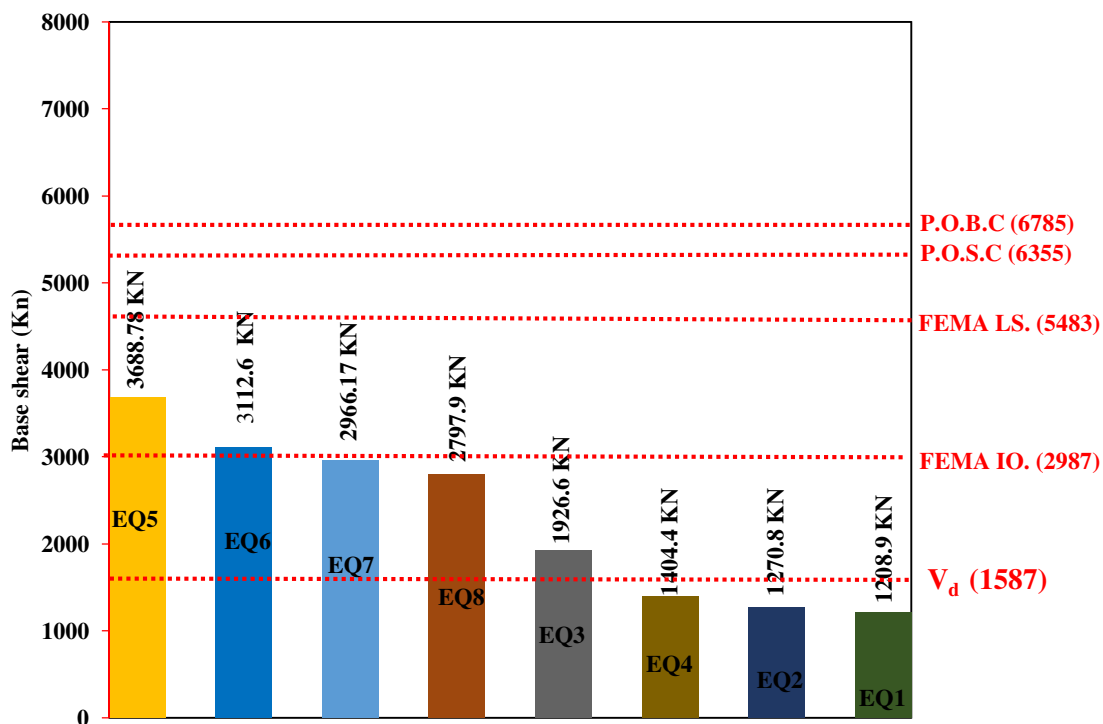

Figure 5.23: Maximum Base Shear of the Nine-Storey SCBF Resulting from Time History Analysis using the Eight Selected Ground Motion Records
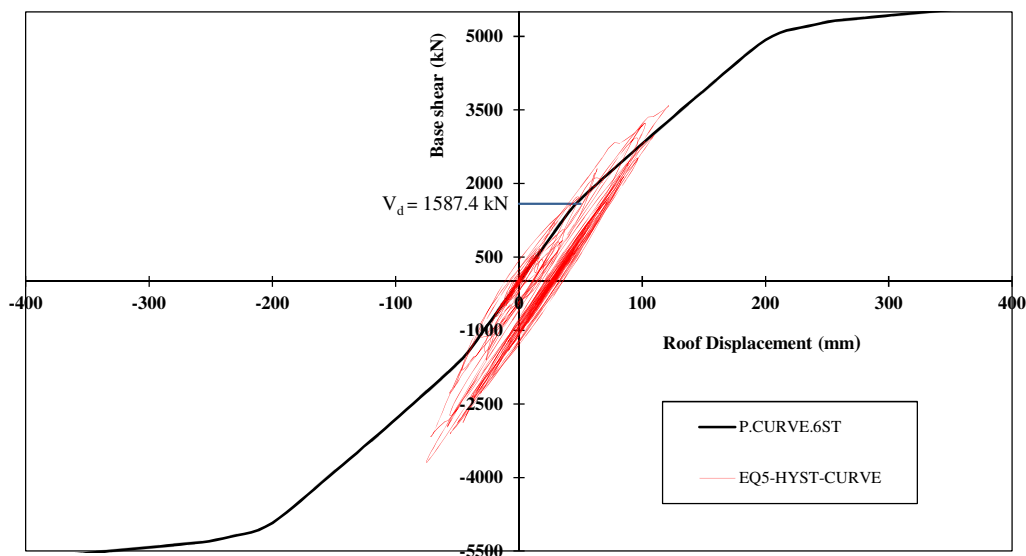
Figure 5.24: Hysteretic Curve (EQ5) versus Pushover Capacity Curve for the Nine-Storey SCBF

As a conclusion, none of the eight ground motion records that are scaled to represent Abu Dhabi seismicity lead to the formation of storey or building collapse mechanism of the nine-storey SCBF. It is important to note that the three ground motions EQ5, EQ6 and EQ7 that caused considerable deformation in the braces resulted in a base shear greater than the design base shear (V_d) as shown in Fig. 5.23. In fact, the low-level repairable damage experienced by the SCBF is attributed to implementing the capacity and ductility concept when sizing the members of the SCBF. It is also important to note the difference between the IDR profiles resulting from time history analysis (Fig. 5.14) and those of pushover analysis of the nine-storey SCBF shown in Fig. 4.16. The difference is due to the fact that the adopted pushover analysis assumes domination of the response by the first mode of vibration. Meanwhile, in time history analysis higher modes have considerable contribution to the response as reflected by the mass participation ratios summarized in Table 5.4.

While the ratio associated with the fundamental mode is 76% only, the contribution of the second mode reached 16%.

5.6.3 Fifteen-Storey SCBF

For the fifteen-storey SCBF, the record EQ6 caused the highest response among all eight excitations leading to a maximum roof drift of 432.58 mm and a maximum base shear of 5372.5 kN as depicted by Figs 5.25 and 5.26, respectively. Meanwhile, static pushover analysis of the fifteen-storey SCBF indicated a roof drift of 2617.44 mm and a base shear of 8263.81 kN at the storey collapse limit as shown in Figs. 5.25 and 5.26, respectively. This reveals that the maximum expected roof drift and base shear from time history analysis are below the values obtained from static pushover analysis. This is also evident by the fact that the hysteretic response of EQ6 is enclosed within the limits of the pushover capacity curve as shown in Fig. 5.27. Similar to the six- and nine-storey SCBFs, this low-level repairable damage is attributed to using the capacity and ductility design provisions when designing the SCBF. The two ground motions EQ5 and EQ6 that caused considerable deformation in the braces resulted in a base shear greater than the design base shear (V_d) as shown in Fig. 5.26. It is worth mentioning that the contribution of higher modes to the response of SCBFs becomes more significant with the increase in the building height. This is expressed by the mass participation ratios summarized in Table 5.4 where the ratio associated with the fundamental mode is about 70% only while the contribution of the second mode exceeds 18%. This explains the difference between the IDR profiles resulting from time history analysis (Fig. 5.18) and those of the pushover analysis of the fifteen-storey SCBF (Fig. 4.20) where the response is assumed to be governed by the fundamental mode only.
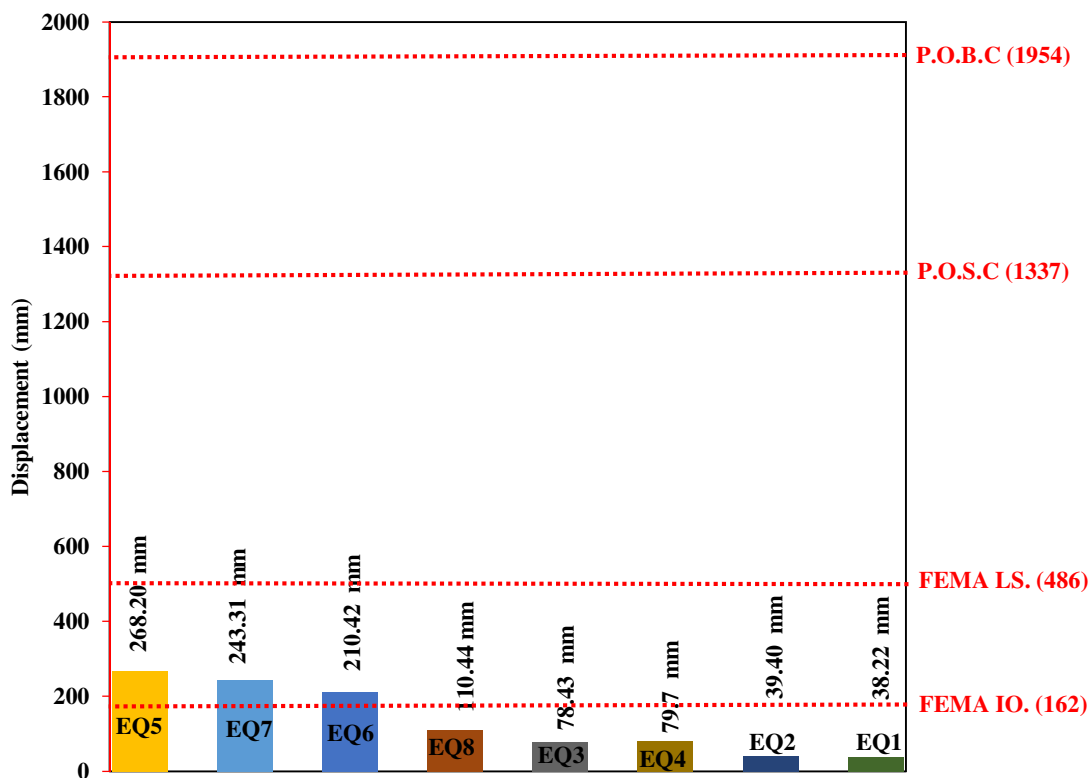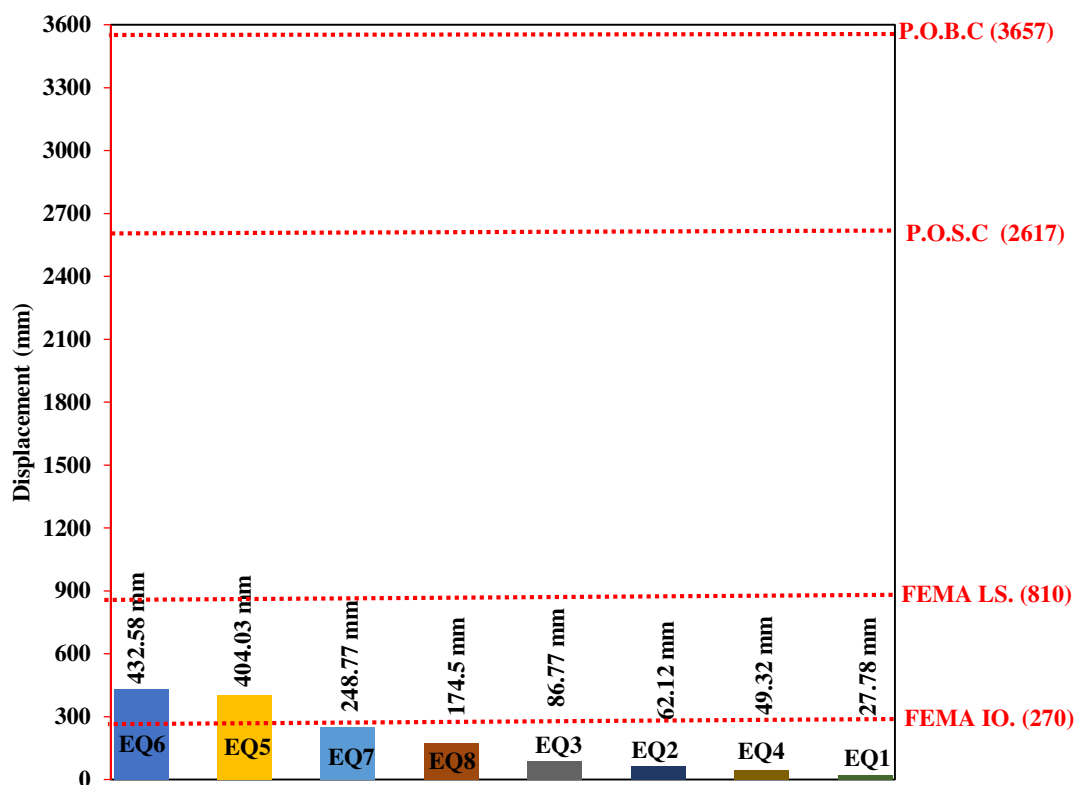
Figure 5.25: Maximum Roof Drift of the Fifteen-Storey SCBF Resulting from Time History Analysis using the Eight Selected Ground Motion Records
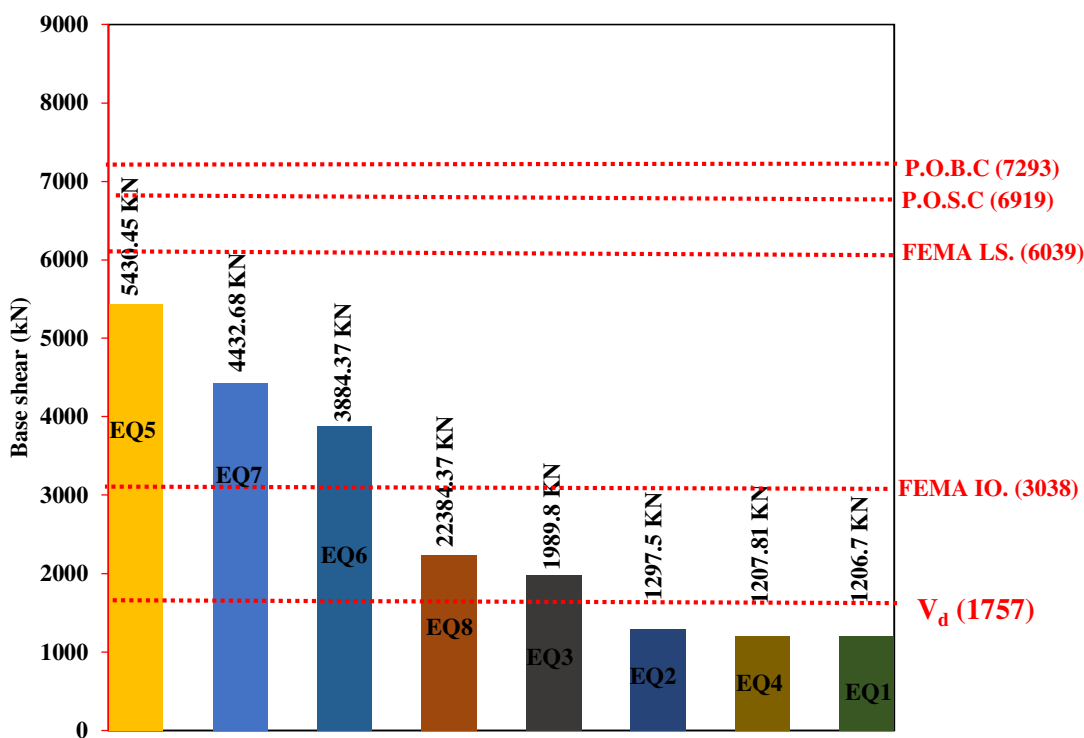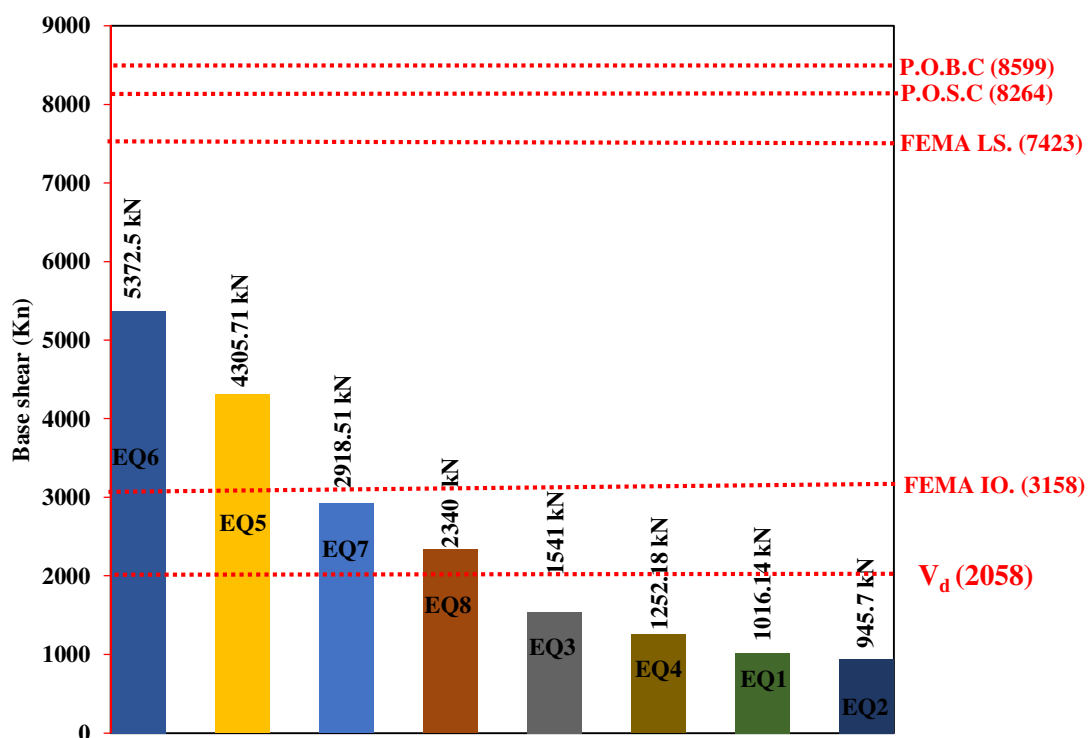

Figure 5.26: Maximum Base Shear of the Fifteen-Storey SCBF Resulting from Time History Analysis using the Eight Selected Ground Motion Records
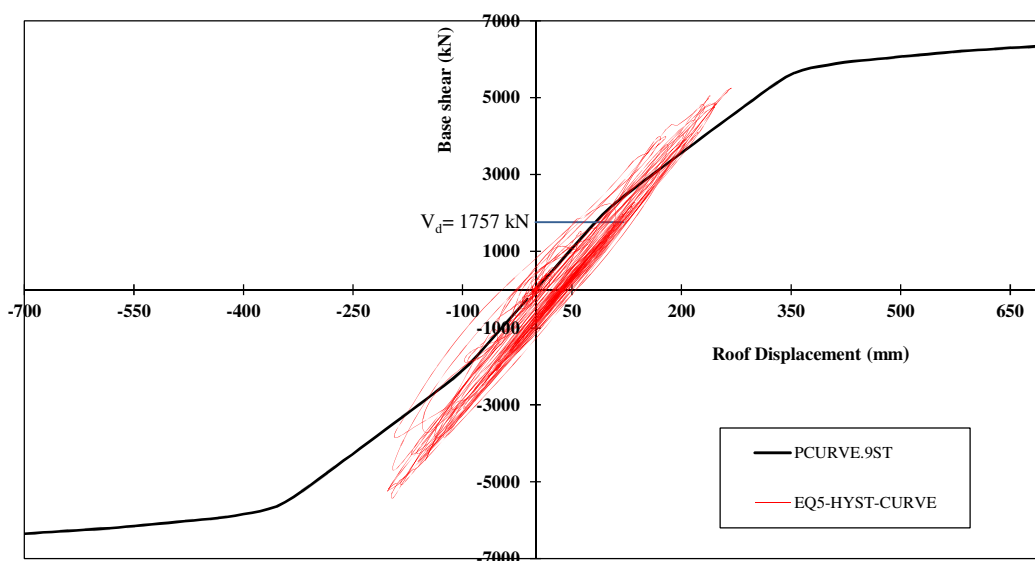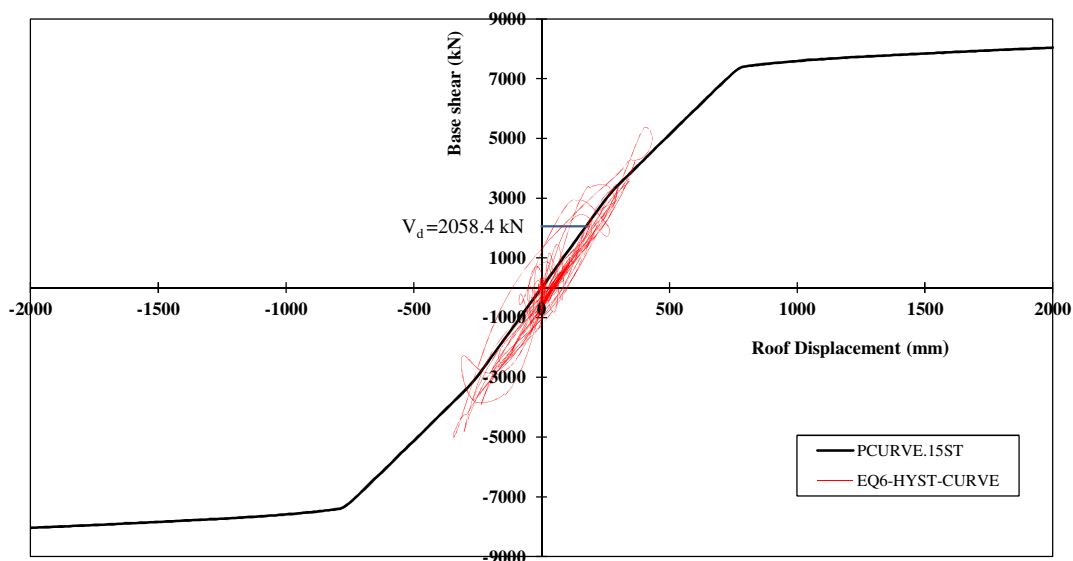
Figure 5.27: Hysteretic Curve (EQ6) versus Pushover Capacity Curve for the Fifteen-Storey SCBF

5.7 Conclusions

This chapter focused on using non-linear time history analysis technique to assess the performance of Special Concentrically Braced Frames (SCBFs) subjected to real earthquake scenarios that represent the seismicity of Abu Dhabi. For this purpose, eight ground motion records representing the possible seismicity levels in Abu Dhabi were selected and scaled to a maximum PGA of 0.17g. Three SCBFs with different heights (six-, nine- and fifteen-storey) were subjected to the eight ground motions. The performance of the modeled SCBFs under these ground motions was satisfactory where minor repairable damages in braces took place with no sign of collapse. None of the structural members reached the Life Safety Structural Performance Level (S-3) while the maximum response observed was in the Damage Control Structural Performance Level range (S-2). Design for the Damage Control Structural Performance Range may be desirable to minimize repair time and operation interruption, as a partial means of protecting valuable equipment

and contents, or to preserve important historic features when the cost of design for immediate occupancy is excessive (FEMA 356, 2000).

Results of the time history analysis of the six-storey SCBF revealed that five of the scaled records (EQ3, EQ5, EQ6, EQ7 and EQ8) caused the deformations in the braces to reach the damage control structural performance range (S-2). All damage was due to relatively high compressive deformations in brace members while tensile deformations were always below this performance level. For these particular records listed above, two damage indicators were used to imply the time sequence of damage occurrence (MDT) and the level of damage incurred by the affected brace elements (MD). A damage severity indicator for influential records was also introduced and its criterion was based on the number of damaged braces, maximum brace deformation, maximum roof drift and maximum IDR. For the particular case of maximum damage severity indicator, response history outcomes indicated the maximum damage to take place in the fourth storey. The recorded maximum brace compressive deformation is 5.34 mm at storey 1 and a maximum roof drift of 121.5 mm with a corresponding maximum inter-storey drift ratio (IDR) of 0.67% at storey 4. These effects took place under the effect of EQ5.

For the nine-storey SCBF, only three of the scaled records; EQ5, EQ6 and EQ7 caused the deformations in the braces to reach the damage control structural performance range (S-2) due to relatively high compressive deformations in brace members. The case of maximum damage severity indicator of the nine-storey SCBF took place under the effect of EQ5. Time history results revealed a maximum damage to occur at storey 1 with a maximum brace compressive deformation is 7.56

mm and a maximum roof drift of 268.2 mm with a corresponding maximum inter-storey drift ratio (IDR) of 0.89% in the mid-height storeys (4 to 7).

Two of the scaled records (EQ5 and EQ6) caused the deformations in the braces of the fifteen-storey SCBF to reach the damage control structural performance range (S-2) due to relatively high compressive deformations in brace members.

For the particular case of maximum damage severity indicator in the fifteen-storey SCBF, response history results indicated the maximum damage to take place at storey 1. The recorded maximum brace compressive deformation is 4.55 mm and a maximum roof drift of 432.58 mm with a corresponding maximum inter-storey drift ratio (IDR) of 1.01% in the upper third of the building height (storey 10 and 11). Unlike the six- and nine-storey SCBFs, these results occurred under the effect of EQ6.

For each of the analyzed CBFs, a comparison was held between the maximum inter-storey drift ratios resulting from time history analysis and those obtained from non-linear pushover analysis. The comparison revealed that the variation of the inter-storey drift along the height of the building differs based on the analysis method. This difference is due to the fact that the pushover analysis conducted used a lateral load pattern that assumes domination of the response by the fundamental mode of vibration. On the contrary, time history results consider the contribution of higher modes of vibration to the response. The contribution of higher modes of vibration to the response was found to be more significant with the increase in SCBF height.

Chapter 6: Conclusions and Recommendations

6.1 Research Summary and Conclusions

The current research work is carried out to investigate the efficiency of using steel concentrically braced frames as lateral force resisting system (LRFS) for office buildings constructed in Abu Dhabi, UAE, with common heights ranging from six to fifteen storeys. Two braced frame systems were considered in the study; namely ordinary concentrically braced frames (OCBFs) and special concentrically braced frames (SCBFs). Three buildings' heights were modeled and analyzed including six-, nine- and fifteen-storey steel braced frames. Structural loads (dead, live, wind and seismic) are calculated in accordance with the ASCE7-10 (2010) standard and the requirements of the International Building Code (IBC, 2012). Design of the various structural elements was performed according to ANSI/AISC 360-10 (2010), and the corresponding seismic provisions ANSI/AISC 341-10 (2010).

Seismic calculations showed that Abu Dhabi is located in a seismic design category (SDC) that is a borderline between categories C and D. As a result, both categories (SDC C) and (SDC D) were considered. For SDC C, a steel OCBF was used as a seismic load resisting system. Due to the seismic code limitations on the height of OCBFs constructed in areas with SDC D, a steel SCBF was considered. Three different building heights (six-, nine- and fifteen-storey) were selected for each system. All six CBFs were modeled and analyzed using the structural analysis software SAP2000 (2009). OCBFs were designed in accordance with strength design requirements only since they are not expected to be subjected to large inelastic demands due to their relatively low response modification factor (R=3.25). For the six- and nine-storey OCBFs strength-designed section sizes were found insufficient

to satisfy the code drift limits. Therefore, brace and column sections were enlarged to control the inter-storey drift values of OCBFs within acceptable code limits. Meanwhile, the SCBFs were subjected to capacity design and ductility requirements as per ANSI/AISC 341-10 (2010) in order to provide significant inelastic deformation capacity primarily through brace buckling and yielding.

For each designed frame, two failure criteria were considered to represent potential levels of damage that could be induced in structural systems during earthquake events. Storey collapse mechanism was utilized to represent the state of a damaged structure that is repairable with a low probability of life-threatening injury as per FEMA 356 (2000) life safety performance level (S-3). A more severe damage scenario was represented by the building collapse mechanism that represents the ultimate state at which the entire structure loses its stability and becomes unable to withstand any additional loads. A finite element model was developed using SeismoStruct software package (2012) to simulate the lateral response of the three building heights using the pushover technique. The accuracy of the finite element model was validated by comparison with relevant experimental measurements reported in the literature. Results of the pushover analysis revealed that SCBFs reach yield before their OCBFs counterparts due to the smaller brace sections used in SCBFs relative to those employed in OCBFs. Pushover capacity curves of the six-storey CBFs indicated considerably different response between OCBFs and SCBFs. This difference becomes less apparent in higher CBFs (i.e.; with nine- and fifteen-storey). This observation is attributed to the close match in section sizes of medium- and high-rise OCBFs and SCBFs due to the need to enlarge the strength designed sections of OCBFs to satisfy drift limitations.

In view of the pushover analysis results, overstrength factors associated with the storey mechanism of the six-, nine-, and fifteen-storey OCBF buildings are 1.59, 2.17 and 2.32, respectively. Higher values (1.91, 2.38 and 2.42, respectively) are found to correspond to overall building collapse. The considerable increase in the estimated reserve strength when height increased from six to fifteen storey is attributed to the fact that sizing of the sections of the six-storey OCBF was solely based on strength design requirements. Meanwhile, those of the nine- and fifteen-storey frames were enlarged to avoid excessive drift values. The obtained reserve strength values for nine- and fifteen-storey buildings satisfy the ASCE7-10 (2010) recommended overstrength value of 2.0 for OCBFs. However, this recommendation may not lead to safe designs of six-storey OCBFs.

Overstrength factors of SCBFs varied slightly (3.96 to 4.01) for the considered at the storey mechanism level. As well as to trigger an overall building collapse mechanism (4.15 to 4.23). The close reserve strength values for all heights of SCBFs were expected since the capacity design requirements led to increasing the sizes of the members in the SCBFs from their original strength-design sizes irrespective of the frame height. The estimated reserve strength factors are more than double the system overstrength factor of 2.0 specified by ASCE7-10 (2010) standards for SCBFs indicating the conservative approach adopted by the ASCE7-10 (2010) for designing SCBFs. It should be noted that the assessment of overstrength being conducted in this study is not intended to reestablish the overstrength as a performance factor. Rather, this is considered in more details by FEMA P695 (2009).

The level of ductility shown by all analyzed models was also explored in the current study. The results implied a significantly higher ductility for SCBF compared

to OCBF of the same height. For short buildings (six-storey model), the ductility of SCBF is about 131% and 72% higher than that of the OCBF at the storey and building collapse mechanisms, respectively. For medium height buildings (nine-storey model), the ductility of SCBF is about 88% and 24% higher than that of the OCBF at the storey and building collapse mechanisms, respectively. Meanwhile, for tall buildings (fifteen-storey model), the ductility of SCBF reached around 21% and 25% higher than that of the OCBF at the storey and building collapse mechanisms, respectively. This comparison revealed that the influence of changing the lateral load resisting system from OCBF to SCBF on the level of ductility is less pronounced with the increase in building height. At the meantime, the ductility of SCBFs is always higher than that of OCBFs. This observation confirms the importance of adopting the code ductility design requirements for SCBFs to attain lateral load resisting systems with high level of ductility.

The inter-storey drift ratio (IDR), at the storey collapse limit, of the six-storey OCBF exceeded the IO (Immediate Occupancy) and LS (Life Safety) limits recommended by FEMA 356 (2000) with the exception of the first storey that did not exceed the LS limit. This behavior is attributed to the formation of storey collapse mechanism due to failure of one of columns in the first storey. Meanwhile, the IDR of the six-storey SCBF showed a typical profile in which the maximum IDR taking place at the first storey with a decreasing trend towards the top of the building. For the nine-storey OCBF, the IDR of all storeys exceeded the IO and LS limits of FEMA 356 (2000) with a typical variation along the height with the maximum IDR of 4.75% at the first storey and the minimum IDR of 2.01% at the ninth storey. The drift control requirements implemented during strength design of the OCBF improved its ductile behavior compared to the six-storey OCBF. A similar IDR

profile is obtained for the nine-storey SCBF with a more ductile behavior relative to its OCBF counterpart as evident by the higher IDR value of 7.3% at the top of the nine-storey SCBF. Almost identical IDR profiles are observed for the fifteen-storey OCB and SCB frames. Both maximum IDR for OCBF (7.42%) and SCBF (7.19%) took place at the first storey where the storey collapse limit was reached. Similar to the nine-storey OCBF, the drift control requirements improved the ductile behavior of the OCBF. The higher drift values associated with the fifteen-storey as compared to the nine-storey OCBF led to a significant increase in the members' sizes to satisfy the drift limits requirements. As such, similar IDR profiles and values are obtained for the fifteen-storey OCBF and SCBF.

Results of the non-linear static pushover analysis revealed that SCBFs provide a better alternative over OCBFs for ductility and overstrength. Thus, the study proceeded with assessing the performance of SCBFs under real earthquake excitations. For this purpose, eight ground motion records were selected and scaled to a maximum PGA of 0.17g to represent the possible seismicity levels in Abu Dhabi. Four of these records (EQ1 through EQ4) represent near-fault local moderate earthquakes with a short distance from the epicenter. Meanwhile, the other four records (EQ5 through EQ8) represent the scenario that is most likely to occur in Abu Dhabi for far-field severe events with a long distance from the epicenter. Three SCBFs with different heights (six-, nine- and fifteen-storey) were subjected to such excitations. In general, the performance of all modeled SCBFs was satisfactory where minor repairable damages in braces took place with no sign of collapse. None of the structural members reached the life safety structural performance level (S-3) while the maximum response observed was in the damage control level range (S-2). In particular, time history results of the six-storey SCBF revealed that five of the

scaled records (EQ3, EQ5, EQ6, EQ7 and EQ8) caused brace compressive deformations to reach the damage control structural performance range (S-2). Two damage indicators were developed to indicate the time sequence of damage occurrence (MDT) and the level of damage incurred by the affected brace elements (MD). A damage severity indicator for influential records was also introduced based on the number of damaged braces, maximum brace deformation, maximum roof drift and maximum IDR. The maximum damage severity indicator took place under the effect of EQ5 where the response history outcomes indicated the maximum damage to occur in the fourth storey. The recorded maximum brace compressive deformation is 5.34 mm and a maximum roof drift of 121.5 mm with a corresponding maximum inter-storey drift ratio (IDR) of 0.67%.

For the nine-storey SCBF, only three of the scaled records (EQ5, EQ6 and EQ7) caused the compressive deformations in the braces to reach the damage control structural performance range (S-2). The case of maximum damage severity indicator of the nine-storey SCBF took place under the effect of EQ5. Time history results revealed a maximum damage to occur in the mid-height storeys (4 to 7) with a maximum brace compressive deformation is 7.56 mm and a maximum roof drift of 268.2 mm with a corresponding maximum inter-storey drift ratio (IDR) of 0.89%.

Two of the scaled records (EQ5 and EQ6) caused the deformations in the braces of the fifteen-storey SCBF to reach the damage control structural performance range (S-2) due to relatively high compressive deformations. For the particular case of maximum damage severity indicator in the fifteen-storey SCBF, response history results indicated the maximum damage to take place in the upper third of the building height (storey 10 and 11). The recorded maximum brace compressive

deformation is 4.55 mm and a maximum roof drift of 432.58 mm with a corresponding maximum inter-storey drift ratio (IDR) of 1.01%. Unlike the six- and nine-storey SCBFs, these results occurred under the effect of EQ6.

For each of the analyzed CBFs, a comparison was held between the maximum inter-storey drift ratios resulting from time history analysis and those obtained from non-linear pushover analysis. The comparison revealed that the variation of the inter-storey drift along the height of the building differs based on the analysis method. This difference is due to the fact that the pushover analysis conducted used a lateral load pattern that assumes domination of the response by the fundamental mode of vibration. On the contrary, time history results consider the contribution of higher modes of vibration to the response. The contribution of higher modes of vibration to the response was found to be more significant with the increase in SCBF height.

6.2 Recommendations for Future Work

This study provides promising outcomes and strong base to motivate future researchers to be further involved in investigating the use of concentrically braced frames in the UAE at large. Continuous research efforts on this subject are expected to enrich literature related to this topic and to provide code developers with relevant basic design information. Some interesting topics that still need to be explored are summarized herein:

- To explore the impact of using various lateral load distribution patterns on the outcomes of nonlinear pushover analysis conducted on concentrically braced frames.

- To investigate the efficiency of other common bracing configurations such as split X-bracing, chevron and inverted chevron for use as lateral force resisting systems in the UAE.

- To compare the performance of buckling restrained bracing systems to that of conventional systems with different configurations.

- To consider the topic of this thesis, along with the future topics listed above, when applied to eccentrically braced frame structures.

Bibliography

Abdalla, J.A., and Al Homoud, AS. (2004). Seismic hazard assessment of United Arab Emirates and its surroundings. *Journal of Earthquake Engineering*, *8*(6), 817–837.

Aldama-Bustos, G., Bommer, J.J., Fenton, C.H., and Stafford, P. (2009). Probabilistic seismic hazard analysis for rock sites in the cities of Abu Dhabi, Dubai and Ras Al Khaimah, United Arab Emirates. *Georisk 3*(1), 1–29.

Annan, Charles D. (December 2008). *Applicability of traditional design procedures to modular steel buildings*- PhD, The University of Western Ontario. London, Ontario, Canada.

ANSI/AISC 341-10, (2010). *Seismic provisions for structural steel buildings,* American Institute of Steel Construction. Chicago, Illinois, USA.

ANSI/AISC 360-10, (2010). *Steel construction manual*, American Institute of Steel Construction. Chicago, Illinois, USA.

Anthony, J. D. (2007). The Gulf States' Construction Boom: Year In Review 2007. (2015). In *Encyclopædia Britannica*. Retrieved from http://www.britannica.com/topic/Gulf-States-Construction-Boom-The-1385117

ASCE, (2010). *SEI/ASCE 7-10: Minimum design loads for buildings and other structures*. ASCE Standard, American Society of Civil Engineers, USA.

Brandonisio, G., Toreno, M., Grande, E., Mele, E., and De Luca, A. (2012). Seismic design of concentric braced frames. *Journal of Constructional Steel Research 78*(11), 22–37.

Broderick, B.M., Elghazouli, A.Y., and Goggins, J. (2008). Earthquake testing and response analysis of concentrically braced sub-frames. *Journal of Constructional Steel Research, 64*(9), 997–1007.

Bruneau, M., Uang, C., and Sabelli, R. (2011). *Ductile design of steel structures* (p.499-590). Second edition. New York, USA: McGraw-Hill Companies, Inc.

Chopra, A. K. (2012). *Dynamics of structures: theory and applications to earthquake engineering*. Fourth edition. Englewood Cliffs, New Jersey, USA: Prentice-Hall.

Clough, R.W. and Penzien, J. (2003). *Dynamics of structures*. Third edition. Berkeley, California, USA: Computers and Structures, Inc.

CSA, (2001) *Handbook of steel construction*, Canadian Institute of Steel Construction. 7th ed., Willowdale, ON, Canada.

D'Aniello, M., Ambrosino, G.L.M., Portioli, F., and Landolfo, R. (2012). Seismic behaviour of dual steel concentric braced frames. *STESSA 2012*. London: Taylor and Francis Group.

Engelhardt, M.D. (2007). *Design of seismic-resistant steel building structures: concentrically braced frames*. University of Texas at Austin with the support of the American Institute of Steel Construction (AISC).

Eurocode 8 (EC8), (2005). *Design of structures for earthquake resistance. Part 1: General rules, seismic actions and rules for buildings*, UNI ENV 1998-1.

Fanella, D.A. (2012). *Structural loads: 2012 IBC and ASCE/SEI 7-10.* Second edition. USA: ICC.

Federal Emergency Management Agency (FEMA-356 (2000)). Prestandard and commentary for the seismic rehabilitation of buildings. Prepared by American Society of Civil Engineers, Washington, D.C., USA.

Federal Emergency Management Agency (FEMA P695 (2009)). Quantification of Building Seismic Performance Factors Prepared by the Applied Technology Council (ATC), California, USA.

Federal Emergency Management Agency (FEMA P-750 (2009)). NEHRP Recommended Seismic Provisions for New Buildings and Other Structures Prepared by the Building Seismic Safety Council of the National Institute of Building Sciences, Washington DC, USA.

Fell, B., Kanvinde, A., Deierlein,G., and Myers, A. (2009). Experimental investigation of inelastic cyclic buckling and fracture of steel braces. *Journal of Structural Engineering, 135*(1), 19–32.

Fenton, C.H., Adams, J., and Halchuk, S. (2006). Seismic hazards assessment for radioactive waste disposal sites in regions of low seismic activity. *Geotechnical and Geological Engineering, 24* (3), 579-592.

Grunthel, G., Bosse, C., Sellami, S., Mayer-Rosa, D., and Giardini, D. (1999). Compilation of the GSHAP regional seismic hazard map for Europe, Africa and the Middle East. *Annali de Geofisica 42*(6), 1215–1223.

Hajirasouliha, I., and Doostan, A. (2010). A simplified model for seismic response prediction of concentrically braced frames. *Advances in Engineering Software 41*(3), 497–505.

Hsiao, P., Lehman, D.E. and Roeder, C.H. (2012). Improved analytical model for special concentrically braced frames. *Journal of Constructional Steel Research 73 (2012) 80–94*

IBC, (2009). *International building code*, International Code Council, Washington, D.C., USA.

IBC, (2012). *International building code*, International Code Council, Washington, D.C., USA.

Issa, A, and Mwafy, A. (2014). Fragility assessment of pre-seismic code buildings and emergency facilities in the UAE. Second European Conference on Earthquake Engineering and Seismology, Istanbul, Turkey, 25-29 August 2014.

Johnson, M., Sloat, D., Roeder, C.H., Lehman, D.E., and Berman, J.W. (2014). Seismic performance of concentrically braced frame connections. Tenth U.S. National Conference on Earthquake Engineering, Anchorage, Alaska, 21-25 July 2014.

Kaviani, A., Paul, A., Bourova, E., Hatzfeld, D., Pedersen, H., and Mokhtari, M. (2007). A strong seismic velocity constant in the shallow mantle across the Zagros collision zone (Iran). *Geophysical Journal International, 171*(l), 399-410.

Khan, Z., El-Emam, M., Irfan, M., and Abdalla, J. (2013). Probabilistic seismic hazard analysis and spectral accelerations for United Arab Emirates. *Natural hazards, 67*(2), 569-589.

Kowalczyk, R.M., Sinn, R., Bennetts, I.D., and Kilmister, M.B. (1995). *Structural systems for tall buildings*. Council on Tall Buildings and Urban Habitat. Committee 3. New York, USA: McGraw-Hill.

Krawinkler, H. (1996). Pushover analysis: why, how, when and when not to use it. *Proceedings of the 65th Annual Convention of the Structural Engineers Association of California*, Maui, Hawaii, 1-6 October 1996.

Lehman, D.E., Roeder, C.W., Herman, D., Johnson, S. and Kotulka, B. (2008). Improved seismic performance of gusset plate connections. *Journal of Structural Engineering, 134*(6), 890–901.

Lindeburg, M.R., and Mcmullin, K.M. (2011). *Seismic design of building structures*. Tenth edition. Belmont, California, USA: Professional Publications, Inc.

Mahmoudi, M., and Zaree, M. (2010). Evaluating response modification factors of concentrically braced steel frames. *Journal of Constructional Steel Research, 66*(10), 1196–1204.

Moghaddam, H., Hajirasouliha, I, and Doostan, A. (2005). Optimum seismic design of concentrically braced steel frames: concepts and design procedures. *Journal of Constructional Steel Research 61*(2), 151–66.

Moghaddam, H. and Hajirasouliha, I. (2006). An investigation on the accuracy of pushover analysis for estimating the seismic deformation of braced steel frames. *Journal of Constructional Steel Research, 62*(4), 343–351.

Mwafy, A., Elnashai, A., Sigbjörnsson, R., and Salama, A. (2006). Significance of severe distant and moderate close earthquakes on design and behavior of tall buildings. *The Structural Design of Tall and Special Buildings, 15*(4), 391-416.

National Earthquake Hazards Reduction Program (NEHRP) 2010, "Evaluation of the FEMA P-695 Methodology for Quantification of Building Seismic Performance Factors", Report prepared for U.S. Department of Commerce Engineering Laboratory, National Institute of Standards and Technology (NIST GCR 10-917-8), Gaithersburg, MD 20899-8600.

Peiris, N., Free, M., Lubkowski, Z., and Hussein, A.T. (2006). Seismic hazard and seismic design requirements for the Arabian Gulf region. *First European conference on earthquake engineering and seismology*, Geneva, Switzerland.

Pong, W.S., Lee, A. and Lee, Z.H. (2006). The international building code and its implications on seismic design. *Fourth International Conference on Earthquake Engineering,* Taipei, Taiwan October 12-13 October 2006.

Rahgozar, M.A. and Humar, J.L. (1998). Accounting for overstrength in seismic design of steel structures. *Canadian Journal of Civil Engineering, 25*(1)*,* 1–15.

Rajendran, C., Rajendran, K., Shah-Hosseini, M., Benti, A. Nautiyal, C., and Andrews, R. (2013). The hazard potential of the western segment of the Makran subduction zone, northern Arabian Sea. *Natural hazards, 65*(l), 219-239.

Sabelli, R., Roeder, C.W., and Hajjar, J.F. (2013). "Seismic design of steel special concentrically braced frame systems: A guide for practicing engineers," NEHRP Seismic Design Technical Brief No. 8, NEHRP Consultants Joint Venture, a partnership of the Applied Technology Council and the Consortium of Universities for Research in Earthquake Engineering, for the National Institute of Standards and Technology, Gaithersburg, MD, NIST GCR 13-917-24.

Salmon, G.S., Johnson, J.E. and Malhas, F.A. (2009). *Steel Structures: Design and Behavior*. Fifth edition. New York, USA: Prentice Hall.

SAP2000, (2009). *Integrated finite element analysis and design of structures*. Computers and Structures, Inc., Version 14.0.0, Berkeley, California, USA.

Sawada, T., Hirao, K., Yamamoto, H., and Tsujihara, O. (1992). Relation between maximum amplitude ratio and spectral parameters of earthquake ground motion, *Proc. 10th World Conference on Earthquake Engineering,* Madrid, Spain, Vol. 2, 617-622.

SeismoStruct - V 6.00. (2012) from Seismosoft - A computer program for static and dynamic nonlinear analysis of framed structures 2003. Available from URL: http://www.seismosoft.com.

Shama, A.A. (2011). *Site specific probabilistic seismic hazard analysis at Dubai Creek on the west coast of UAE. Earthquake Engineering and Engineering Vibration, 10*(1), 143–152.

Sigbjornsson, R., and Elnashai, A.S. (2006). Hazard assessment of Dubai, United Arab Emirates, for close and distant earthquakes. *Journal of Earthquake Engineering*, *10*(5), 749–773.

Taranath, B.S. (2005). *Wind and earthquake resistant buildings: structural analysis and design* (p.261-323). New York, USA: Marcel Dekker.

Tedesco, J.W., McDougal, W.G., and Ross, C.A. (1999). *Structural dynamics: theory and applications*. Menlo Park, California, USA: Addison Wesley Longman.

Tegral Comflo, Composite Flooring. Online resource. Retrieved from: http://www.tegral.com/index.php?page=Comflor, accessed in March 20014.

Uang, C.M., and Bertero, V.V. (1986). Earthquake simulation tests and associated studies of a 0.3-scale model of a 6-storey concentrically braced steel structure. Report No. UCB/EERC-86/10. Earthquake Engineering Research Center; Univ. of California, Berkeley, CA, USA.

UBC, (1997). Structural engineering design provisions. Uniform building code. International conference of building officials, vol. 2.

Uriz, P., and Mahin, S.A. (2008). Toward earthquake-resistant design of concentrically braced steel-frame structures. PEER Report 2008/08. Pacific Earthquake Engineering Research Center; College of Engineering; University of California, Berkeley, CA, USA.

Wakabayashi, M., Matsui, C., Minami, K., and Mitani, I. (1974). Inelastic behaviour of full scale steel frames. *Bull. Disaster Prevention Research Institute, Kyoto Univ., 24*(216), 1–23.

Wakabayashi, M., Nakamura, T., and Yoshida, N. (1977). Experimental studies on the elastic-plastic behavior of braced frames under repeated horizontal loading. *Bull. Disaster Prevention Research Institute, Kyoto Univ., 27*(251), 121–154.

Whitaker, A.S., Bertero, V.V., Alonso J., and Thompson C. (1989). Earthquake simulator testing of steel plate added damping and stiffness elements. Report No. UCB/EERC-89/02, Earthquake Engineering Research Centre, University of California, Berkeley, CA, USA.

Wight, J.K., and Macgregor, J.G. (2011). *Reinforced concrete mechanics and design*. Sixth edition. New Jersey, USA: Pearson.

Williams, A. (2014). *Seismic and wind forces: structural design exemples* (p.267-297). Fourth edition. California, USA: ICC.

Yoo, J.H., Roeder, C.W., and Lehman, D.E. (2008a). Analytical performance simulation of special concentrically braced frames. *Journal of Structural Engineering, 134*(6), 881–889.

Yoo, J.H., Roeder, C.W., and Lehman, D.E. (2008b). FEM simulation and failure analysis of special concentrically braced frame tests. *Journal of Structural Engineering, 134*(6), 902–910.

Yoo, J.H., Roeder, C.W., and Lehman, D.E. (2009). Simulated behavior of multi-storey X-braced frames. *Engineering Structures 31*(1), 182-197

Zhu, T.J., Heidebrecht, A.C., and Tso, W.K. (1988). Effect of peak ground acceleration to velocity ratio on ductility demand of inelastic systems. *Earthquake Engineering and Structural Dynamics 16*(1), 63-79.

Appendix A: Determination of Seismic Design Category

All calculations are based on the ASCE7-10 (2010) provisions.

Site parameters

Site class; C (very dense soil)

Mapped acceleration parameters (Section 11.4.1,):

at short period; $S_S = \mathbf{0.60}$

at 1 sec period; $S_1 = \mathbf{0.19}$

Long-period transition period; $T_L = \mathbf{8.0}$ **sec.**

Site class coefficientat at short period (Table 11.4-1); $F_a = \mathbf{1.20}$

Site class coefficientat at 1 sec period (Table 11.4-2); $F_v = \mathbf{1.60}$

Spectral response acceleration parameters

at short period (Eq. 11.4-1); $S_{MS} = F_a \times S_S = \mathbf{0.696}$

at 1 sec period (Eq. 11.4-2); $S_{M1} = F_v \times S_1 = \mathbf{0.306}$

Design spectral acceleration parameters (Sect 11.4.4)

at short period (Eq. 11.4-3); $S_{DS} = 2/3 \times S_{MS} = \mathbf{0.464}$

at 1 sec period (Eq. 11.4-4); $S_{D1} = 2/3 \times S_{M1} = \mathbf{0.204}$

Seismic design category

Risk category (Table 1.5-1); **II**

Seismic design category based on short period response acceleration (Table 1613.5.6 (1)): **C**

Seismic design category based on 1 sec period response acceleration (Table 1613.5.6 (2)): **C**

TABLE 1613.5.6(1)
SEISMIC DESIGN CATEGORY BASED ON
SHORT-PERIOD RESPONSE ACCELERATIONS

VALUE OF S_{DS}	OCCUPANCY CATEGORY		
	I or II	III	IV
$S_{DS} < 0.167g$	A	A	A
$0.167g \leq S_{DS} < 0.33g$	B	B	C
$0.33g \leq S_{DS} < 0.60g$	C	C	D
$0.60g \leq S_{DS}$	D	D	D

TABLE 1613.5.6(2)
SEISMIC DESIGN CATEGORY BASED ON
1-SECOND PERIOD RESPONSE ACCELERATION

VALUE OF S_{D1}	OCCUPANCY CATEGORY		
	I or II	III	IV
$S_{D1} < 0.067g$	A	A	A
$0.067g \leq S_{D1} < 0.133g$	B	B	C
$0.133g \leq S_{D1} < 0.25g$	C	C	D
$0.25g \leq S_{D1}$	D	D	D

Appendix B: Sample Design Calculations - Levels 1 to 3 (Six-Storey SCBF)

NOTATIONS :		: Manual Input		: Automatic Input Fom another sheet		: Automatic Output

LEVEL 1 to LEVEL 3

BRACES

SECTION	E	F_Y	L	D	t	k	I	A_g	r_I
	Mpa	Mpa	mm	mm	mm		mm^4	mm^2	mm
HSS 152.4x12.7	200000	345	2690.7	152.4	12.7	2	13709679	5573.8	49.59509

CALCULATION OF NOMINAL TENSION & COMPRESSION

Scenario (1) : "Brace Forces are Based on their Expected Strength in Tension and Compression"

Nominal Tensile Str.	$T_{BR} =$	$R_Y \times F_Y \times A_g=$	2115.25	KN	$R_y=$	1.1

| Nominal Compression Str. | $C_{BR} =$ | $1.14 \times F_{cre} \times A_g=$ | 934.267 | KN | = | 0.4262 | $\times T_{BR}$ |

F_{cr} : detailed calculation

Slenderness ratio $\dfrac{Kl}{r_i} =$ 108.5

$4.71\sqrt{\dfrac{E}{R_y F_y}} =$ 108.1

If $\dfrac{Kl}{r_i} > 4.71\sqrt{\dfrac{E}{R_y F_y}}$ → $F_{cr} = 0.877 \times F_e$

If $\dfrac{Kl}{r_i} \leq 4.71\sqrt{\dfrac{E}{R_y F_y}}$ → $F_{cr} = \left[0.658^{\frac{R_y F_Y}{F_e}}\right] \times R_y F_y$

$Fe = \dfrac{\pi^2 E}{\left(\dfrac{Kl}{r_i}\right)^2}$ = 167.655 Mpa

F_{cre} = 147.033 Mpa = 0.4262 $\times F_Y$

Scenario (2) : "Brace Forces are Based on their Expected Tensile Strength and Post-Buckling Compressive Strength"

Expected Tensile Str.	$T_{BR} =$	$R_Y \times F_Y \times A_g=$	2115.25	KN	$R_y=$	1.1

| Post Buckling Compression Str. | $C_{BR} =$ | $0.3 \times F_{cr} \times A_g=$ | 243.801 | KN | = | 0.1153 | $\times T_{BR}$ |

F_{cr} : detailed calculation

Slenderness ratio $\dfrac{Kl}{r_i} =$ 108.5

$4.71\sqrt{\dfrac{E}{F_Y}} =$ 113.4

If $\dfrac{Kl}{r_i} > 4.71\sqrt{\dfrac{E}{F_Y}}$ → $F_{cr} = 0.877 \times F_e$

If $\dfrac{Kl}{r_i} \leq 4.71\sqrt{\dfrac{E}{F_Y}}$ → $F_{cr} = \left[0.658^{\frac{F_Y}{F_e}}\right] \times F_Y$

$Fe = \dfrac{\pi^2 E}{\left(\dfrac{Kl}{r_i}\right)^2}$ = 167.655 Mpa

F_{cr} = 145.802 Mpa = 0.4226 $\times F_Y$

STEEL COLUMNS

SECTION	E	F_Y	L	b	t	k	I	A_g	r_i	Z_p
	Mpa	Mpa	mm	mm	mm		mm⁴	mm²	mm	mm³
TUBE 350X350X35	200000	345	3600	400	35	1	1.145E+09	51100	149.6941	7015750

Nominal Moment strength $M_n =$ $Z_p \times F_Y =$ **2420.43**   KN.m

Nominal Tensile Str. $P_y =$ $F_Y \times A_g =$ **17629.5**   KN

Nominal Compression Str. $P_{ncr} =$ $F_{cr} \times A_g =$ **16899.2**   KN $=$ **0.9586** $\times P_y$

Slenderness ratio $\dfrac{Kl}{r_i} =$ **24.05**

$4.71\sqrt{\dfrac{E}{F_Y}} =$ **113.4**

F_cr : detailed calculation

If $\dfrac{Kl}{r_i} > 4.71\sqrt{\dfrac{E}{F_Y}}$ → $F_{cr} = 0.877 \times F_e$

If $\dfrac{Kl}{r_i} \le 4.71\sqrt{\dfrac{E}{F_Y}}$ → $F_{cr} = \left[0.658^{\frac{F_Y}{F_e}}\right] \times F_Y$

$Fe = \dfrac{\pi^2 E}{\left(\dfrac{Kl}{r_i}\right)^2}$ $=$ **3412.98**   Mpa

F_{cr} $=$ **330.708**   Mpa $=$ **0.9586** $\times F_Y$

DESIGN CHECK

LOADS

ELEMENT	BRACES	GRAVITY FORCES(SERVICE LEVEL)				STRENGTH COMBO{DD,LL &EQ}
	MAX.P(SC.1,SC.2)	P_D	P_L	M_D	M_L	M_U
	KN	KN	KN	KN.m	KN.m	KN.m
COLUMN	10870.562	900	810	-	-	18

1- LOCAL BUCKLING

SEISMICALLY COMPACT SECTION .(AISC 341-10),Table D1.1 (pp. 9.1-12 and 9.1-13)

$\lambda_1 =$ $\dfrac{b - 2xt}{t}$ $=$ **9.43**

$\lambda_{hd} =$ **13.24**

λ1 ≤ λhd ,SEISMICALLY COMPACT SECTION

Element	Width-to-thickness ratio	Limiting width-to-thickness ratio	
		Moderately ductile, λ_md	Highly ductile, λ_mh
Circular HSS[a]	D/t	0.044E/F_y [a]	0.038E/F_y
Rectangular HSS[b]	b/t	0.64(E/F_y)^0.5 [b]	0.55(E/F_y)^0.5
Angles	b/t	0.38(E/F_y)^0.5	0.30(E/F_y)^0.5
Flanges of I-shaped members and channels	b/t	0.38(E/F_y)^0.5	0.30(E/F_y)^0.5
Webs of I-shaped sections used as beams or columns[c]	h/t_w	3.76(1 − 2.75C_a)(E/F_y)^0.5 ... for C_a ≤ 0.125 / 1.12(2.33 − C_a)(E/F_y)^0.5 ≥ 1.49(E/F_y)^0.5 ... for C_a > 0.125	2.45(1 − 0.93C_a)(E/F_y)^0.5 ... for C_a ≤ 0.125 / 0.77(2.93 − C_a)(E/F_y)^0.5 ≥ 1.49(E/F_y)^0.5 ... for C_a > 0.125
Webs of I-shaped sections used as diagonal braces	h/t_w	1.49(E/F_y)^0.5	1.49(E/F_y)^0.5

SECTION IS SEISMICALLY COMPACT & NOT SLENDER

2- GLOBAL BUCKLING

SLENDERNESS :

$\lambda_2 =$ $\dfrac{kl}{r_i}$ $=$ **24.05**

$\lambda =$ **200**

λ2 ≤ λ, NON SLENDER SECTION

if $\frac{P_u}{\phi P_n} \geq 0.2$, then there is **a significant axial contribution,** $\boxed{1}$ becomes : $\boxed{\frac{P_u}{\phi P_{ncr}} + \frac{8}{9}\left(\frac{M_{uc}}{\phi M_n}\right) \leq 1.0}$ $\boxed{2}$

if $\frac{P_u}{\phi P_n} < 0.2$, then there is **unsignificant axial contribution,** $\boxed{1}$ becomes : $\boxed{\frac{1}{2}\frac{P_u}{\phi P_{ncr}} + \frac{M_{uc}}{\phi M_n} \leq 1.0}$ $\boxed{3}$

N.B. In our case the columns are loaded axialy and the moment is small compared to sections capacities , so only equation $\boxed{2}$ **will be used**

$\boxed{P_u}$ $= P(D.S.)+1.2 \times P_D + 1.6 \times P_L =$ $\boxed{13246.56}$ KN

$\boxed{\phi P_{ncr}}$ $= 0.9 \times P_{ncr}$ $=$ $\boxed{15209.25531}$ KN

$\boxed{M_{uc}}$ $=$ $\boxed{B1 \times M_n}$

$$B_1 = \frac{C_m}{1 - \alpha \frac{P_u}{P_{e1}}}$$ ≥ 1.0

$$C_m = 0.6 - 0.4 \times \frac{M_1}{M_2}$$

where M1 and M2, calculated from a first-order analysis, are the smaller and larger moments, respectively, at the ends of that portion of the member unbraced in the plane of bending under consideration.

$\alpha = 1.0$(LRFD DESIGN)

$M_1 =$ $\boxed{0.01}$ KN.m $\quad$ $M_2 =$ $\boxed{3}$ KN.m

$\boxed{C_m}$ $=$ $\boxed{0.5987}$

$$P_{e1} = \frac{\pi^2 \times E \times I}{(K \times L)^2}$$

$\boxed{P_{e1}}$ $=$ $\boxed{174403}$ KN

B_1 $=$ 0.6479

Use $\boxed{B_1}$ $=$ $\boxed{1}$

$\boxed{M_{uc}}$ $=$ $\boxed{18}$ KN.m

$\boxed{\phi M_n}$ $=$ $\boxed{2178.4}$ KN.m

$\boxed{\frac{M_{uc}}{\phi M_n}}$ $=$ $\boxed{0.0083}$

$\boxed{\frac{P_u}{\phi P_{ncr}}}$ $=$ $\boxed{0.871}$

$\boxed{2}$ $\rightarrow$ $\boxed{0.878}$ $\boxed{\leq 1 \text{ ,SECTION IS OK}}$

$$\sum \frac{load\ effects}{Strength}$$

BEAMS

SECTION	E	F_Y	L	h	b	t	s	k	I_min	A_g	r_i min	Z_p
	Mpa	Mpa	mm	mm	mm	mm	mm		mm⁴	mm²	mm	mm³
UB 533x210x109	200000	345	4000	539.5	210.8	18.8	11.6	1	29430000	13900	46.0137608	2830000

Nominal Moment strength $M_n =$ $Z_p \times F_Y =$ 976.35 KN.m

Nominal Tensile Str. $P_y =$ $F_Y \times A_g =$ 4795.5 KN

Nominal Compression Str. $P_{ncr} =$ $F_{cr} \times A_g =$ 2758.98 KN $=$ 0.5753 $\times P_Y$

F_{cr} : detailed calculation

Slenderness ratio $\frac{Kl}{r_i} =$ 86.93

$4.71\sqrt{\frac{E}{F_Y}} =$ 113.4

If $\frac{Kl}{r_i} > 4.71\sqrt{\frac{E}{F_Y}}$ → $F_{cr} = 0.877 \times F_e$

If $\frac{Kl}{r_i} \leq 4.71\sqrt{\frac{E}{F_Y}}$ → $F_{cr} = \left[0.658^{\frac{F_Y}{F_e}}\right] \times F_Y$

$Fe = \dfrac{\pi^2 E}{\left(\frac{Kl}{r_i}\right)^2}$ $=$ 261.207 Mpa

F_{cr} $=$ 198.488 Mpa $=$ 0.5753 $\times F_Y$

DESIGN CHECK

LOADS

ELEMENT	BRACES	GRAVITY FORCES(SERVICE LEVEL)				STRENGTH COMBO(DD,LL &EQ)
	MAX.P(SC.1,SC.2)	P_D	P_L	M_D	M_L	M_U
	KN	KN	KN	KN.m	KN.m	KN.m
BEAM	1390.795541	-	-	80	45	-

1- LOCAL BUCKLING

SEISMICALLY COMPACT SECTION,(AISC 341-10) ,Table D1.1 (pp. 9.1-12 and 9.1-13)

Element	Width-to-thickness ratio	Limiting width-to-thickness ratio	
		Moderately ductile, λ_md	Highly ductile, λ_mh
Circular HSS[a]	D/t	0.044E/F_y [a]	0.038E/F_y
Rectangular HSS[b]	b/t	0.64(E/F_y)^0.5 [b]	0.55(E/F_y)^0.5
Angles	b/t	0.38(E/F_y)^0.5	0.30(E/F_y)^0.5
Flanges of I-shaped members and channels	b/t	0.38(E/F_y)^0.5	0.30(E/F_y)^0.5
Webs of I-shaped sections used as beams or columns[c]	h/t_w	3.76(1 − 2.75C_a)(E/F_y)^0.5 ... for C_a ≤ 0.125 1.12(2.33 − C_a)(E/F_y)^0.5 ≥ 1.49(E/F_y)^0.5 ... for C_a > 0.125	2.45(1 − 0.93C_a)(E/F_y)^0.5 ... for C_a ≤ 0.125 0.77(2.93 − C_a)(E/F_y)^0.5 ≥ 1.49(E/F_y)^0.5 ... for C_a > 0.125
Webs of I-shaped sections used as diagonal braces	h/t_w	1.49(E/F_y)^0.5	1.49(E/F_y)^0.5

WEB CHECK

$C_a =$ $\dfrac{P_u}{\phi P_n}$ $=$ 0.322 $\lambda_{md} =$ 54.142

$\lambda_1 =$ $\dfrac{h - 2xt}{s}$ $=$ 43.27   λ1 ≤ λmd

FLANGE CHECK

$\lambda_2 =$ $\dfrac{b/2}{t}$ $=$ 5.606 $\lambda_{md} =$ 9.14932

λ2 ≤ λmd

SECTION IS SEISMICALLY COMPACT

SECTION IS SEISMICALLY COMPACT & NOT SLENDER

2- SLENDERNESS :

$\lambda_2 =$ $\dfrac{kl}{r_i}$ $=$ 86.93

λ2 ≤ λ, NON SLENDER SECTION

$\lambda =$ 200

3- SECTION CAPACITY CHECK

The column is subjected to Axial compression and flexure, it will be checked as BEAM - COLUMN element:

It should fulfill the following requirement :

$$\sum \frac{load\ effects}{Strength} \leq 1.0 \qquad \boxed{1}$$

if $\frac{P_u}{\phi P_n} \geq 0.2$, then there is **a significant axial contribution,** $\boxed{1}$ becomes : $\boxed{\frac{P_u}{\phi P_{ncr}} + \frac{8}{9}\left(\frac{M_{uc}}{\phi M_n}\right) \leq 1.0}$ $\boxed{2}$

if $\frac{P_u}{\phi P_n} < 0.2$, then there is **unsignificant axial contribution,** $\boxed{1}$ becomes : $\boxed{\frac{1}{2}\frac{P_u}{\phi P_{ncr}} + \frac{M_{uc}}{\phi M_n} \leq 1.0}$ $\boxed{3}$

$P_u =$ **1391** KN

$\phi P_{ncr} = 0.9 \times$ 2759 $=$ **2483.081224** KN

$M_{uc} =$ **B1 x M_u**

$$B_1 = \frac{C_m}{1 - \alpha \frac{P_u}{P_{e1}}} \qquad \geq 1.0 \qquad\qquad C_m = 0.6 - 0.4 \times \frac{M_1}{M_2}$$

where M1 and M2, calculated from a first-order analysis, are the smaller and larger moments, respectively, at the ends of that portion of the member unbraced in the plane of bending under consideration.

$\alpha = 1.0$(LRFD DESIGN)

SIMPLY SUPPORTED BEAM   1
CONTINUOUS BEAM   2 → $M_1=$ **1** KN.m $M_2=$ **1** KN.m

TYPE OF BEAM : **1**

$C_m =$ **1**

$$P_{e1} = \frac{\pi^2 \times E \times I}{(K \times L)^2}$$

$P_{e1} =$ **3631** KN

$B_1 =$ **1.6209**

Use $B_1 =$ **1.621**

$M_u = 1.2M_D + 1.6M_L =$ **168** KN.m

$M_{uc} =$ **272.31** KN.m

$\phi M_n =$ **878.72** KN.m

$\frac{M_{uc}}{\phi M_n} =$ **0.3099**

$\frac{P_u}{\phi P_{ncr}} =$ **0.56**   > 0.2 ,signficant axial contribution, use equation (2)

$\boxed{2}$ → **0.836** ≤ 1 ,SECTION IS OK

$$\sum \frac{load\ effects}{Strength}$$

Appendix C: Bi-Linear Link Element Parameters

- $E = 210,000\ MPa\ (N/mm^2)$ (assumed)
- For Columns: $f_y = 2.53\ t/cm^2\ =\ 2.53\left(\frac{1000x9.81}{100}\right) = 248.193\ MPa$
- For Beams: $f_y = 2.75\ t/cm^2\ =\ 2.75\left(\frac{1000x9.81}{100}\right) = 269.775\ MPa$
- For Braces: $f_y = 2.93\ t/cm^2\ =\ 2.93\left(\frac{1000x9.81}{100}\right) = 287.433\ MPa$

- Brace Buckling Length is calculated in accordance with the description provided by Wakabayashi et al. (1974): the effective length of a bracing used in the analysis is equal to L/2, with L being the length of a bracing shown in Fig. B1. This length was chosen based on experimentally observed deformation behavior of bracing members.

$L = \sqrt{(2500)^2 + (1300)^2} = 2817.8\ mm$
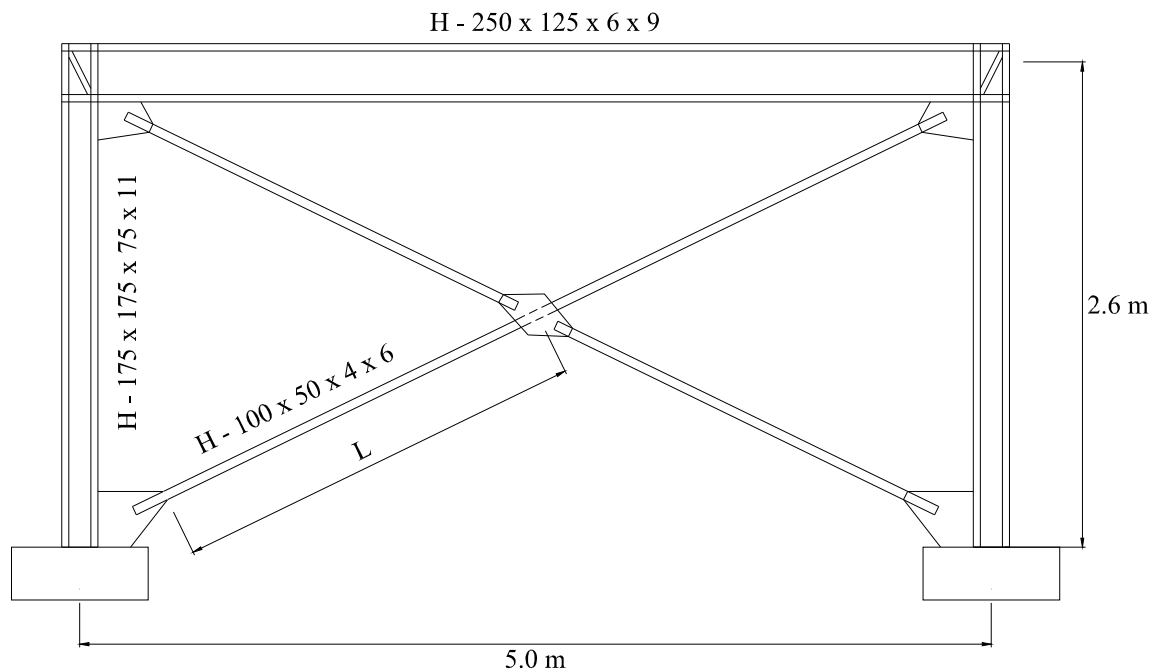
$L_b = 0.5x2817.8 = 1408.9\ mm$

Figure B1: Typical Steel Braced Frame Tested by Wakabayashi et al. (1974)

- Yield strength is used to represent the response of the brace in tension in compliance with the AISC Provisions for Structural Steel Buildings AISC 360-10 (2010) as follows:
  - $F_y^+ = F_y A_g = 287.433x\ 1010 = 290,307.33\ N$
  - $k_0^+ = \frac{EA}{L} = \frac{210,000x1010}{1408.9} = 150,542.977\ N/mm$
  - $r^+ = 1.3\% = 0.013$

- Post-buckling strength is used to represent the response of the brace in compression as per current design practice based on the AISC 360-10 (2010) and Seismic Provisions AISC 341-10 (2010):
  - As given in Wakabayashi et al.(1974):
    A=1010 mm^2 and I$_y$=114,000 mm^4
  - $r_y = \sqrt{114000/1010} = 10.624\ mm$
  - $\frac{b_f}{2t_f} = \frac{50}{12} = 4.167 < 0.3\sqrt{\frac{E}{F_y}} = 8.11$ [Table D1.1, p 9.1–12, AISC 341-10 (2010)] → No Flange Local Buckling
  - $\frac{h}{t_w} = \frac{88}{4} = 22 < 1.49\sqrt{\frac{E}{F_y}} = 40.27$ [Table D1.1, p 9.1–12, AISC 341-10 (2010)] for C$_a$>0.125 → No Web Local Buckling
  - $\frac{L_b}{r_y} = \frac{1408.9}{10.624} = 132.615 > 4.71\sqrt{\frac{E}{F_y}} =$
    $127.31\ (Elastic\ Global\ Buckling)$
  - $F_e = \frac{\pi^2 E}{(L_b/r_y)^2} = 117.8514\ MPa$
  - $F_y^- = 0.877F_e A_g = 0.877x117.8514x\ 1010 = 104,389.235\ N$
    $= 0.36F_y^+$
  - $k_0^- = \frac{EA}{L} = \frac{210,000x1010}{1408.9} = 150,542.977\ N/mm$
  - $r^- = 1.3\% = 0.013$